ILLUMINATING DARK MATTER: LIGHT MICROSCOPY AND RAMAN MICROSPECTROSCOPY THROUGH TRANSPARENT POROUS MEDIA FOR APPLICATIONS IN SOIL AND SEDIMENT MICROBIAL ECOLOGY

Kriti Sharma

A dissertation submitted to the faculty at the University of North Carolina at Chapel Hill in partial fulfillment of the requirements for the degree of Doctor of Philosophy in the Department of Biology.

Chapel Hill
2019

Approved by:

Elizabeth A. Shank

Carol Arnosti

Alecia Septer

Peter White

James Umbanhowar

ABSTRACT

Kriti Sharma: Illuminating dark matter: Light microscopy and Raman microspectroscopy through transparent porous media for applications in soil and sediment microbial ecology
(Under the direction of Elizabeth A. Shank)

Soils offer habitats to an unparalleled abundance and diversity of microorganisms, whose activities are critical to agriculture, ecosystem health, and biogeochemical cycling. A major barrier to understanding soil microbes within their habitats is the opacity of natural soils. Despite a long history of endeavors to visualize life in the soil, and promising advancements in this field, non-destructive approaches that allow dynamic insights into microbial life in soils are particularly lacking. Chapter 1 reviews this field and outlines the history and potential of optically transparent porous media as model soil systems amenable to non-destructive imaging of soil microorganisms within three-dimensional soil-like matrices.

In Chapter 2, I introduce the utility of single-cell Raman spectroscopy (SCRS) for non-destructive stable isotope probing over time, particularly for monitoring the uptake of ^{13}C by bacteria from complex natural polysaccharides. This spatially resolved and non-destructive approach allows us to ask the question, “Do bacterial biofilms allow bacteria to stick together in numbers large enough to initiate cooperative decomposition of necromass?’

In Chapter 3, I assess the polymer Nafion and the crystal cryolite as substrates for optically transparent model soil systems called “transparent soil” (TS) microcosms.

I find that both substrates are compatible with optical microscopy and enable growth, maintenance, and visualization of micron-sized bacteria in three-dimensional porous matrices over time. Both substrates are also compatible with SCRS, and enable stable isotope probing (SIP) using deuterium (D_2O) as a non-destructive marker of microbial activity *in situ*, while cryolite-based microcosms also enable measurement of ^{13}C label uptake in bacteria. I use D_2O label tracing to show that bacterial cells attached to dead fungal hyphae within a Nafion matrix show more metabolic activity after a dry-wet cycle than cells far away from the fungal hyphae, corroborating the important role of fungi in facilitating survival of bacteria in the fluctuating conditions found in soils.

In Chapter 4, I present a method for rapid and inexpensive manufacture of microfluidics devices that were used to construct TS microcosms at the lab bench. Chapter 5 summarizes the dissertation overall and offers suggestions for future research.

To all my relations.

ACKNOWLEDGMENTS

First: Dan McShea at Duke University, who invited me warmly into a country called a “Biology Department” and said, “You could make a home here.” My gratitude to you is as deep as that of anyone who has found herself in an unfamiliar land towards her first and most and necessary host.

My friends and colleagues at Duke University Biology Department – Dave McCandlish, Laurin McCall, Courtney Fitzpatrick, Viviane Callier, Paul Magwene, Debra Murray, Omür Kayikçi, Amy Schmid, Charlie Cooper, Keely Dulmage: you grew me up, you taught me how to hold a pipette and a coherent line of scientific thought, you made the lab a place of care, and I am grateful.

Barbara Herrnstein Smith, Susan Oyama, and Priscilla Wald: were it not for your intellectual kinship, your good influence, the bridges you built for me and the encouragement you held out for me, I surely would have dried up like a tadpole in an evaporating pool, and would never have attempted a metamorphosis into someone amphibious, both capable of swimming and of leaving the pond.

At University of North Carolina, I thank Beth Shank most of all: when I think of how much you’ve made possible for me, I’m moved to be a more generous person towards others. I am so lucky to be your first student – it’s been an honor and an adventure.

My committee – Carol Arnosti, Alecia Septer, James Umbanhowar, Peter White, and (previously) Neel Ahuja: thank you for your generous mentorship, patience, and feedback, on this dissertation and all along the way. I am a better scientist and thinker because of the time each of you took to help be become one.

Gabrielle Grandchamp, Susie Harris, Sarah Yannarell, Alexi Schoenborn, Noam Eckshtain-Levi, Sarah Barr, Jamie Winshell: you are such brilliant, kind, and hilarious labmates. Without you, it would have been such a slog; with you, it was a slog punctuated with a great many moments of ease and joy – also cheese and wine. I will take with me the many things I learned from you – quotes, jokes, protocols, recipes, life hacks, and probably the lab weirwood – and I will miss you very much.

Tony Perdue, UNC Biology Light Microscopy Facility: I liked you from the start, which may be why I liked microscopy from the start, and would you look at me now. Thank you for your mentorship and kindness.

Kenlyn Merritt, Marie Fholer, Tosha Furphy, Shelia Hunnicutt, Madison Hayes Rauscher, Ms. Helen: thank you for the daily ways in which you made my time in graduate school possible.

Sophie Tintori, Alissa Brown, Jenny Heppert, Laura Mudge, Anaïs Monroy-Eklund, Kayleigh O'Keeffe, Bianca Lopez, Alison Earley, Julia Longo, Anna Parker, Elizabeth Moore, Meredith Cenzer, Colin Maxwell: thank you for SSC, for being the place where I felt I most belonged in grad school. I stand by the assessment I made years ago, which was that SSC was probably the best thing I did in grad school.

Aspen Reese, Firas Midani, Rachael Bloom, Max Villa, Erin McKenney, J.P. Balmonte, Adrienne Hoarfrost: thank you for Microbial Ecology Super Group and for the

adventures upon R/V Endeavor, for your company as microbial ecologists I really respect and as people I really like.

Peter Wilfhart, Mandy Maring, Fletcher Halliday, Simone Halliday, Alissa Brown, Bianca Lopez: “there are good ships, and wood ships….”

I thank the University of North Carolina Department of Biology for the Doctoral Dissertation Merit grant, which funded the first year of this doctoral research work. I am also very grateful to the U.S. Department of Energy Bioimaging Energy Research Program – and Program Officer Dr. Prem Srivastava in particular – for the funding that made my dissertation research program possible.

I thank David Berry and the entire Division of Microbial Ecology (DoME) at the University of Vienna for generously hosting me as a visiting scientist and allowing me to conduct the Raman spectroscopy experiments critical to this dissertation research. Thank you for welcoming me to DoME – the experience meant so much.

My friends at DoME – Steffi Imminger, Dimitri Meier, Craig Herbold, Faith Hall-Herbold, Florian Moeller, Candace Williams, Fatima Perreira, Alessandra Riva, Ken Wasmund, Johanna Wiesinger, Petra Pjevac, Nora Grossschmidt, Chris Sedlacek, Franziska Bauchinger, Stephan Köstlbacher, Tamara Matzhold, Anne Daebeler, and all the Domies: however brief my visits were, and however simple and ordinary it may have felt for you to extend your kindness to me in your laid-back Viennese way, having your friendship and being invited into the fold of DoME meant more than I can really say, so

whatever, I'll just bring in a flat of Ottakringers for y'all or something and you can fight over them.

Georgi Nicolov: my collaborator, co-author, and buddy. Thank you so much for all of the centrifuging and the microscoping, for checking up on me every so often to make sure I hadn't died in the Raman room, and for being such good daily company.

Màrton Palatinszky: I would *almost* do the PhD over just to get a chance to collaborate with you again. Almost. I don't really play music, but our collaboration made me appreciate what one might get out of joining a band, what serendipitous miracles might come to people in their attempt to play the same thing together. I am not just a much better scientist for having met you, but also a more joyful and interested person who pays more attention to the world's many details. So, once again, I owe you so much and will always be so grateful to you.

Special thanks to Denise Vandecruze, Sven Rinke, and Eli for also making Vienna home.

Afiya Carter, Alexis Pauline Gumbs, Nia Wilson, Rachael Derello, Kynita Stringer-Stanback, Beth Bruch, Noah Rubin-Blose, Tema Okun, Emily Chavez, Manju Rajendran, Sam Hummel, Mikel Barton, Dannette Sharpley, Sammy Truong, Bryan Proffitt, Nikki Brown, Zachari Curtis, Keagha Carscallen, Shirlette Ammons, Kai Lumumba Barrow: I am because we are, I am because we were, no matter who and what we are now. This dissertation is a zine we started in 2006 on Kai's back porch.

Lea Ray, Tracy Feldman, Glenys Verhulst, Kelly Foyle, Lorrie Guess, Jeff Brown, Tony Macias, Beto Tijerina: thank you for the warmth of your friendship and support,

over the long years we've known each other, but also in particular in these last grad school years. I am lucky to grow with you over life's many stages.

Ginnie Hench, Dhruv Arora, Michael Schulson, Rob Dunn: I've been inspired many times during my time in grad school by the creative ways in which you engage the intersection of science and society, and am grateful for your invitations to do the same.

Michal Osterweil and Arturo Escobar: the invitations you've extended to teach, think, and write together over my grad school years have connected and reconnected me to the questions closest to my heart. In short, they have been a kind of revelation and salvation. To other worlds possible.

RGTT – Russell Herman, Catherine Berman, Manju Rajendran, Noah Rubin-Blose, Roxana Bendezu, Charla Hodges, Andreina Malki, Janet Xiao: one of the great blessings of the last several years has been getting to gather with you regularly and benefit from your thoughtfulness, wisdom, and kindness. In the streets and in science labs, your powerful presence resonates and is deeply felt.

My sangha – Michelle O'Brien, John Paredes, Conal Ho, Natasha Paredes, Kari Hill, Camila Barbosa, Jonathan Iradi, Pavithra Vasudevan, Betsy Dain, elliott turnbull: you are my reminders of what is meant by "bodhisattva" and "precious human birth".

Marjorie Scheer and Carolyn Kapner: for my moment-to-moment gladness-to-be-alive, I have you to thank.

Pavithra Vasudevan, Loni Townsley, Laurin Penland: you are why I feel I am never alone.

Alissa Brown: you were there at the very beginning, all through the middle, and at the very end (!) Take me at my word when I say I could not have done it without you.

Nagars, Sharmas, Joshis, Kakrias, Mulls, Maxwells, Lampmans: my love and gratitude to all of you who have never needed to know what I'm working on or why before you say, "We trust you, and you always belong with us. Now eat up."

Om Sharma, Jyoti Sharma, Santosh Bhardwaj, Sachi Partin, Neel-Gopal Sharma, Rasa Partin, Bharti Sharma: always. But especially these last six years.

Kanai Partin and Avani Partin: I started this before you existed, I finished it after you showed up and kept getting your fingers into everything. When you become paleontologists, I'll help organize your field notes and format your citations.

Colin Maxwell: "otherwise it is just a world with a lot of rough edges/ difficult to get through, and our pockets full of stones."

It will take me years yet to understand and to say all that I learned during the process of completing this PhD, longer still to recognize and thank all who made the journey possible. This dissertation is a start.

TABLE OF CONTENTS

LIST OF TABLES

Table

LIST OF FIGURES

LIST OF ABBREVIATIONS

μCT	Micro-computed X-ray tomography
CARD-FISH	Catalyzed reporter deposition fluorescence in situ hybridization
FISH	Fluorescence in situ hybridization
MRI	Magnetic resonance imaging
NA	Numerical aperture
NanoSIMS	Nanoscale secondary ion mass spectrometry
NMR	Nuclear magnetic resonance
RI	Refractive index
rRNA	Ribosomal ribonucleic acid
SCRS	Single-cell Raman spectroscopy
SIP	Stable isotope probing

CHAPTER 1: *IN MEDIA RES:* HISTORICAL AND EMERGING APPROACHES TO CATCHING SOIL BACTERIA "IN THE MIDDLE OF THE ACTION"

"Progress in science depends on new techniques, new discoveries and new ideas, probably in that order."

–Dr. Sydney Brenner, who established the transparent soil nematode C. elegans *as a model system in developmental biology* (Brenner, 2002)

The cover of the book *The Architecture and Biology of Soils* is arresting. A protist is pictured squeezed thin between two soil particles, almost bisected but for its wasp-like waist. (Figure 1.1) Like the introduction to a compelling story, it seems we have caught our protist protagonist "in the middle of the action".

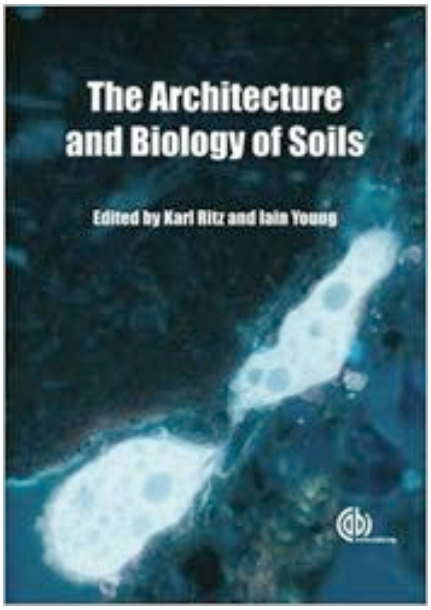

Figure 1.1: Cover of *The Architecture and Biology of Soils*. (Ritz & Young, 2012).

Where is the protist going? How quickly did it move? What contortions did it perform to be able to squeeze its body into such a tiny passage? Was it alive when this photo was taken, or was it laying dormant or dead in the soil? We cannot know the answers to these questions, because this micrograph comes from a fixed sample. Karl Ritz and colleagues used a highly creative and artistic method to obtain this photo (Ritz et al., 2011). They took intact soil cores, poured transparent resin into the cores, allowed the resin to solidify, cut the fixed soil cores into slices with a geological saw, and polished those slices down with diamond paste until they were thin enough for light to shine through. The slices were treated with a fluorescent brightener to highlight biological material in the soils, and then placed under a compound microscope where they could be investigated for signs of life – or rather, of life fixed in place.

These wonderful and painstakingly obtained snapshots are some of our only windows into the microscopic life teeming in soils. By using this same technique to shine light through the dark underground, Nunan and colleagues were able to estimate and model the average distances of bacteria in soils from each other (Nunan et al., 2003). This was one of the only methods available to obtain such information at the time, making these some of the only available biogeographies of microbes in environmental soil samples that are carried out at the scale of microbes themselves.

Plant ecologists survey forests and count trees, and primatologists follow baboons across the savannah. Microbial ecologists, however – and most especially those who study microbes in soils – still struggle with the basic problem of knowing where the subjects of their study are, let alone how they got there, where they are going, who they are interacting with, what they are taking up from their environment,

and how they are transforming that environment. Bulk methods can aggregate this information for thousands, millions, or billions of microbes – for example, by sequencing or extracting metabolites from a gram of soil. However, this is somewhat analogous to aggregating and averaging species or functional data for all the plants on a continent – or even a planet – with no information about their location at a scale appropriate to the size of their bodies.

Plant ecologists would not be satisfied with such a state of affairs, and – fortunately – neither are microbial ecologists. Soil microbial ecologists have long examined the ordinary earth with a fascination and a desire for detail shared by many who study dark and deep worlds: astronomers, oceanographers, and more. In 1938, J. Kubiëna created and carried a specialized microscope to an exposed soil profile, lodged the microscope into the rock face, and looked for microscopic life in rivulets tens of microns wide between aggregates of minerals (Kubiëna, 1938). He sketched and narrated the swimming behaviors of protozoans in these ephemeral microscopic rivers, and became among the first of many who would have to invent new ways of seeing in order to come to know what could not otherwise be known about microscopic life underground.

Beyond what the eye can see: Advances and challenges in soil imaging

Because soils are opaque to light, imaging through soil has depended on other probes, from subatomic particles to electromagnetic radiation outside of the visible spectrum. Micro-computed X-ray tomography (μCT), nuclear magnetic resonance (NMR), magnetic resonance imaging (MRI), neutron radiography, and nanoscale

secondary ion mass spectrometry (NanoSIMS), are all techniques that have been used to image within soils, none of which use visible light as a probe. All of these techniques have contributed to our understanding of soil structure, with each able to highlight particular aspects of the soil environment while obscuring others (Helliwell et al., 2017; Mairhofer et al., 2017, 2013; Metzner et al., 2015; van Dusschoten et al., 2016, Musat et al. 2012).

Micro-computed X-ray tomography (μCT), nuclear magnetic resonance (NMR), and magnetic resonance imaging (MRI) are all promising, non-destructive techniques that have been used to image the soil matrix and plant roots growing through that matrix (Atkinson et al., 2019 for a recent review of advances in root imaging in soils; Helliwell et al., 2017; Mairhofer et al., 2017, 2013; Metzner et al., 2015; van Dusschoten et al., 2016). These are exciting and quickly-advancing developments for plant biology and for the study of soil texture and microbiota on roots. However, these techniques cannot, to date, be used to visualize bacteria because bacteria are not electron-dense enough to be distinguished from soil pore water (Baveye et al., 2018). Neutron radiography is a promising technique for non-destructive visualization of microbes in undisturbed soil cores, but currently lacks the resolution (which is currently on the order of tens and hundreds of microns) to resolve microbes in situ (Tötzke et al., 2017).

The best methods for accurately resolving bacteria in soils are all destructive techniques. NanoSIMS is a particularly powerful method, providing three-dimensional high resolution images including isotopic information of microbes in soil (see Musat et al. 2012 for a review of the history of the method's development and its contributions to microbial ecology), and has recently been used to successfully image rhizosphere

bacteria within a soil matrix (Vidal et al., 2018). Sample preparation for NanoSIMS requires fixation, however, and the image acquisition process is itself destructive. Moreover, with only 22 NanoSIMS instruments in the world (Stanford Nano Shared Facilities, 2019), and the high cost of NanoSIMS instrument time, the technique is not routinely accessible to microbiologists in the way that, say, light microscopy is. Fluorescent in-situ hybridization (FISH) is a powerful tool for identifying prokaryotic cells by 16S rRNA sequence while preserving spatial information, and can be inexpensively carried out at the benchtop (Wagner & Haider, 2012). However, FISH is notoriously difficult in soils due to off-target binding of probes to soil particles and the native autofluorescence of soils which dampens cell signal (Bertaux et al., 2007). The extraction of cells from soils increases cell detection, though at the cost of disrupting the soil matrix and losing positional information (Bertaux et al., 2007; Eichorst et al., 2015). Advances such as CARD-FISH have amplified signal through multiplexing of probes and successfully allowed identification of bacteria within soil samples (Eickhorst & Tippkötter, 2008). Once again, however, this is a destructive technique.

In sum, though great strides have been made in imaging in soils, particularly in the last 15 years, existing techniques that approach the micron-scale resolution needed to detect and visualize soil microbiota are destructive, with no clear candidate yet emerging for non-destructive methods. As Baveye and colleagues (2018) state in their recent and lengthy review of the last decades of research in microscale soil processes, "…it is clear that it is not possible at this stage to monitor in real time, at the microscale, the dynamics of microbial processes in actual soils. And, to be realistic in our

expectations, for bacteria, archaea, and definitely viruses, it may be that we shall never be able to monitor their activity directly in soils."

It is in this context that soil model systems emerge as attractive candidates that can enable non-destructive visualization of microbiota in porous media (i.e. materials, like soils, that have pores or voids). These systems – which are not natural soils but preserve some of the key features of soils depending on the question at hand – allow researchers to model and test our existing assumptions of how soil microbiota cluster, behave, grown, and even metabolize over time.

A history of transparent soils

"Transparent soils" are soil model systems wherein particles saturated with liquids of similar refractive index (RI) allow transmission of light and render the porous, "soil-like" system optically transparent (Iskander, 2010). Transparent soils (TS) have been used for over 25 years in geoengineering and hydrology, where they have helped solve and ground-truth important and otherwise intractable problems in soil physics: from determining how soils compress under weight (with applications for civil engineering), to tracking how oil travels through soil pores (with implications for groundwater quality; see Iskander et al., 2015 for a review of 25 years of work on transparent soils in these fields).

Despite their importance in advancing soil physics, TS systems have only recently and rarely been used for applications in soil biology. Soil physics models have generally not required the maintenance of organisms within TS systems, and have therefore tended to rely on RI-matching strategies using solutions that do not support

organismal growth, such as silicone oil. Foundational work by Leis and colleagues (2005) introduced the synthetic transparent fluoropolymer Nafion (Chemours) as the solid phase of a TS system that could be RI-matched to aqueous, biocompatible solutions, and used to successfully culture sediment microorganisms *in situ*. Downie and colleagues (2012; 2014) built on this work and introduced Nafion-based TS to plant biology as a tool for visualizing roots in a porous transparent medium that gives rise to more naturalistic root phenotypes than roots grown in agar. Though well-cited and lauded as a much-needed advance in the study of roots, no other group (to our knowledge) has used Downie et al's fluoropolymer-based TS system for root phenotyping – though the same research group did significantly advance the method recently for live-cell imaging of nematodes (O'Callaghan et al., 2018). This may be due to the drawbacks of (a) the high cost of Nafion, the fluoropolymer used as the solid substrate in these TS studies, and (b) the RI of Nafion (RI=1.35; Leis et al., 2005), which is close to that of water (RI=1.33) but different enough that image quality deteriorates at the scale of millimeters and centimeters needed for root growth and its visualization. Indeed, a recent work by Ma and colleagues cites these reasons as their motivation for taking Downie and colleagues' Nafion-based system as inspiration, but inventing an inexpensive hydrogel bead-based TS system with a very close RI match with water for root phenotyping studies (Ma et al., 2019).

Nafion may, however, be well-suited to studies in soil microbial ecology, where microcosms utilizing only a few micrograms of particles and requiring imaging depth of tens or hundreds of microns become inexpensive to build, and tolerant of slight RI mismatches, therefore obviating the need for exact RI-matching with bio-incompatible

solutions. For soil microbial studies, Nafion has two major advantages over hydrogel-based systems, despite the clear usefulness of hydrogels for plant studies: (a) Nafion can be milled to fine particle sizes down to 1 μm, which offer micron-sized pores as important habitats for micron-sized bacteria, whereas the lower limit of for the manufacture of hydrogel beads as published by Ma and colleagues is around 500 μm (Ma et al., 2019), and (b) Nafion is a synthetic polymer that is not able to be metabolized by bacteria and fungi, whereas alginate-gellan hydrogel beads are rich carbohydrate sources readily decomposed by many bacteria and fungi (Rice et al., 1992; Lin et al., 2018;).

Another potential substrate for biocompatible, inert TS is cryolite, a naturally occuring and water-insoluble sodium aluminum fluoride crystal. Cryolite's refractive index of 1.339 (Lewis, 2007) is remarkably close to that of water (1.333), rendering it nearly optically transparent in aqueous solutions. Cryolite has been used as a TS medium in a few soil physics studies, though it is not as popular as quartz, due to its relative cost and rareness. A small and intriguing set of studies have used cryolite to gain insight into the biophysics of the burrowing behaviors of marine invertebrates in sediments (Flessa, 1972; Francoeur & Dorgan, 2014; Dorgan, 2018) . As a substrate for soil microbiological studies, cryolite was used by Zhu and colleagues (Zhu et al., 2014) who monitored the swimming behavior of *Bacillus subtilis* bacteria in a packed-cryolite capillary, and by Oates and colleagues (2005) who mapped the spatial patterns of oxygen consumption by *Pseudomonas fluorescens* bacteria in a cryolite matrix using bioluminescent reporters.

The history of transparent soils indicates that the use and development of TS systems was primarily driven by the need to improve predictions in geoengineering and hydrology, and, more recently, to understand plant root biology for agricultural purposes. The recent resurgence of interest in microscale soil biological processes – and therefore the potential application of TS systems to understand these processes – can be attributed at least in part to an additional driver: the need to better understand carbon fluxes in a world experiencing climate change.

A detailed understanding of soil processes is not only essential for building infrastructure, groundwater protection, and agriculture, but also for climate predictions (see Davidson & Janssens, 2006 for a review of concepts in feedbacks between climate predictions and soil processes). Earth systems models used for climate modeling depend on accurate modeling of the flux of carbon between land and air, where carbon moves from the atmosphere to the land through photosynthesis and the exudation of photosynthates to soils through roots, and from land to atmosphere through respiration and decomposition of biomass and soil organic matter (Bardgett et al., 2008; Davidson & Janssens, 2006; IPCC, 2013, 2018). Current models show massive uncertainty regarding the magnitude and even the direction of this flux, as it remains uncertain whether land will act as a carbon source or a carbon sink in an overall warmer and wetter world (IPCC, 2013). Soil microbes are key players in this question, as the primary consumers of root photosynthates and decomposers of biomass and soil organic matter (Bardgett et al., 2008; Wieder et al., 2013). Their metabolic activities are key determinants of how much carbon dioxide is respired from land into the atmosphere – and a great deal of carbon is available to be respired. Large quantities of carbon are

stored in terrestrial soils – 1500 Pg, compared with 800 Pg in the atmosphere and 450 Pg in terrestrial vegetation (IPCC, 2013). This massive carbon pool exists largely as complex soil organic matter (Fontaine et al., 2003). The fate of this carbon – how much of it remains in the ground, and how much is decomposed and respired into the atmosphere – is a question with profound consequences for global climate and for the future of human societies.

More accurate and predictive atmospheric models depend on more realistic soil models – and specifically, more explicit modeling of microbial metabolism in soils as a key determinant of carbon efflux from soils (Pold & DeAngelis, 2013; Wieder et al., 2013). This is where transparent soil models – and specifically micromodels suited to micrometer scale manipulation and measurements – may be particularly useful, as windows into not only microbial spatial distributions but also microbial function and metabolism over time (Baveye et al., 2018).

Raman microspectroscopy in transparent soils and the role of this study

Single-cell Raman spectroscopy (SCRS) has gained interest as a powerful tool for non-destructive characterization of microbial physiology and metabolism (Li et al., 2012). A great deal of information regarding a cell's physiology can be gained from its Raman spectrum, from its lipid content, to its sporulation state, and even, in some cases, species or strain identity (Huang et al., 2004; Xie et al., 2005; Cui et al., 2018). SCRS is also a powerful stable isotope probing (SIP) technique. After incubation with an isotopic variant of water (deuterium or D_2O) or isotopically-labeled carbon-containing compounds (^{13}C), cells can be measured by Raman spectroscopy to determine whether

they took up the isotopic label, which is visible in the cell's Raman spectrum as characteristic peaks or peak shifts (Huang et al., 2004; Li et al., 2013; Berry et al., 2015; Muhamadali et al., 2015). SCRS is essentially a non-destructive technique in the same way that fluorescence microscopy is non-destructive: both depend on excitation of cells with a laser, and resultant signal is dependent on laser power and acquisition time. Overexposure to the laser can harm cells, but given the right acquisition parameters, cells live and grow without phototoxic effects.

Prior work using SCRS as a SIP tool has relied on two main isotopic labels. After foundational work by Berry and colleagues (Berry et al., 2015), the use of SCRS to detect D_2O uptake (as measured by an increase in the peak area between 2045-2080 cm^{-1} in a cell's Raman spectrum) has found widespread use as a marker of microbial activity (Eichorst et al., 2015; Wang et al., 2016). ^{13}C-containing compounds have been used in microbial incubations – from ^{13}C bicarbonate in the cultivation of marine autotrophs, to ^{13}C glucose as a marker for general heterotrophic activity, to ^{13}C naphthalene in monitoring degradation of the compound – and uptake of the ^{13}C label has been detected by the characteristic "red-shift" of a phenylalanine peak from 1003 cm^{-1} to 966 cm^{-1} upon incorporation of ^{13}C into the phenylalanine ring structure present in all cells (Huang et al., 2004; Huang et al., 2009; Li et al., 2012; Li et al., 2013; Kumar et al., 2016).

Raman spectra have not to date been collected from bacterial cells within a soil matrix; rather, cells have been extracted from soils in a relatively pure cell fraction that reduces the particle load in the sample and thereby allows clean detection of cell spectra without interference from soil compounds. SCRS of cells in soils amended with

isotopically-labeled substrates has produced intriguing results. Using this method, Eichorst and colleagues (2015) found that D_2O incorporation could be detected in a subset of cells after soil wetting with D_2O. However, no ^{13}C uptake was detected in cells after incubation with ^{13}C-labeled cellulose. The authors interpreted this finding to mean that the level of ^{13}C incorporation may have been below the level of detection of the assay, due to the high background signal from autofluorescent compounds in soil; or that microbes become active (as indicated by D_2O uptake) before they took up carbon (as indicated by ^{13}C uptake). Alternatively, the soils may be so rich in existing carbon compounds – in humic compounds and cell lysates mobilized and released upon wetting – that the added ^{13}C-labeled cellulose was not the preferred substrate metabolized by microbes.

Raman microspectroscopy through TS systems opens up the exciting possibility of being able to carry out non-destructive live-cell SIP over time within a three-dimensional porous matrix. There is no study to date, to our knowledge, that has attempted SCRS through transparent porous media. One promising study by Brenan and colleagues (1997) used a TS system to show that it is possible to measure the rate of infiltration of water and trichloroethylene (a liquid immiscible with water) into a packed quartz column, and even to monitor how these liquids interact at their interface. Raman spectroscopy through porous substrates is different and quite a bit more challenging than Raman on the same substrates, just as seeing through crushed glass is much more difficult than seeing through intact glass. The complexity of spectra and of out-of-focus contributions to spectra increases greatly with porous substrates, as does the problem of RI mismatch which increases scatter as light bends through pore interfaces.

Brenan and colleagues (1997) showed that it is possible to overcome the difficulties of spectroscopy through porous media. However, this was a cell-free study and involved detecting relatively large volumes of pure liquids with strong characteristic Raman spectra. Detection of single-cell Raman spectra is considerably more difficult due to the tiny size of bacterial cells, and their comparatively small signal relative to the porous medium itself.

Despite these challenges, in this study, we were able to detect cell-specific Raman spectra from single, micrometer-sized bacteria through tightly-packed hydrated Nafion- and cryolite-based TS matrices (see Chapter 3). Moreover, by adding stable isotope probes to the system, we were able to analyze and use these spectra to non-destructively detect bacterial uptake of labeled substrates *in situ*. This capability allowed us to non-destructively measure the metabolic activity of single cells in a spatially resolved way, and in a condition that mimics an ecologically important process in soils: a drying and rewetting cycle (Lopez-Sangil et al., 2018).

A transparent soil model wherein the locations, morphologies, growth dynamics, movements, and even metabolic states of microbes can be resolved non-destructively at the single cell level opens up a wide variety of possible applications. In soil and sediment ecology, previously occluded processes like microbial growth and development, predation and lysis dynamics, migration patterns, conjugation and transduction networks, and interspecies interactions in three-dimensional porous matrices can be monitored by light and fluorescence microscopy. Because TS substrates are mostly pure and inert and do not themselves function as bioavailable sources of carbon or other nutrients, controlled amounts of nutrients can be added to

the system in pore water or as “spike-ins” of minerals or real soil particles to test their effects on soil microbiota. Alternatively, the ready growth of fungi in TS microcosms suggests uses for studying the fungal biology of soils, from elucidating the role of fungi as “highways” for bacterial movement through dry soils (Kohlmeier et al., 2005), to their critical role in biomass decomposition and as natural sources of biomass and nutrients themselves. The compatibility of cryolite with non-destructive ^{13}C tracing suggests a variety of uses to elucidate fundamental processes in soil microbial ecology, from *in situ* tracking of trophic interactions, to monitoring carbon flows in model soils due to viral lysis, to untangling the mechanisms of the widely observed “Birch effect” in soils by direct tracing of ^{13}C fate after dry-wet cycles (Birch, 1958; Unger et al., 2010). Moreover, workers in the field may build on TS microcosm systems by combining them with their own existing methods – such as FISH to identify microbes and their locations *in situ* (a difficult task in natural soils; Bertaux et al., 2007), or using fluorescent reporter strains of interest to explore their own questions in microbial ecology. Though we have suggested just a few possible uses of transparent soil microcosms, their future applications will depend on the questions and creativity of workers in the field.

Conclusion

There is a long tradition of attempting to visualize life in the soil, from direct observation of protozoans in pore water in the field, to catching resin-embedded ameobae in the middle of the action. Technological advances in the last 15 years have substantially expanded the scope of what is possible in the visualization of soil microbiota, and therefore of our understanding of microscale soil processes. The goal

of observing microscale processes in soils non-destructively over time, however, remains elusive, and suggests the need for complex but tractable TS micromodels to test hypotheses about microscale dynamics in soil systems.

Model soils play an important role in advancing our understanding of natural soils. We build them according to our current understanding of soils, and they in turn refine and update our knowledge (Vereecken et al., 2016). Our models of soils reflect and inform the many things that soils are to us: foundation of our infrastructure (Iskander et al., 2015), filter of our drinking water (Ganiyu et al., 2016), cradle and nursery of our agriculture (Atkinson et al., 2019), and – as we have come to appreciate more deeply only recently – regulator of our atmosphere and key determinant of its future (Davidson & Janssens, 2006). These models also have great potential to elucidate the many things that soils are to organisms that inhabit them: they are habitat, moisture, food, breath, and labyrinth for microscopic beings who turn biogeochemical cycles through their metabolism, and thereby make life above and below ground possible.

CHAPTER 2: TESTING THE ROLE OF BIOFILM GENES IN "CRITICAL MASS" FORMATION FOR COOPERATIVE DECOMPOSITION

Summary

Bacterial biofilms allow microbes to stick to substrates, but also to each other. The capacity to produce extracellular biofilm matrices and form aggregates may be advantageous in conditions that favor collectivity of cells. Due to their small size, microbes often cannot initiate extracellular decomposition of substrates as single cells, but rather require larger cell numbers to raise the local concentration of decomposition products high enough to support their survival. Here, we tested the hypothesis that biofilms may allow cells to stick together in numbers large enough to form a "critical mass" that can initiate extracellular decomposition of necromass. We show that *Bacillus subtilis* 3610 attaches to dead hyphae of the fungus *Mucor fragilis*, and that this attachment is dependent on biofilm genes. Fungal cell wall polymers, as well as the extracts and exudates of the fungus *M. fragilis*, induce expression of biofilm genes in *B. subtilis.* We find that single *B. subtilis* cells cannot grow on *M. fragilis* necromass, whereas larger groups of cells can. We estimate the critical mass of *B. subtilis* cells required to initiate decomposition of dead *M. fragilis* biomass as three. We further show that *B. subtilis* biofilm genes enable cells to stick together in clusters of nine or more. We therefore hypothesized that these cell clusters would initiate decomposition and take up ^{13}C from dead *M. fragilis* biomass before single planktonic cells. We used

Raman microspectroscopy of single cells to track uptake of ^{13}C from ^{13}C-labeled dead *M. fragilis* biomass by single planktonic cells and clustersnon-destructively over time. We found that both clusters and single cells take up ^{13}C over time from *M. fragilis* as their sole carbon source, with no significant difference between their uptake dynamics. We speculate that because the estimated critical density of bacteria required for decomposition of fungal biomass is surprisingly low, the effect of biofilm-mediated cell clustering on decomposition and uptake of decomposition products may be below the level of detection of our assay.

Introduction

In part due to their own evolutionary success as ancestors of all eukaryotic and multicellular life (Woese & Fox, 1977), prokaryotes are living in a world full of organisms much larger than themselves. For heterotrophic prokaryotes, breaking down the pool of large and complex polymers found in dead biomass into assimilable parts presents a major challenge, and one that is best approached collectively. The tiny size of prokaryotes constrains the geometry of their membrane transport proteins, which, in many cases sets the upper size limit of molecules they can import into their cytoplasm at about 600 daltons or the size of a trisaccharide (Weiss et al., 1991, though see Reintjes et al., 2017 for evidence of systems that allow uptake of substrates greater than 600 daltons). Prokaryotes therefore produce and secrete extracellular enzymes in order to digest large polymers extracellularly and then import the breakdown products of digestion into their cytoplasm (Arnosti et al., 2011). However, in general, individual cells cannot effectively carry out extracellular digestion on their own. Though some

extracellular enzymes are associated with the cell surface (Traving et al., 2015), non-cell-attached extracellular enzymes diffuse away from single cells faster than breakdown products can diffuse into cells, leading an individual, extracellular enzyme-producing prokaryote to starve, or at least limiting its growth (Rosenberg et al., 1977; Koschwanez et al., 2011). Groups of cells producing extracellular enzymes together, however, can raise the local concentration of breakdown products high enough to support survival and growth (Rosenberg et al., 1977; Koschwanez et al., 2011). In short, as a consequence of their tiny size, heterotrophic prokaryotes must digest the large complex polymers abundant in dead biomass both extracellularly and collectively.

How do prokaryotes then aggregate in groups large enough to carry out extracellular decomposition? Previous work by Koschwanez and colleagues (2011) on collective decomposition of sucrose by budding yeast has highlighted the importance of incomplete division for creating aggregates that can initiate decomposition. However, in the case of bacteria, biofilms may play an equally if not more important role in aggregating cells. Many bacteria in terrestrial and aquatic environments exist primarily not as free-living planktonic cells, but as biofilms – bacterial communities bound together in a self-produced matrix (Vu et al., 2009). This biofilm matrix is composed of extracellular polysaccharides, proteins, and/or nucleic acids (Hobley et al., 2015). Biofilm matrix has been hypothesized to interact with extracellular enzymes (EEs) in a number of ways. The matrix has been shown to (a) protect EEs from denaturation (Tielen et al., 2010; 2013), (b) keep EEs from being carried away by flow or diffusion thereby keeping EEs close to producers (Drescher et al., 2014), or (c) allow EE producers to adhere to the substrates they decompose (Or et al., 2007). It may also (d)

hold aggregates of cells together to form a “critical mass” of EE producers that can initiate decomposition of complex polymers.

This last mechanism has not, to our knowledge, been directly tested. In this study, we test the hypothesis that by holding cells close to each other, biofilm matrix may support the collective growth of EE producers, and allow them to initiate decomposition of complex organic polymers. Biofilms may also help initiate other processes that benefit from numbers, such as antibiotic degradation, luminescence, or further biofilm matrix production itself (West et al., 2007).

The model soil bacterium *B. subtilis* 3610 produces biofilm matrix as well as the EE chitosanase (Rivas et al., 2000). Chitosanase decomposes the complex polysaccharide chitosan, a component of some fungal cell walls that is particularly abundant in the cell walls of zygomycetes in the genus *Mucorales* (Peter, 2005). Indeed, for this reason, chitosanases and chitinases are important known anti-fungal agents, and their producers are used as biocontrol agents to protect crops from fungal pathogens (Kouzai et al., 2012). In forest soils, *B. subtilis* strains have been found growing vegetatively in the presence of fungal hyphae, whereas they were otherwise largely present in this soil as spores (Siala & Gray, 1974). This suggests that *B. subtilis* may live off of fungal hyphae, and fungal chitosan may be a complex carbon source for *B. subtilis* in soils. We therefore use the bacterium *B. subtilis* 3610 and necromass (dead biomass) of the fungal zygomycete *Mucor fragilis* to test the role of biofilm genes in forming a critical mass of cells to initiate decomposition.

Methods

Strain Construction

B. subtilis 3610 strains constitutively expressing fluorescent proteins were constructed by vector cloning, transformation of vectors into *B. subtilis* 168, and phage transduction of *B. subtilis* 168 transformant DNA into *B. subtilis* 3610. *B. subtilis* NCIB 3610 is a commonly-used strain of *B. subtilis* which is less genetically tractable than *B. subtilis* 168, but exhibits biofilm production phenotypes common to wild *B. subtilis* soil isolates that are lost in the 168 lab strain (McLoon et al., 2011). Plasmid pES037 was constructed by standard restriction digest cloning of *B. subtilis* codon-optimized versions of the *YPet* and *mTurquoise2* genes (obtained from Ethan Garner) into the pEA003 parent vector (*amyE::*P*spac*^{C}*-cfp-cam*^{R}; Yannarell et al., 2019), which replaced the *cfp* gene with the new fluorescent protein. Linearized vector was transformed into *B. subtilis* 168 as described previously (Yannarell et al., 2019). Cells were plated onto Lennox-chloramphenicol to select for transformants – *amyE::*P*spac*^{C}*-YPet-cam*^{R} and *amyE::*P*spac*^{C}*-mTurquoise2-cam*^{R}. Phage transduction from *B. subtilis* 168 transformants into *B. subtilis* 3610 using SPP1 bacteriophage was performed as previously described (Yasbin & Young, 1974).

Microorganisms, Media, and Growth Conditions

B. subtilis NCIB 3610 strains were routinely cultured on Lysogeny Broth (LB)-Lennox agar (10 g/L tryptone, 5 g/L yeast extract, 5 g/L NaCl, 15 g/L agar) supplemented with antibiotics (5 ug/mL chloramphenicol final concentration) at 30°C for 16-20 hours. *Mucor fragilis* used in this study was obtained from Fletcher Halliday, who

isolated the strain from a tall fescue plant in the Piedmont region of North Carolina, and created a culture stock by patching *M. fragilis* hyphae onto a malt extract agar (MEA) slant (Difco, malt extract 6 g/L, 6 g/L maltose, 6 g/L dextrose, 15 g/L agar) containing 200 ug/mL chloramphenicol. *M. fragilis* was routinely cultured by patching agar from culture stock into the center of an MEA plate containing 200 ug/mL chloramphenicol and incubating at 30°C for 10 days until a lawn of *M. fragilis* spore bodies was obtained. *M. fragilis* spore stock was obtained by adding 10 mL Milli-Q water to this lawn and aspirating the liquid back up to obtain spores. Spores were pelleted by centrifugation (4000 g on tabletop centrifuge in 15 mL Falcon tube) and washed three times in Milli-Q to remove residual growth medium and hyphae. Spore stock was stored at 4°C for up to one month. Spore concentration was calculated by counting on hemacytometer and diluted back to 10^5 spores per mL for routine use.

MSN medium (minimal salts with free ammonium as nitrogen source; Beauregard et al., 2013; 5 mM potassium phosphate [pH 7], 100 mM morpholinepropanesulfonic acid [MOPS; pH 7], 2 mM $MgCl_2$, 700 µM $CaCl_2$, 50 µM $MnCl_2$, 50 µM $FeCl_3$, 1 µM $ZnCl_2$, 2 µM thiamine, 0.2% NH_4Cl) was used as the base, carbon-free medium to which *M. fragilis* necromass or free sugars were added as sole carbon sources. *M. fragilis* was grown in TS microcosms with MSNglu (MSN with 2% glucose, final concentration). MSNg – MSN with 0.05% glycerol (Beauregard et al., 2013) – was used in necromass attachment, and liquid biofilm gene expression assays. MSgg broth was used as a biofilm-inducing medium (5 mM potassium phosphate [pH 7], 100 mM morpholinepropanesulfonic acid [MOPS; pH 7], 2 mM $MgCl_2$, 700 µM $CaCl_2$,

50 μM $MnCl_2$, 50 μM $FeCl_3$, 1 μM $ZnCl_2$, 2 μM thiamine, 0.5% glycerol, 0.5% glutamate (Branda et al., 2001)).

Preparation of Fungal Biomass and Necromass

M. fragilis spore stock (100 μL of 10^5 spores per mL stock) was inoculated into 25 mL MEA broth and incubated 16 to 20 hours at 30°C. *M. fragilis* hyphae were washed by filtering the culture through a 40 μm cell strainer and washing hyphae on the strainer three times with 10 mL MSN medium. Washed *M. fragilis* was resuspended in MSN and 1 mL hyphal suspension was filtered through a 0.45 μm filter, dried, and weighed to calculate dry weight of fungal biomass. Suspension was diluted to 6 mg dry weight of biomass per mL. Live hyphae were used in the *B. subtilis* attachment assay.

To prepare dead *M. fragilis* hyphae (necromass), *M. fragilis* was cultured and washed as above. The washed fungal suspension was heated for 1 hour at 70°C in a heat bath or oven to kill hyphae and spores (Thom et al., 1916). Heat-killed culture was inoculated onto an MEA plate to test for growth; none appeared. The heat-killed suspension was washed three times in MSN by filtering, then resuspended, weighed, and diluted to 6 mg dry weight necromass per mL as above. Necromass was resuspended in MSN, MSNg, or MSgg depending on its use.

Biofilm Formation on Fungal Biomass and Necromass

Wild-type and biofilm mutant (*epsA-O::kan tasA::tet,* biofilm gene knockout, abbreviated below as *eps-tasA*) *B. subtilis* 3610 strains were grown for 2.5 hours at 37°C shaking in LB broth, washed 5x in MSNg, and added to 2 mL of *M. fragilis*

biomass or necromass suspension in MSNg to a final concentration of OD_{600} of 0.05 (~2.5 x 10^7 cells/mL) in wells of a 24-well plate. The final concentration of fungus in each well was 3 mg/mL dry weight of fungus. The plate was sealed with an air-permeable cover (AeraSeal) and incubated at 30°C for 48 hours without shaking. Each culture was then strained through a 40 µm cell strainer, and hyphae and associated bacteria were gently washed by washing the filter with MSNg. Filter-caught hyphae and associated bacteria were then suspended in 1 mL PBS, sonicated to separate cells from hyphae and from each other, and dilution-plated to count CFU (colony-forming units)/mL. Three separate experiments (different biological replicates, different days) were performed. Control *B. subtilis* cultures with no *M. fragilis* biomass or necromass were washed as above; no CFU were detected, indicating that the assay detects only hyphae-associated bacteria.

Biofilm Gene Expression on Chitosan and Chitin

Colloidal chitin was prepared as described previously, with slight modification (Saima et al., 2013). Briefly, 40 g of chitin powder (Sigma) was slowly added to 600 mL of 1 M HCl while stirring vigorously and heated to 30°C to dissolve (about 30 minutes). Dissolved chitin was precipitated by adding slowly to 1 L ice water (4 to 10°C), then the precipitate (colloidal chitin) was concentrated by filtering through a Grade 1 Whatman filter over a Buchner funnel with suction. Colloidal chitin was washed three times by resuspending the filter cake in 3L water and refiltering, until the pH of the suspension was 3.5. The final washed filter cake was resuspended in 150 mL distilled water and autoclaved to sterilize. An aliquot of the autoclaved solution was dried and weighed to

calculate dry weight of chitin per mL, then added to agar plates as described below (4 g dry weight chitin for 1 L chitin agar). Dissolved chitosan was prepared as described previously with slight modification (Shimosaka et al., 1995). Briefly, 10 g chitosan powder (Sigma) was added to a glass beaker with a stir bar, and wet with acetic acid. 400 mL distilled water was added slowly while stirring vigorously and heating to about 40°C, then 90 mL 1 M acetic acid was added to dissolve the powder. 1 M sodium acetate was added to raise pH to 5.0 (about 180 mL required). The solution was brought to 1 L with water and autoclaved to sterilize, then used to make agar plates as below (100 mL of 1% chitosan solution for 1 L chitosan agar). Petri plates with 0.1x LB agar (1 g/L tryptone, 0.5 g/L yeast extract, 0.5 g/L NaCl, 15 g/L agar), 0.1x LB agar with 0.4% (final concentration) colloidal chitin (Sigma), and 0.1x LB agar with 0.1% (final concentration) dissolved chitosan were prepared.

B. subtilis 3610 with a biofilm gene fluorescent reporter (*amyE::*P*tapA-YPet*) was grown for 2 hours in LB at 37°C shaking. One µL of this culture was spotted onto each agar plate (3 colonies per plate) and incubated for 24 hours at 30°C. Images of colonies were taken using a Zeiss Stereo Discovery.V8 dissecting stereomicroscope (Oberkochen, Germany) with 0.63x objective under white light illumination and YFP fluorescence. Average YFP fluorescence intensities of whole colonies were quantified in Fiji image analysis software (n=3 replicate colonies).

Biofilm Gene Induction by Fungal Exudates and Extracts

M.fragilis exudates were obtained by growing the fungus from spores (100 µL of 10^5 spores/mL spore stock into 25 mL MSNg) for 48 hours and filtering to obtain liquid

media conditioned by the organism. Extracts were obtained by crushing the filtered *M. fragilis* biomass in liquid nitrogen into a fine powder. Extract powder was added to wells at a concentration of 1% w/v. *B. subtilis* 3610 with a biofilm gene luminescent reporter (*amyE::*P*tapA-luxA*) was grown for 2.5 hours at 37°C shaking in LB broth, washed three times in MSNg, and added to a final density of OD_{600}=0.05 (2.5 x 10^7 cells/mL) into 300 µL of MSNg with or without fungal extracts or exudates in a 96-well culture plate. The plate was sealed (AeraSeal) and shaken at 300 rpm at 30°C. 100 µL of culture was transferred to a white-bottom 96-well plate and luminescence readings were taken on a luminescence plate reader. Readings were normalized by dividing luminescence per well by luminescence of an MSNg only (no extract, no exudate) control. Readings were further normalized to the number of bacteria in each well by dividing the luminescence reading by the CFU/mL count. Four biological replicates were conducted.

Decomposition of Fungal Necromass by *B. subtilis*

B. subtilis 3610 wild type and chitosanase mutant (*csn::erm*) were grown for 2.5 hours at 37°C shaking in LB broth and washed 5x in MSN. *B. subtilis* was added to 1 mL of MSN containing *M. fragilis* necromass (final concentration of 3 mg/mL) in wells of a 24-well plate to a final density of OD_{600} =0.05 (2.5 x 10^7 cells/mL). They were incubated at 30°C without shaking for 7 days. Dry weight of fungal biomass remaining in each well was calculated by filtering spent medium through a 0.45 µm filter and measuring dry weight, and dividing as a percentage of initial weight.

Critical Cell Number Assay

B. subtilis 3610 *epsA- tasA* biofilm gene knockout was grown for 2.5 hours at 37°C shaking in LB broth, washed 5x in MSN, diluted to OD_{600}=0.5 (2.5 x 10^8 cells/mL), and diluted appropriately and added to a 96-well plate in MSN medium (Table 3.1). Dilutions were plated and CFU counted to verify that cell number estimates were accurate. Fungal necromass was added to the wells in a 96-well plate at a final concentration of 4 mg/mL, making dead *M. fragilis* the sole carbon source for *B. subtilis*. The biofilm mutant strain was used to measure the effect of cell number only, independent of the effect of aggregation on *M. fragilis* hyphae (see Figures 2.7 and 2.8).

Plates were sealed (AeraSeal) and cultures were incubated on a shaker table for 10 days at 30°C. Wells with turbidity at the end of this period were scored as “wells with growth”, and those with clear supernatants were scored as “wells with no growth”. The predicted proportion of wells with growth was drawn from a Poisson distribution of lambda=2 or lambda=0.2, which estimates the number of wells that should have zero cells by chance if the original population had 2 cells or 0.2 cells on average per well respectively. A chi-squared test (one-tailed) was performed comparing observed versus expected growth versus no growth counts (Table 2.1). Bootstrap 95% CI for mean observed proportion of cells with growth were generated (100,000 iterations), and the observed mean and bootstrap 95% CI were used to produce an estimate of cell number required to initiate growth.

B. subtilis Aggregate Size on Iron-Coated Silica

B. subtilis 3610 and *eps-tasA* mutant strains, both constitutively expressing YPet fluorescent protein (*amyE::*P*spac*^{C}*-YPet*), were grown for 2.5 hours at 37°C shaking in LB broth, washed 3x in MSgg, diluted to OD_{600}=0.05 (2.5 x 10^7 cells/mL) and incubated with *M. fragilis* necromass (4 mg/mL final concentration) or iron-coated silica particles as an alternate surface for cells to attach (8 mg/mL final concentration) in MSgg (biofilm-inducing growth medium) for 7 hours without shaking at 30°C. To obtain hyphae-associated cell fraction, *B. subtilis*-with-necromass cultures were filtered through a 40 µm cell strainer and washed three times in MSN (minimal salts, no carbon). To obtain silica-associated cell fraction, silica was allowed to settle to the bottom of a centrifuge tube and particles were washed three times in MSN by carefully removing the supernatant. Hyphae- or silica-associated cell fraction was imaged under a DeltaVision epifluorescence microscope.

Thirty silica particles (as prepared above, see Figure 2.7) were selected at random from a field of view at 10x magnification, where bacterial cells could not be seen. The number of cells associated with each particle were then counted by obtaining micrographs at 40x magnification and counting cells manually.

^{13}C Stable Isotope Probing by Raman Microspectroscopy

M. fragilis spores were inoculated into MSN (minimal salts) medium with 2% ^{13}C-labeled glucose and grown overnight at 30°C without shaking (10 uL spore stock with 10^5 spores/mL into 50 uL final volume of MSN ^{13}C -glucose). The resultant *M. fragilis* hyphae were ^{13}C-labeled. This ^{13}C -labeled biomass was heat-killed (incubated at 70°C

for 1 hour) and washed 5x in MSN by filtering over a 40 μm cell strainer. *B. subtilis* 3610 cells were grown for 2.5 hours at 37°C shaking in LB broth, washed 5x in MSN, and diluted to OD_{600}=0.05. They were incubated in 1.7 mL microcentrifuge tubes for 48 hours at 30°C without shaking (to mimic the non-shaking conditions of later experiments conducted in microfluidics chips) in MSN with or without ^{13}C-labeled *M. fragilis* necromass. After incubation, *B. subtilis* cells were washed in Milli-Q water by centrifugation and spotted onto an aluminum slide. Thirty individual microbial cell spectra per treatment were acquired using a LabRAM HR800 Raman microscope (Horiba) equipped with a 532-nm neodymium-yttrium aluminum garnet laser and 300 grooves/mm diffraction grating. Spectra were acquired in the range of 400–3,200 cm^{-1} with the following acquisition parameters: 30 s acquisition time, 70% laser power, 10% ND filter, slit=150, hole=300 (resulting in resolution of about 1 μm).

"Percent ^{13}C" was calculated individually for each raw (not baselined, not normalized) cell spectrum as $(A_{966}/(A_{966} + A_{1003}))x100$, where A_{966} is the average intensity between 960 and 968 cm^{-1} minus the average intensity of the nearby 945 to 955 cm^{-1} baseline region (^{13}C phenylalanine peak) and A_{1003} is average intensity between 998 and 1005 cm^{-1} minus the 945 to 955 cm^{-1} baseline region (^{12}C phenylalanine peak).

For experiments comparing carbon uptake of necromass-associated clumps versus unattached cells over time, ^{13}C-labeled *M. fragilis* necromass was prepared as described above. *B. subtilis* 3610 cells expressing constitutive YFP fluorescence (P*spac*^{C}-YPet) were grown for 2.5 hours at 37°C shaking in LB broth, washed 5x in biofilm-inducing MSgg medium, diluted to OD_{600}=0.05, and incubated with ^{13}C-labeled

M. fragilis necromass in MSgg for 7 hours at 30°C to allow *B. subtilis* clusters to form on hyphae. Unattached bacteria were washed off of hyphae by filtering hyphae through 40 µm cell strainer, washing 5x with MSN medium, and resuspending in MSN medium. These hyphae were then inoculated into three replicate microfluidics devices, sealed, and incubated at 30°C. Hyphae-associated clusters and the few non-hyphae-associated cells ("planktonic" cells) that remain after washing were measured for ^{13}C uptake over time by Raman microspectroscopy. Chambers were sealed with tape and incubated between measurements at 30°C in 50 mL centrifuge tubes with wet absorbent paper in order to maintain humidity over time. Raman cell spectra were acquired as above, except laser power was increased to 100%, and ND filter increased to 50%. Moreover, for each cell spectrum acquired, a "background" spectrum in the same z-plane but approximately 10-20 µm away in the x-y plane was acquired as a measure of the Raman spectrum of the microfluidics device itself.

Spectra were baselined and normalized using scattr software (Berry et al., 2015). Briefly, each spectrum was fitted with a 6^{th} degree polynomial function then normalized to total spectral intensity. All spectra collected from a single microcosm were normalized together. Then, the matching background spectrum was subtracted from each cell spectrum to obtain a background-subtracted cell spectrum for each cell. "Percent ^{13}C" for each background-subtracted cell spectrum was calculated as described above.

Results

B. subtilis 3610 attachment to *M. fragilis* hyphae

To determine whether *B. subtilis* attaches to *M. fragilis* hyphae, and whether biofilm genes facilitate this attachment, *B. subtilis* 3610 strains (wild type and *eps-tasA* biofilm gene knockout) were co-cultured with *M. fragilis* in liquid MSNg medium, where the fungus was either alive or heat killed. MSNg medium was chosen because it was previously shown to not induce biofilm gene expression in *B. subtilis* by itself (Beauregard et al., 2013), making it a suitable medium for testing the effect of added compounds on *B. subtilis* biofilm formation but allowing minimal growth without stimulating starvation responses such as sporulation.

We found that neither wild-type *B. subtilis* nor the biofilm mutant attached to live *M. fragilis* hyphae (Fig. 2.1; CFU/mL of hyphae-associated bacterial fraction below level of assay detection). Both wild-type *B. subtilis* and the biofilm mutant attached to dead, heat-killed fungal hyphae (Fig. 2.1). Wild-type *B. subtilis* attached to dead fungi in larger numbers than the biofilm mutant (Fig 2.1, $p<0.001$, Student's t-test two-tailed, n=4 biological replicates per strain).

When incubated with dead *M. fragilis* hyphae, wild-type *B. subtilis* forms clusters on the hyphae. Moreover, by using a biofilm gene reporter (*amyE::PtapA-YPet*), we observed that biofilm genes are expressed within a subset of cells within these *Mucor*-associated aggregates (Fig. 2.2).

Fungal cell wall polymers, and *M. fragilis* extracts and exudates induce biofilm gene expression in B. subtilis

To determine whether components of fungal cell walls induce biofilm gene expression in *B. subtilis*, a *B. subtilis* with a biofilm gene fluorescent reporter (*amyE::*P*tapA-YPet*) was grown on 0.1x LB agar alone or with chitosan or chitin, and whole-colony fluorescence was measured. Colonies grown on chitosan- or chitin-containing media were much more fluorescent than colonies grown on control media, indicating high amounts of biofilm gene expression on these media (Fig 2.3, $p<0.001$, Student's t-test two-tailed, n=3 biological replicates per medium). The wrinkling morphology of colonies grown on chitosan is also a clear indicator of biofilm matrix production (Fig 2.3).

Having determined that chitin and chitosan induce biofilm gene expression in *B. subtilis*, we asked whether extracts and exudates from *M. fragilis* specifically induce biofilm gene expression. *B. subtilis* with a biofilm gene luminescent reporter (*amyE*::P*tapA-luxA*) was incubated with *M. fragilis* extracts and exudates. A luminescent gene reporter was used instead of a fluorescent gene reporter in this assay in order to increase the signal of the bacterial gene reporter over the background signal of the dead hyphae, which are autofluorescent, but not luminescent. *B. subtilis* cultures grown in *M. fragilis* extracts and in *M. fragilis* exudates were more luminescent than cultures grown in the base medium without extracts or exudates (Fig. 2.4, $p<0.001$, Student's t-test two-tailed, n=4 biological replicates per medium).

B. subtilis decomposes *M. fragilis* necromass, dependent on the chitosanase (*csn*) gene.

B. subtilis 3610 wild type and chitosanase mutant (*csn::erm*) were grown with *M. fragilis* necromass as their sole carbon source. Macroscopic observations of culture wells show large clumps of necromass remaining when *M. fragilis* is incubated alone, and the reduction or disappearance of these necromass clumps when they are incubated with either strain of *B. subtilis* (Fig. 2.5). When incubated with *B. subtilis csn, M. fragilis* necromass is reduced to 70.0% of its original mass (bootstrap 95% CI [53.45%, 85.93%], n=3 biological replicates per medium), indicating that the chitosanase mutant is able to decompose the fungal necromass. When incubated with wild-type *B. subtilis, M. fragilis* necromass is reduced to 28.4% of its original mass (bootstrap 95% CI [12.6%, 44.2%], n=3 biological replicates per medium), indicating that wild-type *B. subtilis* decomposed significantly more necromass than the chitosanase mutant (Fig. 2.5, $p<0.001$, Student's t-test two-tailed, n=3 biological replicates per medium).

B. subtilis 3610 cells can grow on dead *M. fragilis* as a sole carbon source, but single cells cannot initiate growth.

To estimate whether single *B. subtilis* cells can initiate growth on *M. fragilis* necromass, *B. subtilis* biofilm gene knockout mutant was cultured with *M. fragilis* necromass as its sole carbon source. *B. subtilis* was added to *M. fragilis* in ten-fold dilutions. Biofilm gene knockout strain was used to measure effect of cell number (i.e. the initial inoculum size) on decomposition of necromass, independent of effect of aggregation on *M. fragilis* hyphae (see Figures 2.7 and 2.8). Cultures were incubated

for 10 days at 30°C shaking; in these favorable growth conditions, any cultures that would grow at all would grow to stationary phase within this period of time.

Wells with turbidity at the end of this period were scored as “wells with growth”, and those with clear supernatants were scored as “wells with no growth”. The predicted proportion of wells with growth was drawn from a Poisson distribution of lambda=2 or lambda=0.2, which estimates the number of wells that should have zero cells by chance if the original population had 2 cells or 0.2 cells on average per well respectively. A chi-squared test (one-tailed) was performed comparing observed versus expected growth versus no growth counts (Table 2.1). The observed number of wells with growth is equal to the expected number for wells with initial inoculum sizes of 20 cells on average or more, indicating that *B. subtilis* can initiate growth on dead *Mucor* when inoculated as tens of cells or more. However, the observed number of wells with growth is significantly lower than expected if one cell was sufficient to initiate growth. The null hypothesis – that one cell is sufficient to initiate growth – is therefore rejected (Table 2.1).

Estimate of number of *B. subtilis* cells needed to initiate growth on *M. fragilis* as a sole carbon source.

We assumed that the number of cells in the previously described experiment were distributed into wells according to a Poisson distribution. For the case where the average number of cells in each well was 2, the distribution of cells in each well is modeled by a Poisson distribution where lambda (i.e. the mean number of countable events, in this case, cells) equals 2 (Fig. 2.6). The area under this curve (cumulative Poisson distribution, Fig. 2.6) at any integer value represents the number of wells in

which growth is expected if that number of cells *or greater* is able to initiate growth. The observed proportion of wells with growth (0.325) is very close to the proportion expected if 3 or more cells can initiate growth (0.323). To obtain an estimate of variance around this observed mean estimate (0.325), we calculated generated a bootstrap 95% CI of the observed mean, which was found to be [0.175, 0.325]. This CI is graphed in Fig. 2.6, and corresponds to an estimate of the mean number of cells required to initiate growth as between 2 and 4.

Effect of *eps-tasA* genes on formation of stable aggregates and attachment to substrates.

To test whether biofilm genes enable *B. subtilis* cells to attach to surfaces and to each other, we incubated *B. subtilis* 3610 wild-type and biofilm mutant strains (*epsA-tasA* biofilm gene knockout) with *M. fragilis* necromass or iron-coated silica particles in MSgg (a biofilm-inducing growth medium). Iron-coated silica was chosen as a substrate because previous work has shown that *B. subtilis* cells will stick to iron-coated silica due to charge interactions (Ams et al., 2004), allowing us to assess the importance of charge interactions in initial attachment of *B. subtilis* cells to substrates relative to the importance of biofilm matrix production. Wild-type cells formed aggregates on both *M. fragilis* necromass and on iron-coated silica particles that held together even after the fungi and particles were gently washed to remove unattached cells (Fig. 2.7). Biofilm mutant cells, however, remained attached to the substrates only as singletons or doublets.

We quantified the number of cells attached to each silica particle by microscopy. We randomly selected particles from a field of view, then magnified to count the number

of cells on each particle (Fig. 2.8). Most particles (about 70%) had no cells associated with them, regardless of strain. However, wild-type *B. subtilis* cells that attached to particles stayed attached in clusters of 9 or more cells, whereas biofilm gene mutants stayed attached only as singletons or doublets. More wild-type cells remained attached to each particle after washing than *eps-tasA* cells (Tukey HSD p-value <0.0001, n=30 particles), indicating that biofilm genes enable cells to remain aggregated even after washing.

Raman microspectroscopy reveals uptake of ^{13}C-labeled *M. fragilis* by *B. subtilis* cells.

To determine whether we could use Raman spectroscopy to detect the uptake of ^{13}C-labeled *M. fragilis* hyphae by *B. subtilis* cells, we incubated ^{13}C-labeled *M. fragilis* with *B. subtilis* cells and collected Raman cell spectra. *M. fragilis* spores were grown in media containing ^{13}C-labeled glucose as their sole carbon source; the resultant *M. fragilis* hyphae were fully ^{13}C-labeled. This ^{13}C-labeled biomass was heat-killed and washed thoroughly. *B. subtilis* 3610 cells were incubated with this ^{13}C -labeled *Mucor* necromass. The Raman spectra of individual *B. subtilis* cells were measured by Raman microspectroscopy. Averages of 30 individual cell spectra are shown (Fig. 2.9). Shift of the dominant phenylalanine peak from 1003 to 966 wavenumber indicates incorporation of ^{13}C into *B. subtilis* phenylalanine molecules and therefore into its overall biomass (Fig. 2.9).

Both necromass-associated clusters and non-associated planktonic cells take up ^{13}C from ^{13}C-labeled necromass over time, with no significant difference between them.

We tested whether clusters of *B. subtilis* cells on *M. fragilis* hyphae take up carbon from the hyphae earlier than planktonic, non-attached cells. ^{13}C-labeled *M.*

fragilis hyphae were heat-killed, washed, and incubated with *B. subtilis* 3610 cells in rich, biofilm-inducing MSgg medium for 7 hours to allow *B. subtilis* clusters to form on hyphae (Fig. 2.10 bottom right panel). The -7 hour measurements represent *B. subtilis* cells immediately after they were mixed with dead *Mucor* biomass as planktonic cells and before they had time to form clusters or take up appreciable ^{13}C from *Mucor.* Unattached bacteria were then washed off of the hyphae, and the washed hyphae were then inoculated into microfluidics devices. Hyphae-associated clusters and the few non-hyphae-associated cells ("planktonic" cells) that remained after washing were measured for ^{13}C uptake over time by Raman microspectroscopy.

Using this technique, we asked whether clusters of *B. subtilis* cells on *M. fragilis* hyphae take up carbon from the hyphae earlier than planktonic, non-attached cells. The null hypothesis was that the *B. subtilis* clusters take up the same amount of ^{13}C over all time points as planktonic cells. Our results failed to reject the null hypothesis. Our ANOVA model including category (clusters versus planktonic), time point (0, 12, 24, or 48 hours) and biological replicate (n=3 replicates) detects time point and biological replicate as statistically significant factors ($p = 6.505 \times 10^{-9}$ and 4.947×10^{-4} respectively), but category is not found to be significant (p=0.9321).

After 48 hours, cells were significantly more enriched in ^{13}C than at 0 hours, for both clusters and planktonic cells (one-way ANOVA for all categories F-statistic 4.98, p-value 2.85×10^{-5}; Tukey-Kramer p-value <0.01 comparing t0 to t48 for both clusters and planktonic cells). However, there were no significant differences in ^{13}C enrichment between clusters versus planktonic cells at any time point (Fig. 2.11, Tukey-Kramer p-

value > 0.05 for all pair-wise comparisons of clusters versus planktonic samples at each time point).

Discussion

In this study, we found that *B. subtilis* cells form biofilms on fungal necromass, and that these biofilms are important to form and maintain aggregates of nine cells or more. We found that single bacterial cells cannot initiate decomposition of fungal necromass, and estimated that the critical number of bacteria required to initiate decomposition is three. We therefore reasoned that biofilm genes enable the formation and maintenance of aggregates with a sufficiently large number of cells (three or more) to initiate decomposition of fungal necromass. We hypothesized that these aggregates may initiate decomposition more quickly than would single cells. We tested this hypothesis by measuring uptake of isotopically-labeled fungal necromass using Raman microspectroscopy. Though we found that both aggregates and single cells took up carbon from fungal necromass over time, we found no difference in uptake dynamics between them.

B. subtilis 3610 was previously shown to form biofilms on plant roots, and that plant cell wall components, extracts, and exudates induce biofilm gene expression in plant roots (Beauregard et al., 2013). We show that *B. subtilis* 3610 responds similarly to fungal hyphae, cell wall components, extracts, and exudates. Fungi – and particularly fungal necromass – may be an important ecological niche for *B. subtilis* in soils. *B. subtilis* strains have been found to exist mainly as spores in soils *except* when in the presence of dead fungal hyphae, where they were found to grow vegetatively

(Siala & Gray, 1974). Worrich and colleagues (2017) found that *B. subtilis* cells draw water and nutrients from fungal hyphae in dry, oligotrophic environments, and that *B. subtilis* spores that come into contact with fungal hyphae are more likely to germinate than spores far from fungal hyphae. Moreover, *B. subtilis* is a prodigious producer of extracellular polysaccharide-degrading enzymes, with dozens of these enzymes encoded in the *B. subtilis* 3610 genome (Priest, 1977). Some of these enzymes are specific to substrates found in fungi, such as the chitosanase enzyme which breaks down chitosan – a polysaccharide which is not found in plants, but is a component of some fungal cell walls and particularly abundant in the cell walls of zygomycetes like *Mucor fragilis* (Peter, 2005). Interestingly, we found that *B. subtilis* did not form aggregates on live *M. fragilis* hyphae, but only on dead *M. fragilis* hyphae. This suggests the presence of anti-bacterial or anti-biofilm agent on or in the live hyphae. Alternatively, dead hyphae may be "stickier" than live hyphae, due to different charge properties or surface chemistry. Our macroscopic examination of dead hyphae showed that they clumped more to each other than did live hyphae, suggesting a change in surface properties after heat-killing.

Previous work has shown that surface properties and charge interactions are important for *B. subtilis* initial attachment to substrates. *B. subtilis* cells will stick to iron-coated silica particles due to charge interactions (Ams et al., 2004). We show that both wild-type and biofilm gene mutants of *B. subtilis* have the same probability of attaching to iron-coated silica particles. However, wild type *B. subtilis* cells that attach to particles will stay attached in clusters of 9 or more cells, whereas biofilm gene mutants will stay attached only as singletons or doublets. This suggests that charge interactions are

more important than biofilm matrix in the initial attachment of cells to particles, but biofilm matrix plays an important role in attaching cells to one another. That is, in *B. subtilis,* biofilm genes may be more important in enabling cells to stick to each other than in enabling cells to stick to substrates. Attachment and clustering habits are similar between *B. subtilis* interactions with iron-coated silica and interactions with dead *M. fragilis* biomass, suggesting a similar process of initial attachment due to charge and subsequent aggregation due to biofilm genes.

We found that a critical number of cells are required for extracellular decomposition of fungal necromass, corroborating previous work that shows the importance of cell number for extracellular decomposition of other substrates (Rosenberg et al., 1977; Koschwanez et al., 2011). Unlike these previous studies, which examined the role of critical number in decomposing a single, pure substrate, we examined decomposition of a complex natural necromass containing many different components. Because multiple EEs are required for the decomposition of the multiple substrates found in natural biomass and necromass (da Costa et al., 2018), the loss of any one enzyme does not completely block necromass decomposition, since other enzymes can still facilitate decomposition of other substrates in the necromass (Dashtban et al., 2010). We found that a *B. subtilis* 3610 strain lacking the chitosanase gene was not able to degrade as much fungal necromass as the wild-type strain, but was still able to decompose a significant amount of necromass despite lacking this one enzyme (Fig. 2.5). A number of studies have concluded that cells that do not produce extracellular enzymes are “cheaters”, since they can benefit from the decomposition products made available by extracellular enzyme producers without bearing the

metabolic costs of production. However, many of these studies are specifically set up to measure the metabolic costs and benefits of degrading a single substrate in a condition where that one substrate is the only available nutrient source (Allison et al., 2014; Drescher et al., 2014). Our study suggests that in a more naturalistic case where multiple substrates tend to co-occur (such as in almost any necromass), organisms lacking any one EE gene or even a set of EEs needed to degrade one specific substrate can still participate in decomposition.

Based on our results, we had hypothesized that by increasing the probability that *B. subtilis* cells will aggregate on *M. fragilis* in clusters, biofilm-mediated aggregation increases the probability that *B. subtilis* will be able to initiate extracellular decomposition and take up nutrients from the dead biomass. However, this hypothesis was difficult to test directly. We opted to use Raman microspectrosopy to test the hypothesis because it is a non-destructive stable isotope probing method that allowed us to monitor nutrient uptake over time, and its high spatial resolution allowed us to measure single cells either attached to or not attached to *M. fragilis*.

Using this technique, we asked whether clusters of *B. subtilis* cells on *M. fragilis* hyphae take up carbon from the hyphae earlier than planktonic, non-attached cells. The null hypothesis was that the *B. subtilis* clusters take up the same amount of ^{13}C over all time points as planktonic cells. Our results failed to reject the null hypothesis. Our ANOVA model including category (clusters versus planktonic), time point (0, 12, 24, or 48 hours) and biological replicate (A, B, or C) detects time point and biological replicate as statistically significant factors ($p = 6.505 \times 10^{-9}$ and 4.947×10^{-4} respectively), but category is not found to be significant ($p=0.9321$). Cells at t48 were significantly more

enriched in ^{13}C than cells at t0, for both clusters and planktonic cells (one-way ANOVA for both categories and all time points F-statistic 4.98, p-value 2.85×10^{-5}; Tukey-Kramer p-value <0.01 comparing t0 to t48 for both clusters and planktonic cells).

The failure to reject the null hypothesis that clusters and planktonic cells took up equal amounts of ^{13}C from *M. fragilis* over time could be attributed to a number of different factors. Perhaps because the critical mass of cells required to initiate growth is so low that the total number of cells in our microfluidics microcosms – which numbered in the tens – was more than sufficient to initiate decomposition at an early timepoint and swamped the effect of local decomposition and uptake in clusters. The chambers we used were very small, containing about 2 µL of liquid, in order to facilitate visualization of cells throughout the microcosm, and to decrease the number of cells within each microcosm. This small volume, and the fact that there was no liquid flow through the microfluidics device, meant that the concentration of EEs could rise quickly within the microcosm even with a small number of cells. Alternatively, research by Grossart and colleagues suggests that cells attach and detach repeatedly from particles and aggregates, suggesting perhaps that in the time frame of our experiments, cells that were classified as “planktonic” may recently have detached from clusters, and vice versa, potentially obscuring differences between the classes (Grossart et al., 2007).

Our study highlights the potential of fungal biomass and necromass as substrates for stable isotope probing studies. Obtaining ^{13}C-labeled plant biomass is difficult and costly because plants must be grown in specialized chambers where they are provided with ^{13}C-labeled carbon dioxide in air. We found that ^{13}C-labeled fungal biomass is considerably less difficult and expensive because, as heterotrophs, fungi can

be cultured from spores in medium containing ^{13}C-labeled sugar. We obtained highly-labeled fungus using this approach, with phenylalanine peak shifts clearly visible in the Raman spectra of ^{13}C-labeled fungus.

Overall, our study underscores the importance of biofilm matrix formation in not only enabling cells to adhere to surfaces and substrates, but importantly, to adhere to each other. Future research is needed to understand the possible role of biofilm-mediated aggregation in other cooperative processes like detoxification of antibiotics, and the potential fitness advantages of aggregation in the soil environment (West et al., 2007).

Acknowledgments

We sincerely thank Fletcher Halliday (University of North Carolina at Chapel Hill) for the kind gift of the wild *Mucor fragilis* strain used in this study; Ethan Garner (Harvard University) for the *B. subtilis* codon-optimized fluorescent protein gene sequences used in strain construction; the Maddox Labs (Amy and Paul Maddox) for generous access to their DeltaVision instrument for light microscopy; Ilon Weinstein for assistance in replicating “critical cell number assay” experiments; Jamie Winshell (University of North Carolina at Chapel Hill) for assistance in strain construction; the Division of Microbial Ecology (University of Vienna) for use of their Zeiss AxioObserver epifluorescence microscope, and Horiba high resolution confocal Raman microspectroscopy system, and Markus Schmid for training and assistance on these instruments.

Figures

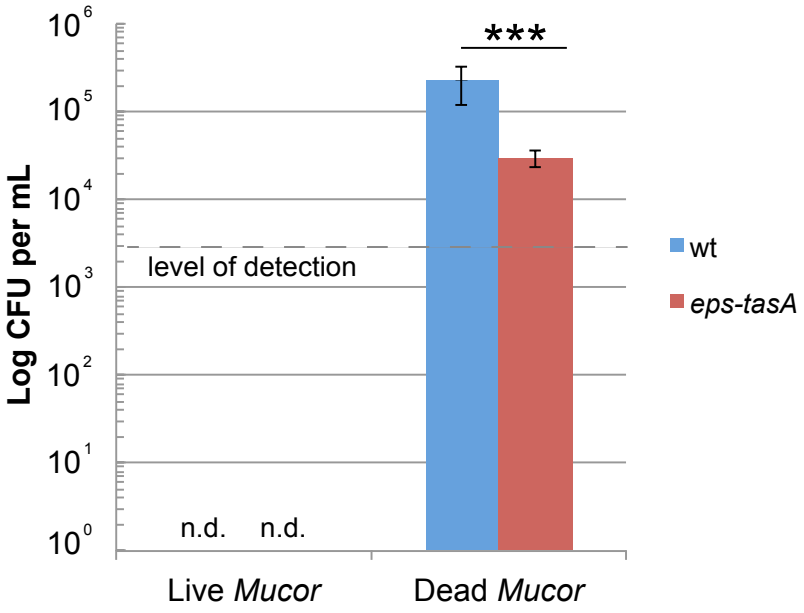

Figure 2.1: *Bacillus subtilis* 3610 attaches to dead but not live *Mucor fragilis* hyphae, dependent on eps-tasA biofilm genes. *Bacillus subtilis* 3610 strains (wild type and *epsA-tasA* biofilm gene knockout) were co-cultured with *Mucor fragilis,* where the fungus was either alive, or heat killed. *B. subtilis* and *M. fragilis* were incubated together in MSNg medium (minimal salts with free ammonium and 0.05% glycerol), and filtered through a 40 µm cell strainer to obtain only the hyphae-associated fraction of bacteria. Hyphae were sonicated to remove bacteria, and colony-forming units were counted. ***p<0.001, Student's t-test two-tailed, n=4 biological replicates per strain, error bars = 95% confidence intervals.

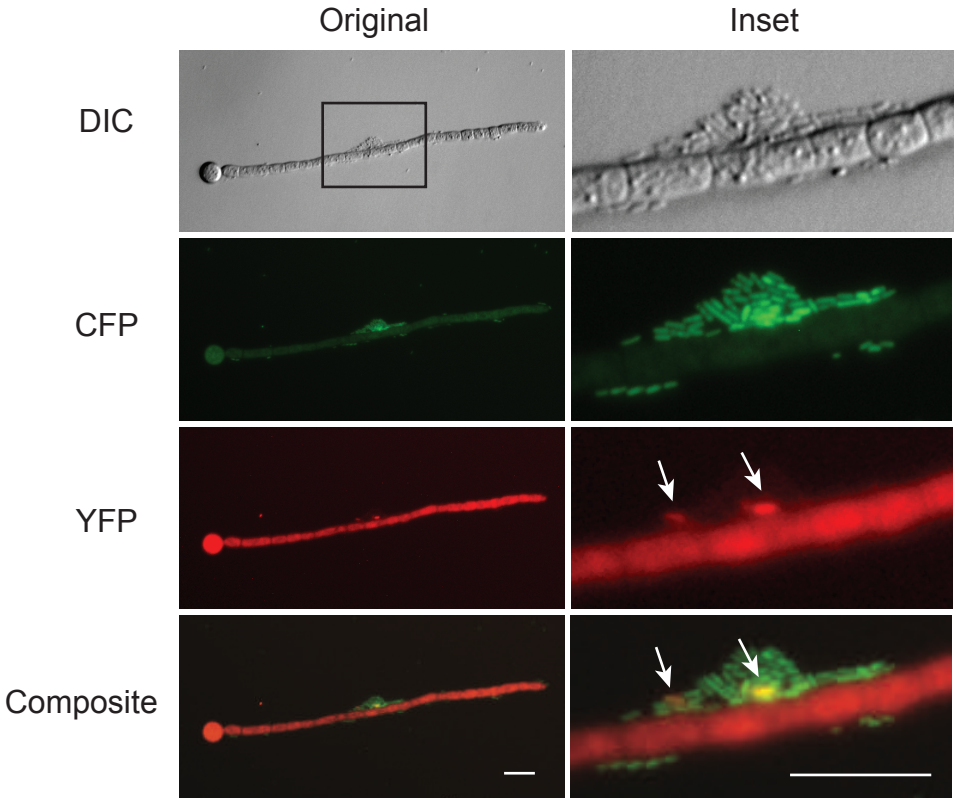

Figure 2.2: *B. subtilis* aggregates on dead *M. fragilis.* *B. subtilis* 3610 with constitutive fluorescent reporter (false-colored blue) and biofilm gene reporter (Pt*apA-YPet*, false-colored green, appearing cyan in picture due to color mixing with blue channel) was incubated for 48 hours at 30°C in MSNg medium with dead *M. fragilis*. Image acquired on widefield epifluorescence microscope with 40x oil objective lens. Overlay of CFP, YFP, and DIC channels. Green color of *M. fragilis* hypha due to autofluorescence in YFP channel. Note biofilm gene reporter expressed in small cluster of cells in center of clump near hypha.

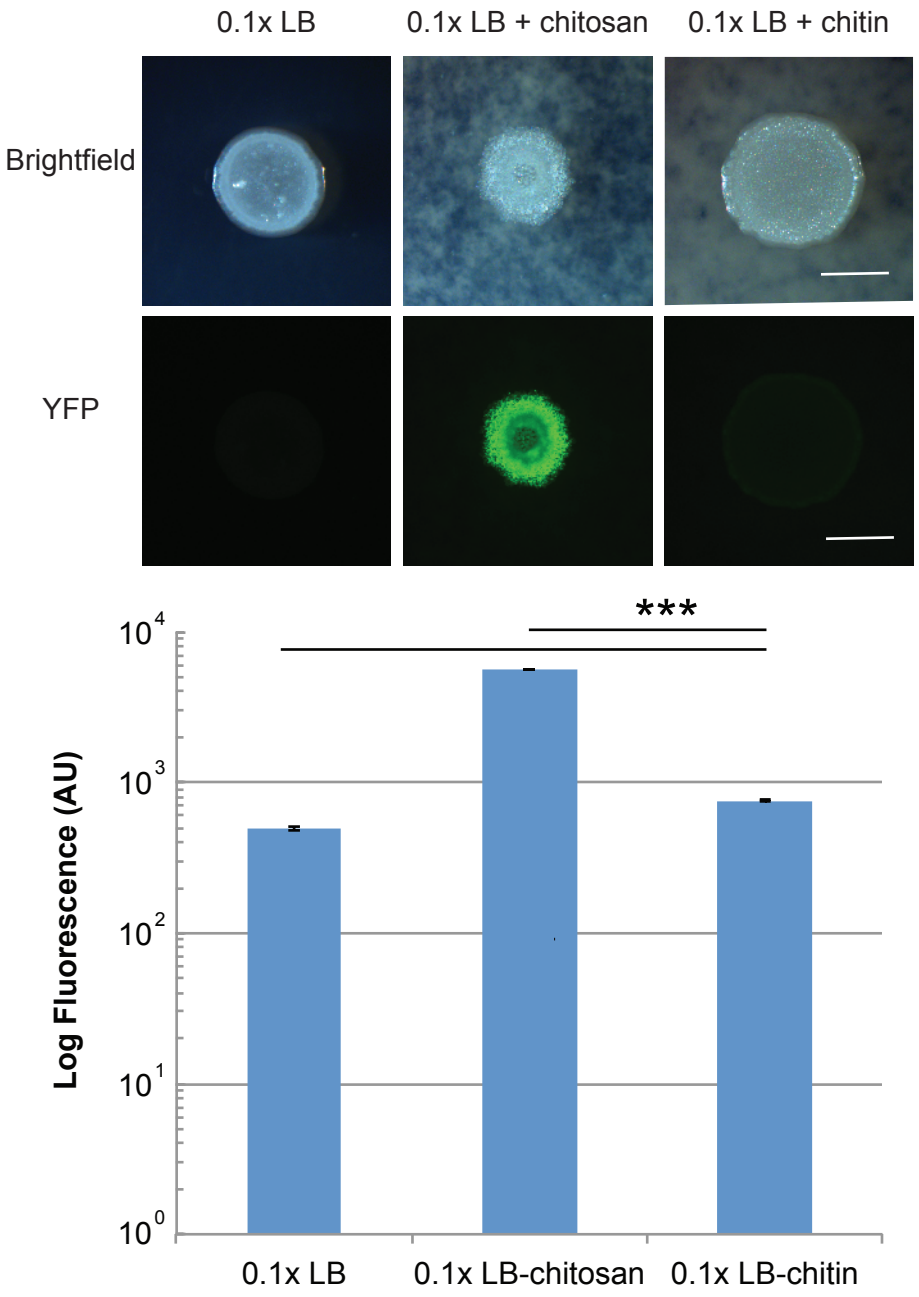

Figure 2.3: Fungal cell wall polymers induce biofilm gene expression in *B. subtilis* 3610. *B. subtilis* 3610 with a biofilm gene fluorescent reporter (*amyE*::P*tapA-YPet*) was grown for 24 hours on agar plates at 30°C. Fluorescence in the YFP channel was quantified for 3 replicate colonies. ***p<0.001, Student's t-test two-tailed, n=3 biological replicates per medium, error bars = 95% confidence intervals.

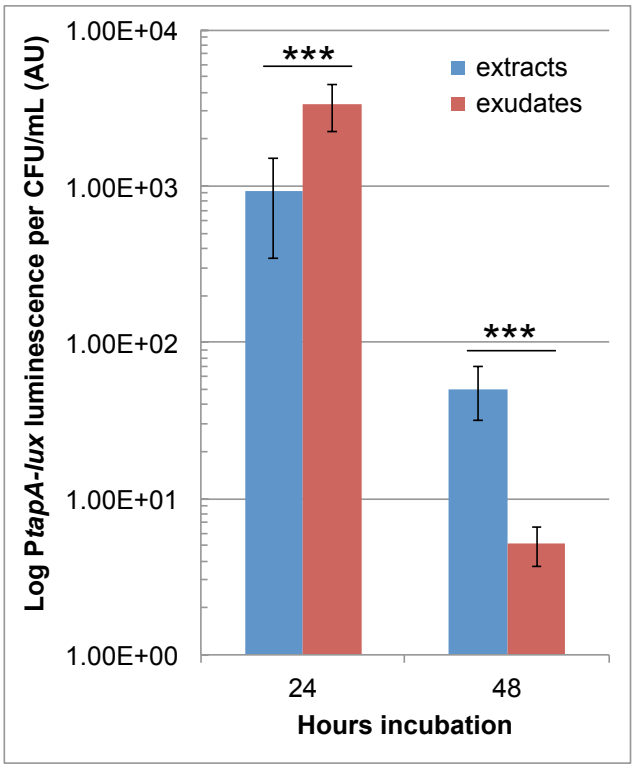

Figure 2.4: *M. fragilis* extracts and exudates induce biofilm gene expression in *B. subtilis* 3610. *B. subtilis* 3610 with a biofilm gene luminescent reporter (*amyE*::P*tapA-luxA*) was incubated in liquid MSNg medium with *M. fragilis* extracts and exudates. Luminescence readings were obtained by reading cell culture in a luminescence plate reader. Readings were normalized by dividing luminescence per well by luminescence of a MSNg only (no extract, no exudate) control. Readings were further normalized to the number of bacteria in each well by dividing the luminescence reading by the CFU/mL count. N=4 biological replicates per strain, error bars = 95% confidence intervals.

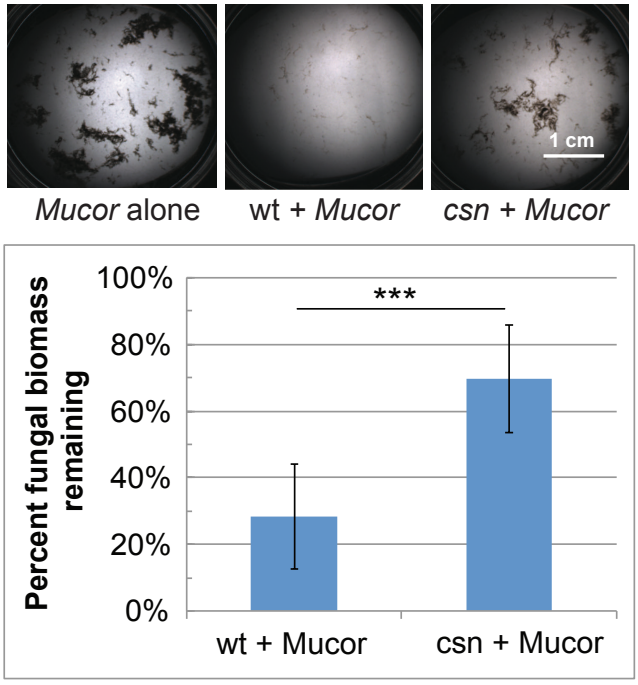

Figure 2.5: *B. subtilis* decomposes dead *M. fragilis*, dependent on the chitosanase (*csn*) gene. *B. subtilis* 3610 wild type and chitosanase mutant (*csn*::*erm*) were grown in 1 mL MSNg in 24 well plates at 30°C without shaking for 7 days with 6 mg/mL dead (heat-killed and washed) *M. fragilis* biomass. Dry weight of remaining fungal biomass calculated by filtering spent medium through 0.45 µm filter and measuring dry weight, and dividing as a percentage of initial weight. ***p<0.001, Student's t-test two-tailed, n=3 biological replicates per medium, error bars = 95% confidence intervals.

Average number of cells per well	Predicted percentage of wells with growth (if single cells can grow)	Total number of wells inoculated	Expected number of wells with growth	Observed number of wells with growth	Observed percentage of wells with growth	Chi-squared test statistic	p-value (based on chi-squared test)	Observed < Expected (p< 0.050)?
2000	100.00	8	8	8	100.0	0.000	1	No
200	100.00	8	8	8	100.0	0.000	1	No
20	100.00	8	8	8	100.0	0.000	1	No
2	86.47	40	35	13	32.5	99.587	<0.00001	Yes
0.2	18.13	80	15	6	7.5	6.090	0.0136	Yes

Table 2.1: *B. subtilis* 3610 cells can grow on dead *M. fragilis* as a sole carbon source, but single cells cannot initiate growth. *B. subtilis* 3610 *epsA-O::kan tasA::tet* biofilm gene knockout was added in ten-fold dilutions to a 96-well plate in MSN medium (minimal salts with free ammonium as a nitrogen source, with no carbon sources). Dead (heat-killed, washed) *M. fragilis* was added to the wells in a 96-well plate at a final concentration of 4 mg/mL fungal biomass, making dead *M. fragilis* the sole carbon source for *B. subtilis*. Biofilm gene knockout strain was used to measure effect of cell number only, independent of effect of aggregation on *M. fragilis* hyphae (see Figures 2.7 and 2.8). Cultures were incubated for 10 days at 30°C shaking; in these favorable growth conditions, any cultures that would grow at all would grow to stationary phase within this period of time. Wells with turbidity at the end of this period were scored as “wells with growth”, and those with clear supernatants were scored as “wells with no growth”. The predicted proportion of wells with growth was drawn from a Poisson distribution of lambda=2 or lambda=0.2, which estimates the number of wells that should have zero cells by chance if the original population had 2 cells or 0.2 cells on average per well respectively. A chi-squared test (one-tailed) was performed comparing observed versus expected growth versus no growth counts. The observed number of wells with growth is equal to the expected for wells with starting inocula of 20 cells on average or more, indicating that *B. subtilis* can initiate growth on dead *Mucor* when inoculated as tens of cells or more. However, the observed number of wells with growth is significantly lower than expected if one cell was sufficient to initiate growth.

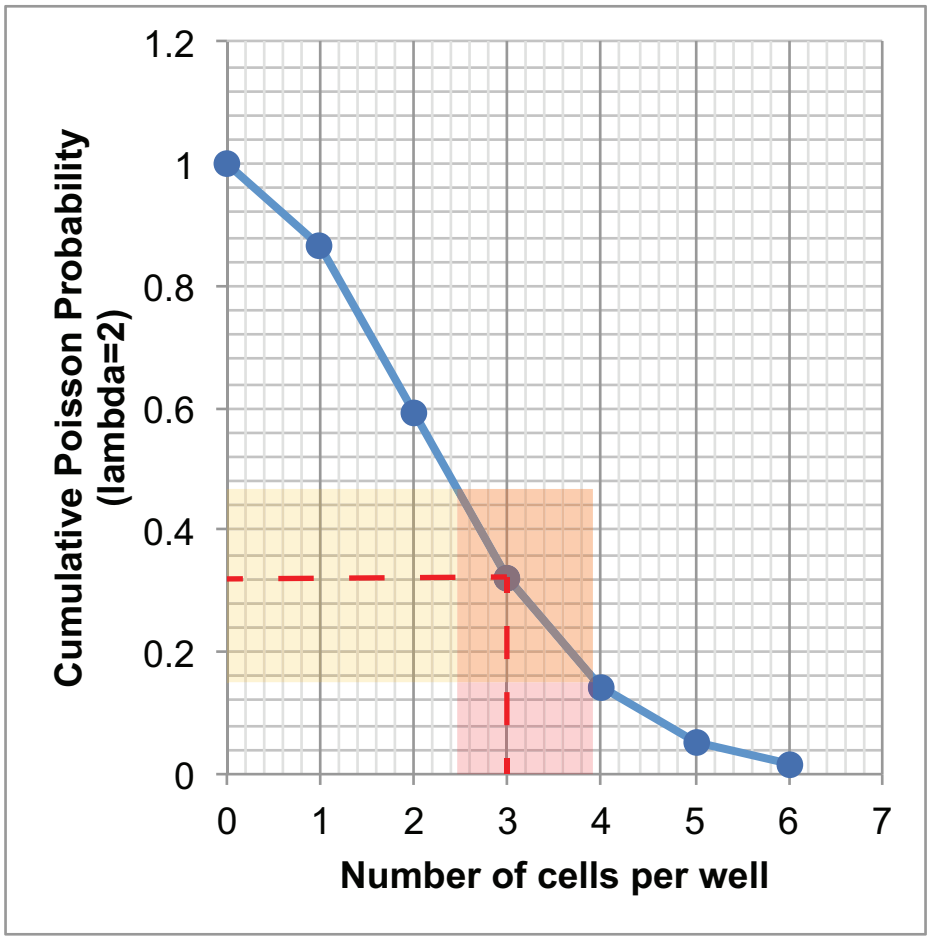

Figure 2.6: Number of *B. subtilis* cells needed to initiate growth on *M. fragilis* as a sole carbon source is estimated as greater than one. Blue dots and trace models cumulative Poisson distribution of lambda = 2, i.e. the area under the curve of the lambda=2 Poisson distribution. This value represents number of wells in which growth is expected if that number of cells *or greater* is able to initiate growth. Horizontal red dashed trace indicates the observed proportion of wells with growth (0.325) when wells were inoculated with n=2 cells on average. Reading from the graph (vertical red trace), this proportion of wells is very close to the proportion expected if 3 or more cells can initiate growth. Shaded yellow area indicates bootstrap 95% CI for mean value of proportion of wells with growth. This CI corresponds to an estimate of between 2 and 4 cells expected to initiate growth (red shaded area).

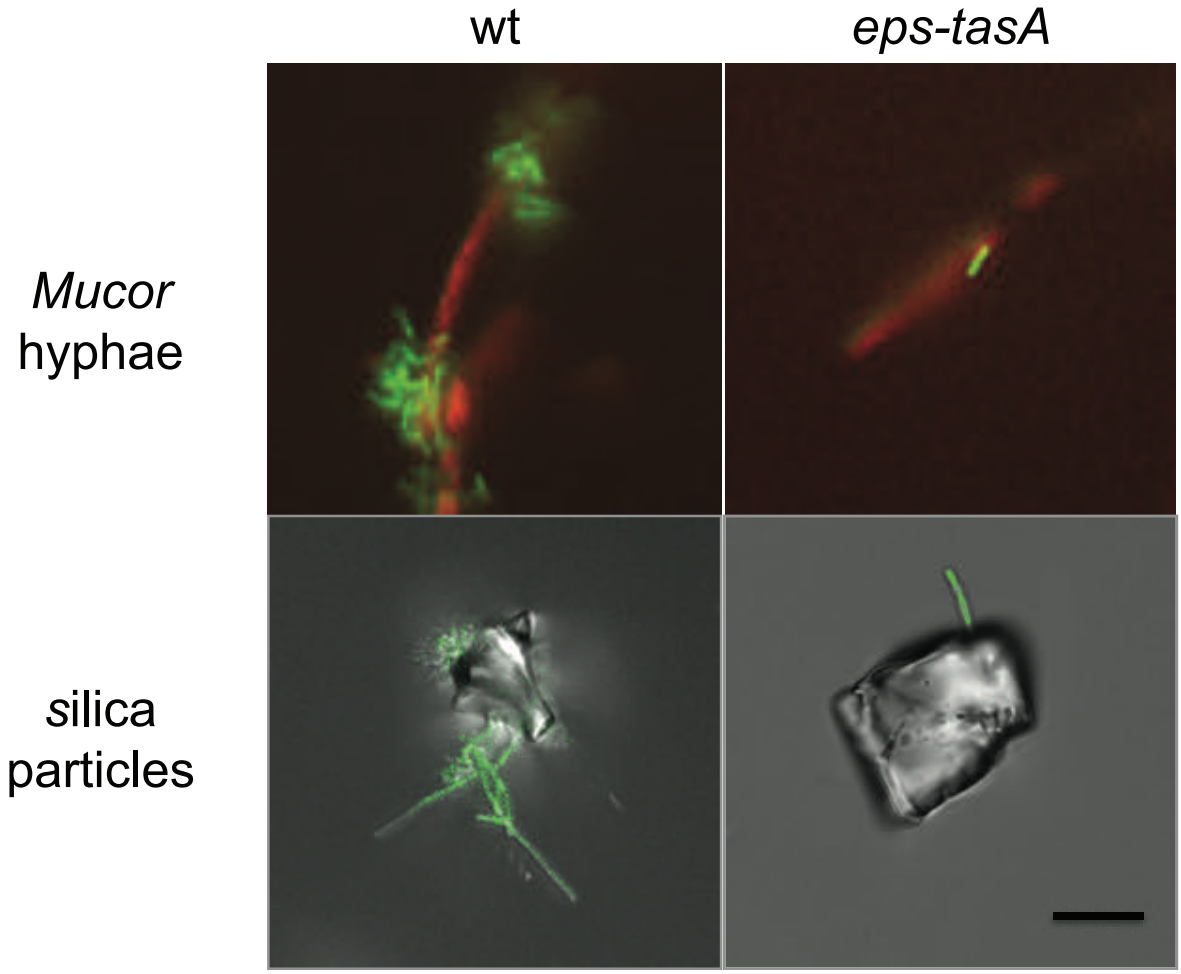

Figure 2.7: *B. subtilis* wt forms clusters on both dead *Mucor* hyphae and positively-charged silica particles that remain intact even after washing, whereas e*ps-tasA* cells stay attached only as singletons or doublets. *B. subtilis* 3610 and *eps-tasA* mutant strains, both constitutively expressing YPet fluorescent protein (P*spacC-YPet*), were incubated with dead *M. fragilis* or iron-coated silica particles in MSgg (biofilm-inducing growth medium) for 7 hours without shaking at 30°C. To obtain hyphae-associated cell fraction, *B. subtilis*-dead *Mucor* cultures were filtered through a 40 µm cell strainer and washed three times in MSN (minimal salts, no carbon). To obtain silica-associated cell fraction, silica was allowed to settle to the bottom of a centrifuge tube and particles were washed three times in MSN by carefully removing the supernatant. Hyphae- or silica-associated cell fraction was imaged under a DeltaVision epifluorescence microscope and 20 µm-thick z-stacks flattened into maximum intensity projections. *Mucor* hyphae are autofluorescent in RFP channel (red), and silica particles are visible under DIC channel (gray). *B. subtilis* cells are YFP fluorescent (green). Scale bar = 10 µm.

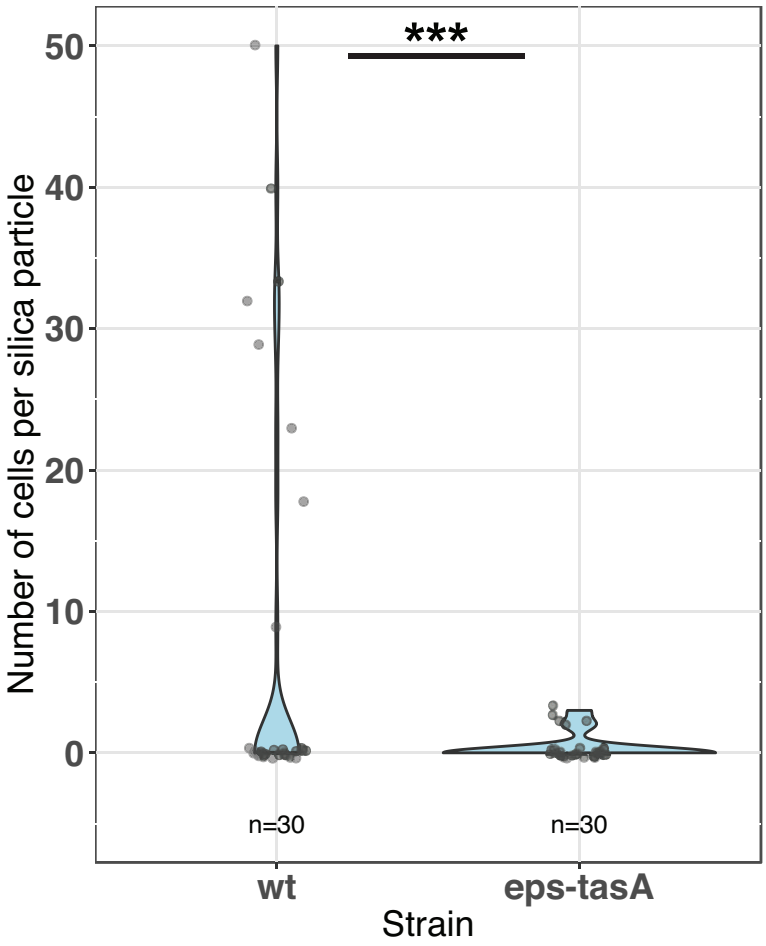

Figure 2.8: Number of cells per silica particle. Thirty silica particles (as prepared above, see Figure 2.7) were selected at random from a field of view at 10x magnification, where bacterial cells could not be seen. The number of cells associated with each particle were then counted by obtaining micrographs at 40x magnification and counting cells manually. Silica particles had more wild type cells per particle than *eps-tasA* cells (Tukey HSD p-value <0.0001).

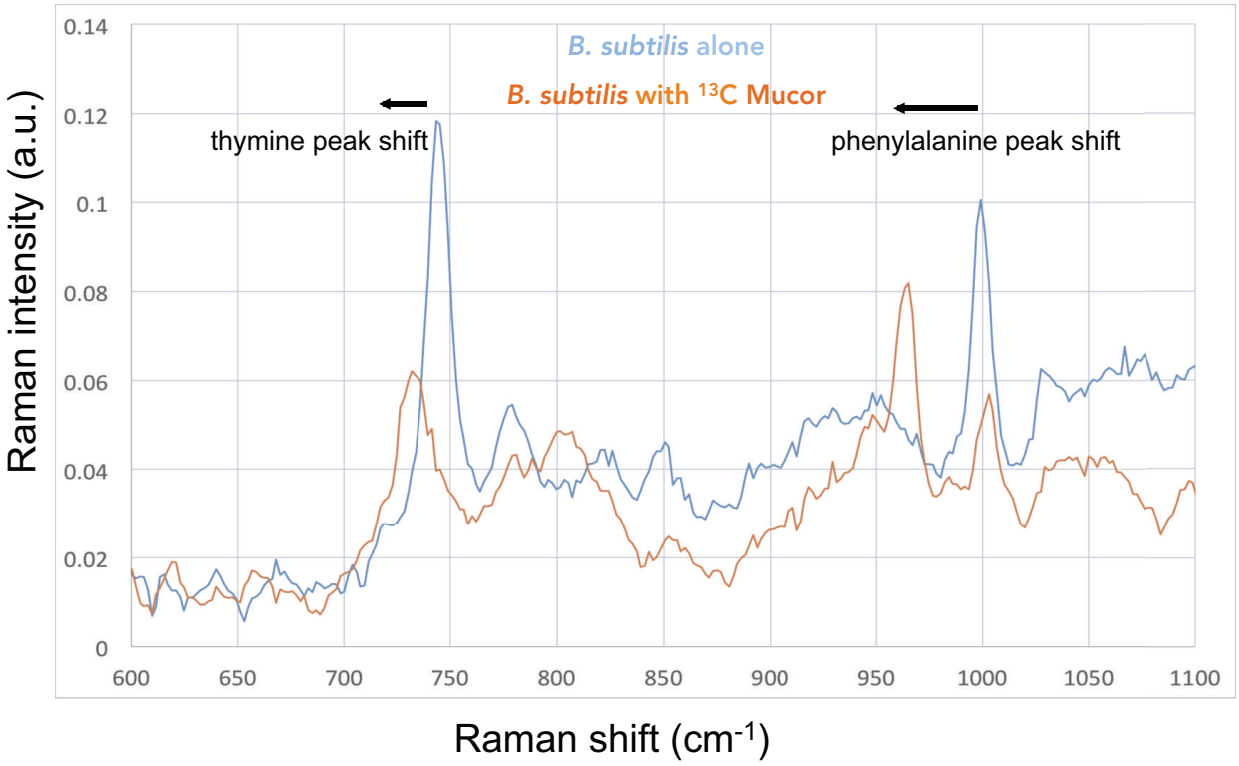

Figure 2.9: Raman microspectroscopy reveals uptake of ^{13}C-labeled *M. fragilis* by *B. subtilis* cells. *M. fragilis* spores were inoculated into MSN (minimal salts) medium with 2% ^{13}C-labeled glucose and grown overnight at 30°C without shaking. The resultant *M. fragilis* hyphae were ^{13}C-labeled. This ^{13}C-labeled biomass was heat-killed and washed multiple times in MSN. *B. subtilis* 3610 cells were incubated for 48 hours at 30°C without shaking in MSN (minimal salts) with or without ^{13}C-labeled dead *Mucor* biomass. *B. subtilis* cells were spotted onto an aluminum slide and cell spectra were measured by Raman microspectroscopy. Averages of 30 individual cell spectra are shown. Shift of dominant phenylalanine peak from 1003 to 966 wavenumber indicates incorporation of ^{13}C into *B. subtilis* phenylalanine molecules and therefore into its overall biomass.

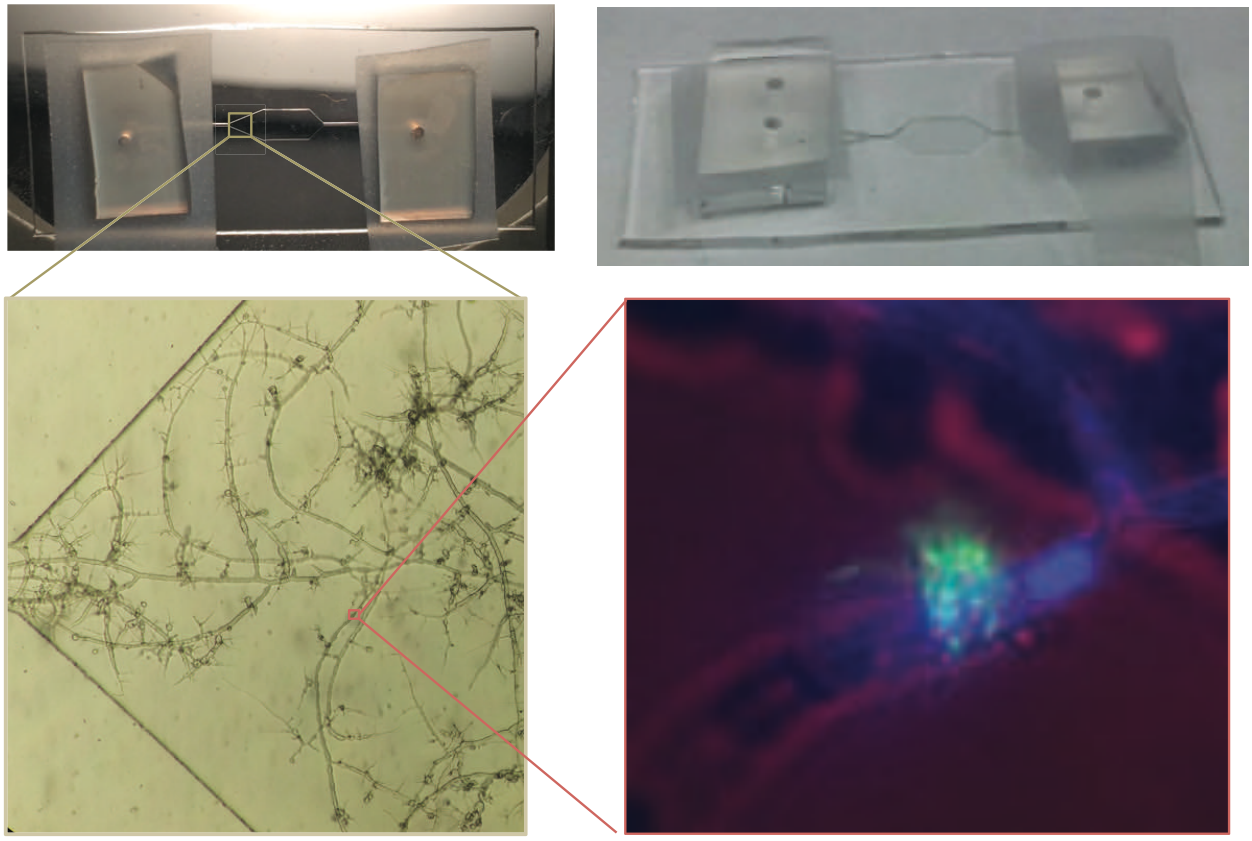

Figure 2.10: Microfluidic chambers allow growth, visualization, and non-destructive dynamic stable isotope probing of *B. subtilis* cells over time. ^{13}C-labeled *M. fragilis* is heat-killed, washed, and incubated with *B. subtilis* 3610 cells expressing constitutive YFP fluorescence (P*spacC*-YPet) at 30°C in rich, biofilm-inducing MSgg medium for 7 hours to allow *B. subtilis* clusters to form on hyphae (bottom right panel). Hyphae and hyphae-associated bacteria are then washed of unattached bacteria by filtering through 40 µm cell strainer and resuspending in MSN medium (minimal salts, no added carbon). These hyphae are then inoculated into microfluidics devices, sealed, and incubated at 30°C. Hyphae-associated clusters and the few non-hyphae-associated cells ("planktonic" cells) that remain after washing are measured for ^{13}C uptake over time by Raman microspectroscopy.

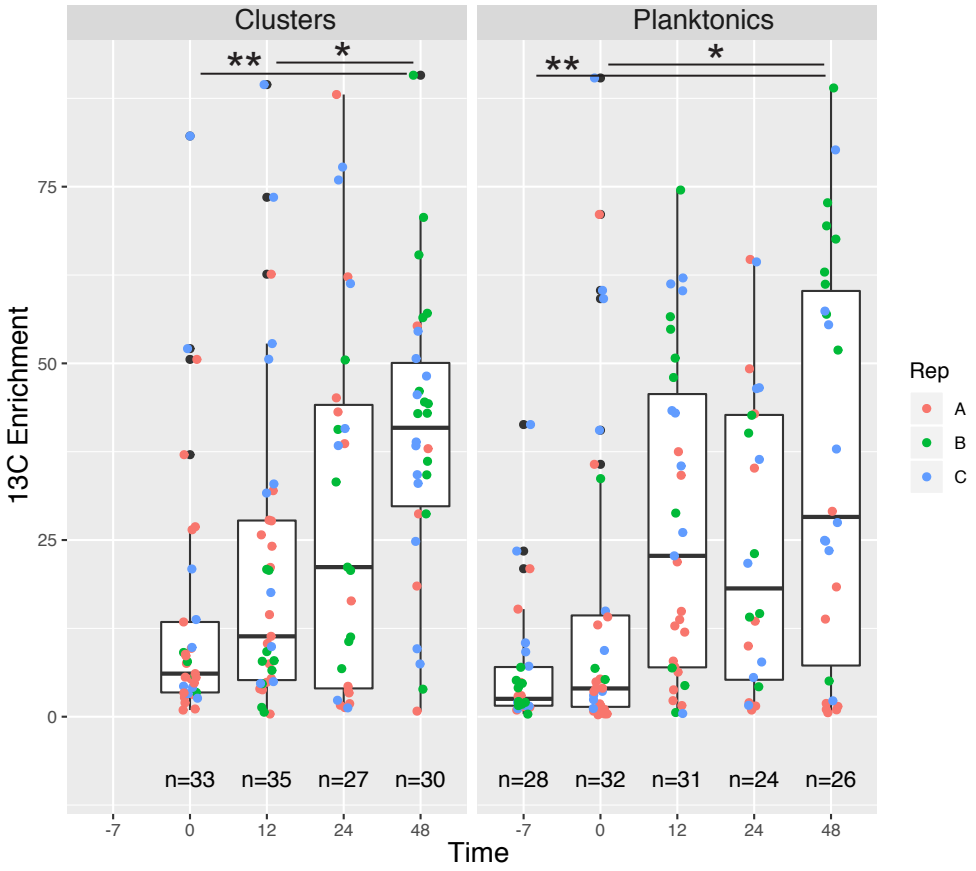

Figure 2.11: Both hyphae-associated clusters and non-attached planktonic cells take up ^{13}C from ^{13}C-labeled *M. fragilis* over time, with no significant difference between them. "^{13}C enrichment" is calculated individually for each background subtracted cell spectrum as $(A_{966}/(A_{966} + A_{1003}))x100$, where A_{966} is peak height at 966 cm^{-1} (^{13}C phenylalanine peak) and H_{1003} is peak height at 1003 cm^{-1} (^{12}C phenylalanine peak). "Time -7" measurements represent *B. subtilis* cells immediately after they were mixed with dead *Mucor* biomass as planktonic cells and before they had time to form clusters or take up appreciable ^{13}C from *Mucor.* Results from 3 separate biological replicates in separate microfluidics chambers shown in color. Cells at t48 were significantly more enriched in ^{13}C than cells at t0, for both clusters and planktonic cells (one-way ANOVA for all categories F-statistic 4.98, p-value $2.85x10^{-5}$; Tukey-Kramer p-value <0.01 comparing t0 to t48 for both clusters and planktonic cells). However, there were no significant differences in ^{13}C enrichment between clusters versus planktonic cells at any time point (Tukey-Kramer p-value > 0.05 for all pair-wise comparisons of clusters versus planktonic samples at each time point).

CHAPTER 3: "TRANSPARENT SOIL MICROCOSMS" ENABLE SUBMICRON RESOLUTION IMAGING AND NON-DESTRUCTIVE STABLE ISOTOPE PROBING OF BACTERIA AND FUNGI WITHIN A THREE-DIMENSIONAL POROUS MATRIX OVER TIME

Summary

Microscale soil processes are critically important to larger scale ecological and biogeochemical processes, yet are difficult to study due to the opacity and spatial and chemical complexity of soils. We have constructed "transparent soil" (TS) microcosms that enable multimodal visualization of microbial growth and assembly, combining fluorescence microscopy and Raman microspectroscopy to measure microbial activity and carbon uptake using stable isotope probing of bacteria *in situ*. We used and assessed both the polymer Nafion and the crystal cryolite as substrates for optically transparent model soil systems. We found that both substrates enable growth, maintenance, and visualization of submicron features of bacteria and fungi in deep (100 μm) three-dimensional porous matrices over time by light microscopy. Both Nafion-based and cryolite-based "transparent soil" microcosms are compatible with stable isotope probing of heavy water as a non-destructive marker of microbial activity *in situ*, while cryolite-based microcosms are also compatible with tracing uptake of ^{13}C substrates by bacteria. We use deuterium label tracing to show that bacterial cells attached to dead fungal hyphae within a Nafion matrix have greater metabolic activity after a dry-down and rewetting cycle than cells far away from the fungal hyphae,

corroborating the important role of fungi in facilitating survival of bacteria in the fluctuating conditions found in soils.

Introduction

"Until someone invents transparent soil," writes plant and soil scientist David Robinson, "roots will be imperfectly understood" (Robinson, 2012). The same could be said for the lives of soil microorganisms. Terrestrial soils offer habitats to an unparalleled abundance and diversity of bacteria and fungi, whose metabolic activities drive critical biogeochemical processes with biosphere-level effects (Pold et al., 2013; Wieder et al., 2013). A major barrier to understanding soil microbes in their habitats is the opacity of natural soils.

"Transparent soils" (TS) are soil model systems wherein particles saturated with liquids of similar refractive index allow transmission of light and render the porous, "soil-like" system optically transparent (Iskander, 2010). Transparent soils (TS) have been used for over 25 years in geoengineering and hydrology, where they have helped solve and ground-truth important and otherwise intractable problems in soil physics, from determining how soils compress under weight (with applications for civil engineering), to tracking how oil travels through soil pores, (with implications for groundwater quality) (see Iskander et al., 2015 for a review of 25 years of transparent soils work in these fields).

Despite their importance in advancing soil physics, TS systems have only recently and rarely been used for applications in soil biology. Soil physics models have generally not required the maintenance of organisms within TS systems, and have

therefore tended to rely on RI-matching strategies using solutions that do not support organismal growth, such as silicone oil. Foundational work by Leis and colleagues (2005) introduced the synthetic transparent fluoropolymer Nafion (Chemours, Wilmington, DE) as the solid phase of a TS system that could be RI-matched to aqueous, biocompatible solutions, and used to successfully culture sediment microorganisms *in situ*. Downie and colleagues (2012; 2014) built on this work and introduced Nafion-based TS to plant biology as a tool for visualizing roots in a porous transparent medium that gives rise to more naturalistic root phenotypes than roots grown in agar. Though well-cited and lauded as a much-needed advance in the study of roots, no other group (to our knowledge) has used Downie et al's fluoropolymer-based TS system for root phenotyping – though the same research group did significantly advance the method recently for live-cell imaging of nematodes (O'Callaghan et al., 2018). This may be due to the drawbacks of (a) the high cost of Nafion, the fluoropolymer used as the solid substrate in these TS studies, and (b) the RI of Nafion (RI=1.35; Leis et al., 2005), which is close to that of water (RI=1.33) but different enough that image quality deteriorates at the scale of millimeters and centimeters needed for root growth and its visualization. Indeed, a recent work by Ma and colleagues cites these reasons as their motivation for taking Downie and colleagues' Nafion-based system as inspiration, but inventing an inexpensive hydrogel bead-based TS system with a very close RI match with water for root phenotyping studies (Ma et al., 2019).

Nafion may, however, be well-suited to studies in soil microbial ecology, where microcosms utilizing only a few micrograms of particles and requiring imaging depth of

tens or hundreds of microns become inexpensive to build, and tolerant of slight RI mismatches, therefore obviating the need for exact RI-matching with bio-incompatible solutions. For soil microbial studies, Nafion has two major advantages over hydrogel-based systems, despite the clear usefulness of hydrogels for plant studies: (a) Nafion can be milled to fine particle sizes down to 1 μm, which offer micron-sized pores as important habitats for micron-sized bacteria, whereas the lower limit of for the manufacture of hydrogel beads as published by Ma and colleagues is around 500 μm (Ma et al., 2019), and (b) Nafion is a synthetic polymer that is not able to be metabolized by bacteria and fungi, whereas alginate-gellan hydrogel beads are rich carbohydrate sources readily decomposed by many bacteria and fungi (Rice et al., 1992; Lin et al., 2018;).

Another potential substrate for biocompatible, inert TS is cryolite, a naturally occuring and water-insoluble sodium aluminum fluoride crystal. Cryolite's refractive index of 1.339 (Lewis, 2007) is remarkably close to that of water (1.333), rendering it nearly optically transparent in aqueous solutions. Cryolite has been used as a TS medium in a few soil physics studies, though it is not as popular as quartz, due to its relative cost and rareness. A small and intriguing set of studies have used cryolite to gain insight into the biophysics of the burrowing behaviors of marine invertebrates in sediments (Flessa, 1972; Francoeur & Dorgan, 2014; Dorgan, 2018) . As a substrate for soil microbiological studies, cryolite was used by Zhu and colleagues (Zhu et al., 2014) who monitored the swimming behavior of *Bacillus subtilis* bacteria in a packed-cryolite capillary, and by Oates and colleagues (2005) who mapped the spatial patterns

of oxygen consumption by *Pseudomonas fluorescens* bacteria in a cryolite matrix using bioluminescent reporters.

In this study, we evaluate both Nafion and cryolite as TS substrates for studies in soil microbial ecology. We have optimized a laboratory model system – "transparent soil (TS) microcosms" – to non-destructively visualize bacteria and fungi with micrometer resolution within a three-dimensional particulate matrix of Nafion or cryolite, thus creating pore spaces analagous to those characteristic of bacterial habitats in natural terrestrial soils (Dal Ferro & Morari, 2015; Deng et al., 2015; Baveye et al., 2018). Critical to soil microbial ecology is elucidating microbial spatial distributions, migration, and growth dynamics, as well as gaining insight into the physiological states and ecological functions of individual cells and species (Fike et al., 2008; Berry et al., 2015). We therefore evaluate these TS systems not only for their amenability to high-resolution, three-dimensional imaging by fluorescence and confocal microscopy, but also for their compatibility with Raman microspectroscopy – a powerful non-destructive optical method to obtain physiological information about cell state and, when paired with the addition of stable isotopes, to obtain information about microbial metabolic activity and nutrient uptake (Huang et al., 2004; Huang et al., 2009; Li et al., 2012; Li et al., 2013; Berry et al., 2015; Kumar et al., 2016). To our knowledge, this is the first study that attempts Raman microspectroscopy of cells within a transparent porous matrix, with important potential applications to fundamental problems in soil and sediment microbial ecology.

We use this complex but tractable system to expose bacteria to a dessication and rehydration event within a TS-matrix and measure how metabolically active bacteria

are within the matrix depending on their proximity to fungal hyphae. Finally, we demonstrate that in addition to enabling the measurement of deuterium uptake as a marker of microbial activity, cryolite-based TS microcosms enable the measurement of isotopically-labeled carbon uptake by microbes and therefore enable non-destructive dynamic monitoring of carbon flow through a complex, porous, soil-like system.

Methods

Strain Construction

Bacillus subtilis 3610 strains constitutively expressing fluorescent proteins were constructed by vector cloning, transformation of vectors into *B. subtilis* 168, and phage transduction of *B. subtilis* 168 transformant DNA into *B. subtilis* 3610 (Yannarell et al., 2019). *B. subtilis* NCIB 3610 is a commonly-used strain of *B. subtilis* which is less genetically tractable than *B. subtilis* 168, but exhibits biofilm production phenotypes common to wild *B. subtilis* soil isolates and lost in the 168 lab strain (McLoon et al., 2011). Plasmid pES037 was constructed by standard restriction digest cloning of *B. subtilis* codon-optimized versions of the *YPet* and *mTurquoise2* genes (obtained from Ethan Garner, Harvard University) into the pEA003 parent vector (*amyE*::P*spac*^{C}*-cfp-cam*^{R}), which replaced the *cfp* gene with the new fluorescent protein. Linearized vector was transformed into *B. subtilis* 168 as described previously (Yannarell et al., 2019). Cells were plated onto Lennox-chloramphenicol to select for transformants – *amyE*::P*spac*^{C}*-YPet-cam*^{R} and *amyE*::P*spac*^{C}*-mTurquoise2-cam*^{R}. Phage transduction from *B. subtilis* 168 transformants into *B. subtilis* 3610 using SPP1 bacteriophage was performed as previously described (Yasbin & Young, 1974).

Microorganisms, Media, and Growth Conditions

B. subtilis NCIB 3610 strains were routinely cultured on Lysogeny Broth (LB)-Lennox agar (10 g/L tryptone, 5 g/L yeast extract, 5 g/L NaCl, 15 g/L agar) supplemented with antibiotics (5 µg/mL chloramphenicol final concentration) at 30°C for 16-20 hours. *Mucor fragilis* used in this study was obtained from Fletcher Halliday (University of North Carolina at Chapel Hill), who isolated the strain from a tall fescue plant in the Piedmont region of North Carolina, and created a culture stock by patching *M. fragilis* hyphae onto a malt extract agar (MEA) slant (Difco, malt extract 6 g/L, 6 g/L maltose, 6 g/L dextrose, 15 g/L agar) containing 200 µg/mL chloramphenicol. *M. fragilis* was routinely cultured by patching agar from culture stock into the center of an MEA plate containing 200 µg/mL chloramphenicol and incubating at 30°C for 10 days until a lawn of *M. fragilis* spore bodies was obtained. *M. fragilis* spore stock was obtained by adding 10 mL Milli-Q water to this lawn and aspirating the liquid back up to obtain spores. Spores were pelleted by centrifugation (4000 x *g* on tabletop centrifuge in 15 mL Falcon tube) and washed three times in Milli-Q to remove residual growth medium and hyphae. Spore stock was stored at 4°C for up to one month. Spore concentration was calculated by counting spores on hemacytometer and diluting back to 10^5 spores per mL for routine use.

MSN medium (minimal salts with free ammonium as nitrogen source; Beauregard et al., 2013) was used as the base (carbon-free) medium to which various amendments were added for growth and isotope-labeling experiments (5 mM potassium phosphate [pH 7], 100 mM morpholinepropanesulfonic acid [MOPS; pH 7], 2 mM $MgCl_2$,

700 μM $CaCl_2$, 50 μM $MnCl_2$, 50 μM $FeCl_3$, 1 μM $ZnCl_2$, 2 μM thiamine, 0.2% NH_4Cl). *M. fragilis* was grown in TS microcosms with MSNglu (MSN with 2% glucose, final concentration). *B. subtilis* was grown in TS microcosms with MSNglu or MSgg, a biofilm-inducing medium (5 mM potassium phosphate [pH 7], 100 mM morpholinepropanesulfonic acid [MOPS; pH 7], 2 mM $MgCl_2$, 700 μM $CaCl_2$, 50 μM $MnCl_2$, 50 μM $FeCl_3$, 1 μM $ZnCl_2$, 2 μM thiamine, 0.5% glycerol, 0.5% glutamate).

Nafion Particle Preparation

Nafion particles were acid washed and rendered hydrophilic and cation-exchanging as previously described (Downie et al., 2012), with modifications. Briefly, 30 g PowdION Nafion powder (IonPower) was suspended in 300 mL 15% KOH/35% DMSO aqueous solution in a glass beaker and heated for 5 hours at 80°C to hydrolyze Nafion. Particles were washed 3 times with Milli-Q water. All washes were carried out by centrifugation unless otherwise noted (4000 x *g* in 50 mL centrifuge tube in table top centrifuge for 5 minutes). To convert Nafion to ion-exchanging form, particles were suspended in 15% nitric acid and incubated at room temperature for 1 hour in a glass beaker, then washed with Milli-Q water, and resuspended with nitric acid and left at room temperature overnight. To remove impurities from Nafion surfaces, particles were washed 3 times with Milli-Q water, incubated in 1 M sulfuric acid for 1 hour at 65°C in a glass beaker, washed with Milli-Q water, and incubated again at 65°C for one hour. Particles were then washed 3 times with Milli-Q water, suspended in 3% hydrogen peroxide, incubated at 65°C for 1 hour, and washed 3 times with Milli-Q water. Finally, to replace protons held by Nafion with biologically important cations, particles were

washed repeatedly with MSN medium until supernatant pH stabilized at 7.

To obtain particle size fractions small enough to fit in microfluidic microcosms, a dilute particle slurry (1:20 particles to water) was sieved through a 40 μm cell strainer. Particles in the flow-through were collected by centrifugation (see Figure 3.3 for particle size distributions). Particles were then sterilized by autoclaving slurry (1:1 particles to water by volume).

Cryolite Particle Preparation

Cryolite particles were obtained by grinding 5 g of cryolite crystal (Wilhelm Niemutz Mineralien, Vienna) with a mortar and pestle, washing 3 times in Milli-Q water by centrifugation, sieving through a 40 μm cell strainer to obtain small particles in flow-through, and autoclaving particle slurry.

TS Microcosm Manufacture and Preparation

The TS microcosm construction process is summarized in Figure 3.1. Sylgard 184 PDMS (Dow Chemical) was mixed 10:1 base:curing agent, poured over either a standard SU-8 silicon master or a craft epoxy master (see Chapter 4), and baked overnight. Inlets and outlets were punched with a 1 mm biopsy puncher (Cole-Parmer). Devices were rendered hydrophilic using a handheld corona treater (Electro-Technic), passed over the chip 10-20 times at full power. A TS slurry of either Nafion or cryolite particles (1:1 particles to water) was vigorously vortexed and 3 μL of slurry pipetted quickly into PDMS chambers. A glass cover slip (60 x 20 x 0.15 mm) was corona

treated as above and pressed firmly onto the PDMS chamber to seal, then baked at 70°C for 1 hour to bond.

TS in chambers was washed by gently flowing in liquid at a rate of 0.5 µL/min with a syringe pump using a 1 mL syringe (Oxford Instruments). Nafion-based microcosms were rehydrated with 3 uL 20% ethanol, then washed with 20 µL of desired culture medium before inoculation with microorganisms. Cryolite-based microcosms were simply wet with 3 µL of desired medium (enough to wet the TS) before inoculation (see Figure 3.2).

Bacterial and Fungal Culture in TS Microcosms

B. subtilis 3610 cells were grown for 2.5 hours at 37°C shaking in LB broth, washed 5x in appropriate growth medium (MSN or MSgg, see figure captions for details), diluted back to OD_{600} of 0.05 (~2.5 x 10^7 cells/mL) and inoculated into TS microcosms by syringe pump at a rate of 0.5 µL/min, 3 µL total volume. *M. fragilis* spores were resuspended 1:10 (from 10^5 spores/mL spore stock in sterile Milli-Q water) into MSN-glu growth medium, and inoculated into TS microcosms by syringe pump. TS microcosms were sealed with Scotch tape on the inlet and outlet and either imaged immediately or placed in a 50 mL Falcon tube with a small piece of wet paper towel to maintain humidity and incubated horizontally at 30°C until removed for imaging.

B. subtilis Culture for Isotope Labeling Experiments

B. subtilis 3610 cells were grown for 16 to 20 hours at 37°C shaking in MSN 2% glucose medium made with either: 2% regular glucose (termed ^{12}C H_2O cells), 2% ^{13}C

glucose (^{13}C H_2O cells), 1% regular glucose and 1% ^{13}C glucose (half-^{13}C H_2O cells), or 2% regular glucose and 50% (final volume) D_2O (^{12}C D_2O cells). Cells were then inoculated directly into TS microcosms by pipetting ~3 µL cell culture into inlet. In the case of ^{12}C D_2O cells, cells were first washed 5x in regular MSN to remove background D_2O (which interferes with Raman cell spectrum signal) and then inoculated into TS microcosms. Cells were measured by Raman microspectroscopy immediately after inoculation.

Confocal Raman Microspectroscopy and Spectral Processing

Single microbial cell spectra were acquired using a LabRAM HR800 Raman microscope (Horiba) equipped with a 532-nm neodymium-yttrium aluminium garnet laser and 300 grooves/mm diffraction grating. Spectra were acquired in the range of 400–3,200 cm^{-1}. Only cells over 15 µm away from either the glass coverslip or PDMS side of the microcosm were measured to reduce interference from glass or PDMS. Acquisition parameters were as follows: 30 s acquisition time, 100% laser power, 50% ND filter, slit=150, hole=300 (resulting in resolution of approximately 1 µm). For each cell spectrum acquired, a "background" spectrum in the same z-plane but approximately 10-20 µm away in the x-y plane was acquired as a measure of the Raman spectrum of the local TS matrix around the cell.

Spectra were baselined and normalized using scattr software (Single Cell Analysis and Testing Tools for Raman microspectroscopy; Berry et al., 2015). Briefly, each spectrum was fitted with a 6^{th} degree polynomial function then normalized to total spectral intensity. All spectra collected from a single microcosm were normalized

together. The matching background spectrum was then subtracted from each cell spectrum to obtain a background-subtracted cell spectrum for each cell.

"CD region" for an individual cell spectrum was calculated as the area under the curve between 2145 and 2090 cm^{-1} (average intensity of region between 2145 and 2090 cm^{-1} minus average intensity between the flat baseline region between 2040 and 2060 cm^{-1}). "Percent ^{13}C" was calculated individually for each background subtracted cell spectrum as $(A_{966}/(A_{966} + A_{1003}))x100$, where A_{966} is the average intensity between 960 and 968 cm^{-1} minus the average intensity of the nearby baseline 935 to 945 cm^{-1} region (^{13}C phenylalanine peak) and A_{1003} is average intensity between 998 and 1005 cm^{-1} minus the nearby baseline 980 to 985 cm^{-1} region (^{12}C phenylalanine peak).

Dessication and Rehydration Treatment of TS Microcosm

M. fragilis spores were inoculated into a Nafion TS microcosm with MSN-glu growth medium and incubated at 30°C for 24 hours. Hyphae were heat killed *in situ* the next day, and the microcosm washed with fresh MSN medium. *B. subtilis* 3610 cells were then inoculated into the microcosm in MSN medium, with dead *Mucor* as their sole carbon source. The fully-hydrated microcosm was then dried down by leaving ports on the microfluidics device unsealed and leaving exposed to air in a 50 mL Falcon tube at 30°C for 6 hours. After full dessication of the Nafion (i.e. macropores filled with air, Nafion reverts to white appearance and not transparent/translucent as when hydrated), microcosms were incubated for an additional 36 hours at 30°C with ports unsealed and the system exposed to air. After this dry period, 15% ethylene glycol was slowly percolated into the microfluidics device using a syringe pump (3 µL total volume, 0.5

μL/min) to rehydrate the hydrophobic Nafion, followed by washing with MSN medium to remove ethylene glycol (20 μL total volume, 0.5 μL/min). Finally, the system was fully hydrated with MSN made with 50% D_2O (20 μL total volume, 0.5 μL/min) and incubated 16 hours at 30°C, with ports sealed to maintain full hydration. The next day, the microcosm was washed with fresh sterile distilled water to remove excess non-metabolized D_2O. Single *B. subtilis* cells were measured by Raman microspectroscopy as described in the previous section. *B. subtilis* cells measured were classified as either "on" (cells attached to *M. fragilis* hyphae), "near" (cells attached to Nafion on *M. fragilis* -inoculated side of microcosm, within a 20 μm radius of the nearest hypha), or "far" (cells attached to Nafion on the side of the microcosm lacking *M. fragilis* hyphae). "Far" cells are 3 mm or more away from nearest *M. fragilis* hyphae.

Results

Visualization of TS matrix itself

We first tested whether particle edges and pore water can be rendered visible in TS matrices. Nafion particle edges are visible through water by brightfield or DIC microscopy. As shown previously (Downie et al., 2012), Nafion can be rendered fluorescent in the RFP channels by staining with sulphorhodamine (Fig. 3.2). We found that particles are also slightly autofluorescent in CFP and YFP channels.

Cryolite particle edges, by contrast, are not visible through water by brightfield microscopy, presumably due to close RI matching (Fig. 3.8). They are visible by DIC microscopy or other polarized light microscopy, and are partly visible in the PMT channel of a confocal microscope (Fig. 3.8, Fig. 3.10). Cryolite particles were not able

to be stained by sulphorhodamine, fluorescein or by AF647 amine dye (Fig. 3.10). They were not autofluorescent in the DAPI, CFP, YFP, RFP, or AF660 channels.

The cryolite particle matrix can be visualized by staining the pore water around particles. Adding non-toxic fluorescent dyes – sulphorhodamine, fluorescein or Alexa Fluor dyes (amine form used here) – makes particles visible as unstained negative space (Fig. 3.10). Pore water in a Nafion particle matrix can be visualized using these same dyes, which is particularly helpful when imaging unsaturated systems where it is important to be able to distinguish liquid- from air-filled pores (Fig. 3.6). However, both fluorescein and AF647 amine dye stain Nafion particles themselves after a dry-wet cycle. The particles still remain easily distinguishable from the pore space, but the added strong fluorescent signal from particles can add background noise, making it more difficult to image bacteria, which are much smaller than particles and tend to have a much weaker fluorescent signal.

Rehydration of Nafion

Nafion is very hydrophobic until its sulfonyl group is functionalized by acid washing, which renders Nafion hydrophilic and submersible in water (Downie et al., 2012; Moilanen et al., 2007). After drying, Nafion becomes very hydrophobic again, and cannot be re-wet with water alone. We used 20% ethanol, 15% ethylene glycol, or 0.1% Tween-20 to rehydrate Nafion after drying. 20% ethanol was the fastest and most effective re-wetting agent, and therefore a good choice for initial wetting after microcosm manufacture, when the system is still sterile (Fig. 3.1). However, this high concentration of ethanol is toxic to most cells. We found that 15% ethylene glycol or

0.1% Tween-20 were effective and non-toxic agents (Blank et al., 1987; Man et al., 2017) for re-wetting Nafion microcosms already inoculated with bacteria or fungi (Fig 3.17).

TS microcosms enable submicron resolution imaging of bacteria and fungi in three dimensions over time within a porous matrix

Though previous work has focused on RI matching of particles and liquid in order to improve image quality through the particle matrix (Downie et al., 2012; Leis et al., 2005; O'Callaghan et al., 2018), we found that exact RI matching was not necessary to obtain well-resolved images of bacteria and fungi through 100 μm of particles, where the particle size distribution was between 2 um and 40 um (Fig. 3.4, 3.9, 3.11). Sub-micron fine features of the fungus such as textural bumps on the hyphal surface are resolved even through 100 μm of liquid-saturated cryolite matrix (Fig. 3.9). A 3 μm line profile (Fig. 3.9, yellow line in bottom images) was taken of two bumps on *M. fragilis* in liquid (Fig. 3.9, blue border) and *M. fragilis* in cryolite (Fig. 3.9, red border) imaged 100 μm into a cryolite-filled microfluidics chamber. Full width at half-maximum (FWHM) values were estimated for each bump as a measure of resolution. Resolution through cryolite saturated with aqueous medium for features of this size was comparable to resolution when imaging through aqueous medium alone (between 0.5 and 0.6 μm for imaging through aqueous medium, compared to between 0.6 and 0.7 μm for imaging through saturated cryolite). Even finer features are resolvable by eye through 100 μm cryolite (note fine scaly texture of *Mucor* hyphae in top right corner of red-bordered image in Fig. 3.9), but were not measured. Bacteria expressing fluorescent proteins are visible by confocal microscopy even through 100 μm of Nafion (Fig. 3.4) or cryolite (Fig.

3.11). Indeed, in the cryoilte matrix, they are visible even in the non-fluorescent PMT channel (Fig 3.11, PMT).

B. subtilis bacteria and *M. fragilis* fungi were able to grow, be maintained, and be visualized non-destructively over time in both Nafion- and cryolite-based TS microcosms (Fig. 3.5, Fig. 3.6, Fig 3.7). We found that *B. subtilis* cells were still active in hydrated microcosms (as indicated by motility within liquid-filled pores) after 2 weeks in MSgg medium. *M. fragilis* inoculated as spores into TS microcosms grew into full mycelial masses within 48 hours (Fig. 3.7).

Growth in TS matrix influences bacterial and fungal morphology

By milling Nafion or cryolite to coarse or fine particle sizes, a variety of pore sizes can be obtained, which in turn appear to influence the morphologies of bacteria and fungi grown within the matrix (Holden, 2011). Larger Nafion particle sizes (40 to 100 μm) resulted in larger pores, and *B. subtilis* took on a more filamentous morphology within these larger pores than in the smaller pores afforded by smaller Nafion particles (1 to 40 μm; Fig. 3.6). *M. fragilis* hyphae grown in Nafion-based TS matrix have less variation in hyphal width and more tortuous growth habit (as defined by deviation from straight lines of growth) than *M. fragilis* hyphae grown without TS (Fig. 3.7).

TS microcosms are compatible with Raman microspectroscopy and enable *in situ* single-cell detection of microbial activity as measured by uptake of D_2O

Almost all microbial metabolism involves the uptake of water and incorporation of hydrogen from water into the cellular biomass. By tracking the incorporation of a non-toxic, isotopically-labeled variant of water (D_2O) into biomass through peak shifts in the

Raman spectra of cells (Berry et al., 2015), it is possible to detect which cells within the TS matrix are active and which are not. We grew *B. subtilis* cells in H_2O and in 50% D_2O media and inoculated them into Nafion and cryolite TS microcosms. Single-cell Raman spectra were taken from cells embedded 15 to 85 μm deep within a packed TS matrix. We found that the D_2O-grown cells have a significantly larger CD area than H_2O-grown cells in Nafion microcosms (Fig. 3.12; n=23 for D_2O- and for H_2O-grown cells, Student's t-test p-value = 1.99×10^{-8}, bootstrap 95% confidence interval [CI] testing difference in means [1.08, 2.09]), as well as in cryolite microcosms (Fig. 3.13; n=41 for H_2O-grown cells, n=26 for D_2O-grown cells, Student's t-test p-value = 2.16×10^{-7}, bootstrap 95% CI testing difference in means [0.58, 1.29]). Larger peaks in this area between 2030 and 2300 cm^{-1} are correlated with greater D_2O uptake, a measure of cell metabolic activity (Berry et al., 2015).

In Nafion microcosms, the cutoff for cells to be classified as D_2O-labeled can be set at CD region area = 0.5, since all H_2O-labeled cells fall below this cutoff (Fig. 3.12). This cutoff produces two false negative values (D_2O-labeled cells misclassified as H_2O-labeled cells, 9%). In cryolite microcosms, the cutoff for cells to be classified as D_2O labeled can be set at CD region area = 0.75, since this is the third quartile of H_2O labeled cells (Fig. 3.13). This cutoff produces eight false positive values (H_2O-labeled cells misclassified as D_2O labeled, 20%), and five false negative values (D_2O labeled cells misclassified as H_2O labeled, 19%).

TS microcosms enable the detection of ^{13}C uptake by populations of bacteria *in situ* by Raman microspectroscopy

Raman spectroscopy can be used to detect the uptake of ^{13}C-labeled compounds into cellular biomass measuring the characteristic "red-shift" of the phenylalanine peak from 1003 cm^{-1} to 966 cm^{-1} upon incorporation of ^{13}C into phenylalanine molecules in the cell (Huang et al., 2004; Huang et al., 2009; Li et al., 2012; Li et al., 2013; Kumar et al., 2016). We found that Raman microspectroscopy of *B. subtilis* cells through a Nafion TS matrix could not reliably distinguish single cells grown in ^{13}C glucose-containing media from single cells grown in ^{12}C glucose-containing media. Though over 75% of ^{13}C-labeled cells in Nafion have a "Percent 13C" value of over 75%, a large number of ^{12}C-labeled also have high "Percent 13C" values and are misclassified as ^{13}C-labeled (Fig. 3.14, right). As seen in the average spectra traces, ^{12}C-labeled cell spectra have a high background peak at around 965 cm^{-1} (Fig. 3.14, left). To inspect why this peak occurs even in ^{12}C-treated cells, we examined the background spectra of single ^{12}C-grown cells. A representative background spectrum of a single ^{12}C-grown cell shows the same high peak at 965 cm^{-1} (Fig. 3.15). The background-subtracted cell spectrum retains this peak, resulting in the cell being misclassified as ^{13}C-labeled.

Though single ^{12}C-treated cells could not be reliably distinguished from ^{13}C-treated cells within a Nafion matrix, the *population* of ^{12}C-treated cells was distinguishable from the population of ^{13}C-treated cells. ^{13}C-labeled cells have significantly higher "Percent ^{13}C" values than ^{12}C-labeled cells (Student's t-test p-value = 0.001209, bootstrap 95% CI testing difference in means [8.96, 42.42]).

In cryolite-based TS microcosms, populations of ^{13}C-treated *B. subtilis* cells can also be distinguished from populations of ^{12}C-treated cells (Fig. 3.16). ^{13}C -grown cells measured within the cryolite matrix have significantly higher "Percent ^{13}C" values than ^{12}C -grown cells and half-^{13}C -grown cells (Fig. 3.16; n=39 ^{12}C-grown-cells, n=25 half-^{13}C-grown cells, n=20 ^{13}C-grown cells; One-way ANOVA for comparison of all three categories F-statistic = 10.52, p-value = 0.0001; Tukey-Kramer HSD p-value <0.005 when comparing ^{13}C-labeled cells to both ^{12}C- and half-labeled cells; bootstrap 95% CI testing difference in means for ^{13}C-labeled versus half-^{13}C-labeled cells = [22.42, 57.65], and for ^{13}C-labeled versus ^{12}C-labeled cells = [8.42, 45.81]). However, half-^{13}C-labeled cells are found to not be significantly different from ^{12}C-labeled cells (Tukey-Kramer HSD p-value = 0.58 when comparing ^{12}C-labeled cells to half-labeled cells; bootstrap 95% CI testing difference in means = [-30.36, 5.66]).

B. subtilis cells attached to dead fungal biomass are more metabolically active after a dry-wet cycle in Nafion than cells far away from fungus

Having established that Raman spectroscopy can be used to distinguish single D_2O-treated cells from single H_2O-treated cells within a Nafion matrix, and knowing that D_2O uptake can be used as a marker of microbial activity, we applied our method to an ecologically relevant question: how does a dessication and rehydration cycle within a porous matrix affect microbial activity, and does proximity to a fungus affect whether cells will remain active after this cycle?

M. fragilis spores were inoculated into Nafion-based TS microcosms and grown overnight in MSN-glucose, then hyphae were heat-killed and washed *in situ.* *B. subtilis* cells were then inoculated into the TS microcosm, with the dead *M. fragilis* hyphae as

their only carbon source, and the microcosm was dessicated for two days. The microcosm was then rehydrated with 50% D_2O-containing medium as a probe for microbial activity following this dessication and rehydration cycle. *B. subtilis* cells were classified as either, on, near, or far from fungal hyphae (Fig. 3.17).

Cells with CD>0.5 were classified as D_2O-labeled, based on the previously-established threshold (see Fig. 3.12). We found that most *B. subtilis* cells (60 to 70% of cells in each microcosm, n=3 microcosms) do not show any detectable uptake of D_2O after dessication and rehydration (Fig. 3.18, left panel, all cells with CD area less than 0.5, indicating no activity detectable by D_2O uptake). However, of the cells that did show uptake of D_2O (Fig. 3.18, right panel, cells with CD area > 0.5), those attached to dead *M. fragilis* hyphae took up more of the D_2O label than cells far away from the hyphae (i.e. cells attached to Nafion particles outside of a 3 mm radius from any *M. fragilis* hyphae; Fig. 3.18; n=13 cells on *M. fragilis*, n=10 cells near *M. fragilis*, n=11 cells far from *M. fragilis*, one-way ANOVA of all three categories F-statistic 4.5988, p-value = 0.01782; Tukey-Kramer HSD p-value = 0.01352 for “on” vs “far” cells; bootstrap 95% CI testing difference in means between “on” vs “far” cells = [0.2550, 0.7602]). Cells *near* but not *on M. fragilis* hyphae – i.e. cells attached to Nafion within 20 μm of the hyphae – showed slightly but not significantly higher D_2O uptake than cells far away (Tukey-Kramer HSD p-value = 0.4047 for cells near *M. fragilis* versus far from *M. fragilis*).

Discussion

In this study, we imaged through TS with the aim of achieving resolution appropriate to the visualization of micrometer-sized bacteria, through microcosm

volumes that represent large habitats for bacteria (hundreds of microns). Though three other studies have used light microscopy to investigate bacteria with single-cell resolution in transparent porous media (Leis et al., 2005; Oates et al., 2005; Drescher et al., 2013), this is the first work, to our knowledge, that attempts Raman microspectroscopy of cells through such media. This is an ambitious goal, as it asks a great deal of the Raman spectrophotometer instrument. Photons from the excitation laser must not only make their way to the cell embedded within the matrix while passing through tens of microns of solid transparent particles, pore liquid, and glass, but the resultant photons produced by Raman scattering must find their way back to the Raman detector through this same set of materials. Moreover, the intensity of the Raman signal from the measured cell must be high enough that it is detectable over the Raman spectra of the particle-liquid matrix as well as the imaging chamber itself – a complex combination of materials producing an intense and complex composite Raman spectrum in its own right (Everall, 2010). Even with perfect refractive index matching, surface refraction (worsened if the material is not flat) and surface scattering (worsened if the material is not smooth) can both contribute strongly to background contributions to the cell spectrum (Freebody et al., 2010), which we would expect in the non-flat, rough surfaces found in TS systems.

Despite these challenging conditions, we were able to detect cell-specific Raman spectra from single, micrometer-sized bacteria through tightly-packed hydrated TS matrices. Moreover, by adding stable isotope probes to the system, we were able to analyze and use these spectra to non-destructively detect bacterial uptake of labeled substrates *in situ*. This capability allowed us to non-destructively measure the

metabolic activity of single cells in a spatially resolved way, using a treatment that mimics an ecologically important process in soils: a drying and rewetting cycle.

Comparing Nafion and Cryolite as Transparent Porous Substrates for Microbial Studies

We assessed both the polymer Nafion and the crystal cryolite for their suitability to soil microbial ecology studies according to a number of criteria, summarized in Table 3.1. Both substrates support the growth of heterotrophic bacteria and fungi, are inert (i.e. not readily decomposed by heterotrophs), enable visualization of submicron features and fluorescent cells through 100 μm of particle matrix, have cation exchange properties (empirically measured for Nafion [Downie et al., 2012], theoretically inferred for cryolite [see below]), and are compatible with SIP by Raman microspectroscopy. However, the substrates have important differences that are useful for the potential user to consider.

Nafion has the advantage of being reliably commercially available, consistent and pure – as opposed to cryolite crystal, which is rare and acquired through gem vendors, and includes small impurities like siderite, fluorite, and quartz (Pauly & Bailey, 1999). Importantly, although synthetically-produced cryolite is readily commercially available through scientific suppliers and is inexpensive, it is not recommended as a transparent porous medium substrate due to (a) the prevalence of very fine, sub-micron particle sizes that highly scatter light, (b) the presence of highly opaque aluminum oxides (even in synthetic formulations with 99% purity) that render the substrate opaque within a few microns (Flessa, 1972) and (c) its amorphous molecular structure, which produces a greater diversity of Raman peaks and higher baseline Raman spectra than

crystalline cryolite, whose lattice arrangement results in a few sharp, clear Raman bands (Tushcel, 2017). We therefore used natural crystalline cryolite for this study.

Despite the paucity of sources for this cryolite crystal and the variability of this unprocessed natural material, cryolite has several advantages over Nafion. Cryolite crystal is considerably cheaper than Nafion (tens of cents per gram, as opposed to tens of dollars per gram), readily ground into powder to desired particle sizes by mortar and pestle (as opposed to Nafion, which must be cryomilled or bought pre-ground), and requires no pre-treatment before use (unlike Nafion which requires an extensive number of washes to functionalize). We found that cryolite also has the advantage of being extremely optically transparent, such that micron-sized bacteria can be resolved through even 100 μm of cryolite matrix hydrated with aqueous microbial growth medium even under brightfield or DIC illumination on a compound microscope (Fig 3.9, Fig 3.11). This makes it an attractive candidate for soil microbial ecology studies, since it may obviate the need for genetic manipulation and fluorescent labeling of bacteria for tracking in microcosms.

Cryolite also has more natural dry-down and wet-up behavior than Nafion. After drying, Nafion becomes very hydrophobic again, and cannot be re-wet with water alone. This is a major difficulty and limitation of using Nafion-based systems, which we overcame by using small amounts of surfactants as rewetting agents then removing them from the system with subsequent washes. Both of the rewetting agents we used – 15% ethylene glycol and 0.1% Tween – are non-toxic to the organisms used in this study at these relatively low concentrations and short (i.e. 10 minutes maximum) exposure times (Blank et al., 1987; Man et al., 2017). However, both can cause cell

stress – ethylene glycol is an osmolyte, and Tween-20 is a detergent (Hallsworth et al., 2003; Nielsen et al., 2016). They can also be potential contaminating sources of carbon and nutrients in the system – particularly ethylene glycol which is readily metabolized by a number of microbial heterotrophs (Man et al., 2017).

In addition to hydrophobicity and drying-wetting behavior, an important consideration for soil model materials is their surface charge properties – notably cation exchange capacities. After acid washing, the sulfonyl group of Nafion particles become negatively charged and they participate in cation exchange reactions, with a measured cation exchange capacity of 81 meq100 g^{-1} (Downie et al., 2012). For cryolite particles, we were unable to find a published measured cation exchange capacity value. However, the point of zero charge of cryolite has been measured as 1.5 (Kosmulski, 2009), meaning cryolite particle surfaces carry a negative charge when immersed in solutions with pH greater than 1.5 (Lindblad & Duroux, 2017). They are therefore predicted to participate in cation exchange reactions in the pH ranges found in soils (pH 3 to 10; Slessarev et al., 2016). For comparison, the point of zero charge for clays are 2.5 for montmorillonite and 4.6 for kaolinite, both of which are important determinants of the cation-exchange capacities of soils (Kosmulski, 2009).

Capabilities and Limitations of Single-Cell Raman Microspectroscopy for Stable Isotope Probing Through TS

We have demonstrated, for the first time, that it is possible to collect Raman cell spectra through TS matrices (specifically, Nafion- and cryolite-based TS matrices), and we attempted to use Raman spectroscopy detect the uptake of stable isotopes by bacteria. We chose D_2O and ^{13}C as the stable isotopes of interest since they have both

previously been shown to produce clear changes in cell Raman spectra upon uptake, and because they are powerful tools for studying questions of interest in soil microbial ecology: microbial activity and carbon metabolism and cycling in soils.

D_2O-treated cells measured through a Nafion matrix were clearly distinguishable from H_2O-treated cells (Fig. 3.12), with all H_2O-treated cells falling below the CD area = 0.5 threshold, and all but 9% of cells (2 out of 23 cells) falling above that threshold. The threshold is conservative, resulting in a few false negatives, but no false positives. We can therefore assume with confidence that any single cells measured in a Nafion-based matrix with a CD area over 0.5 is D_2O labeled. We therefore conclude that single-cell D_2O uptake measurements can be made using Raman microspectroscopy through Nafion-based TS microcosms.

In cryolite-based microcosms, however, background-subtracted cell spectra were quite variable in the CD area, resulting in a large number (20%) of false positives – H_2O-treated cells misclassified as D_2O-labeled cells (Fig. 3.13). We were therefore unable to say with confidence that single cells above a certain CD area were D_2O -labeled when measured through a cryolite matrix. However, the entire population of D_2O-treated cells as a whole has a significantly higher CD area than a population of H_2O-treated cells, suggesting that *population-level* comparisons of D_2O uptake in cryolite can be made – for example, comparing the CD area of 30 cells exposed to a dessication and rehydration event versus 30 cells that were not exposed to such an event.

Berry and colleagues (2015) previously found that an accurate metric for D_2O uptake is the Percent CD, defined as the area of the CD region over the sum of the CD

region and the CH region of the cell spectrum. The CH region is the area between 2800 and 3100 cm^{-1}, and represents the carbon-hydrogen bonds in cells, which are depleted in deuterium-labeled cells (Berry et al 2015). In TS microcosms, CD peak cannot be normalized to the CH region because the measurements are taken in water-filled pores, which produces a large background signal in the CH region (2800 to 3100 cm^{-1}) due to the Raman spectrum of water itself. In addition, interference from glass and PDMS is high in this region (Lee et al., 2019). This may contribute to the greater variability in CD region area when cells are measured in TS matrices than when D_2O-grown cells are measured on aluminum slides (Berry, 2015).

Having established that D_2O uptake can be detected through TS matrices by Raman microspectroscopy, we attempted to similarly detect ^{13}C uptake. This presented more of a challenge because the signal intensities for the Raman peaks associated with ^{13}C-labeled compounds tend to be weaker than those for D_2O-labeled compounds, making ^{13}C uptake detection more challenging than D_2O uptake detection even in ideal conditions (Huang et al., 2004; Berry et al., 2015; Eichorst et al., 2015).

We found that it is not possible to accurately distinguish single ^{13}C-labeled cells from ^{12}C-labeled cells through a Nafion matrix using Raman microspectroscopy. When cells are embedded in the Nafion matrix and cell spectra measured by Raman microspectroscopy, we show that an intrinsic peak within the Nafion polymer around 965 cm^{-1} interferes with the 966 peak expected in the cell spectrum itself, thereby resulting in unlabeled cells being mislabeled as ^{13}C labeled (Fig. 3.15). In their study of the Raman spectrum of Nafion 117 membrane (sulphonated, and therefore similar in structure to the pellets used in this study), Bribes and colleagues (1991) found a broad

Raman peak at 971 cm^{-1} that they assigned to the symmetric stretch of C-O-C bonds intrinsic to Nafion, which is likely what we detect here. Nafion has intrinsic Raman peaks in all of the regions that would indicate ^{13}C uptake into cellular biomass (Bribes, El Boukari, & Maillols, 1991), perhaps because it contains so many carbon-based bonds, similar to biological materials.

Crystalline cryolite, in contrast, has no carbon bonds, resulting in a simple Raman spectrum with a few clear peaks outside the biological cell spectrum (Lafuente et al., 2016). We found that population-level differences in ^{13}C uptake are detectable through cryolite TS microcosms. We showed that a population of ^{13}C-treated cells had a significantly higher Percent ^{13}C measure than a population of ^{12}C-treated cells in a cryolite matrix (Fig. 3.16), suggesting that population-level comparisons of ^{13}C uptake in cryolite can be made – for example, comparing "Percent 13C" for 30 cells near a ^{13}C-labeled polysaccharide versus 30 cells far from a ^{13}C-labeled polysaccharide. Though we also found a statistically significant difference between ^{12}C-treated and ^{13}C-treated cell populations measured in Nafion (Fig. 3.15), the high intrinsic background of Nafion resulted in a much higher median "Percent 13C" value for ^{12}C-treated cells measured in Nafion (median=59.46; Fig. 3.14) than for ^{12}C-treated cells measured in cryolite (median=9.54; Fig. 3.16). With fully ^{12}C-labeled cells exhibiting such high "Percent 13C" values in Nafion, the threshold for classifying cells as ^{13}C-labeled needs to be high, and there is little range in which to detect cells with intermediate levels of labeling (Fig. 3.14; note that the median "Percent 13C" of ^{12}C-treated cells is relatively close to the median of ^{13}C-treated cells). In cryolite, however, the low background signal results in a low median "Percent 13C" value for ^{12}C-labeled cells, which allows a broad range to detect

intermediate levels of ^{12}C-labeling (Fig. 3.16; note that the median "Percent 13C" of ^{12}C-treated cells is relatively far from the median of ^{13}C-treated cells, and the median of half-treated cells is intermediate between them). Cryolite is therefore preferable to Nafion as a TS substrate in which to conduct studies involving ^{13}C-SIP.

Drying and Rewetting in TS and in Soils

Having established that D_2O uptake can be detected in single cells in Nafion microcosms by Raman spectroscopy, we used this D_2O-SIP approach to ask whether bacteria in this soil-like porous matrix can be protected from dessication and rehydration stress by proximity to fungal hyphae. As soils dry and are rewet, microorganisms in soils must rapidly adapt to enormous changes in osmolarity and nutrient availability, causing cellular stress (Chen & Alexander, 1973; Hallsworth et al., 2003; Barnard et al., 2013; Kakumanu et al., 2013). We found that most *B. subtilis* cells (60 to 70% in each replicate microcosm) do not show any detectable uptake of D_2O after dessication and rehydration (Fig. 3.18) – an indicator of how stressful dry-wet cycles can be even to bacterial species that are considered well-adapted to life in the soil. However, of the cells that did show uptake of D_2O, those attached to *M. fragilis* hyphae took up more of the label than those cells far (i.e. 3 mm away in Euclidean space) from any *M. fragilis* hyphae. Cells *near* but not *on M. fragilis* hyphae – i.e. cells within 20 μm of the hyphae – showed slightly but not significantly higher D_2O uptake than cells far away.

Cells in the TS microcosms were moved around by liquid flow during microcosm washing and rehydration. We therefore only measured cells that were *attached* to a surface – either Nafion or *M. fragilis* – reasoning that attached cells would not have

moved due to liquid flow. By examining microcosms before and after washing, we observed that at the low flow speeds we used (0.5 µL/min), the TS matrix, fungal hyphae, and attached bacteria stayed in place before and after flow, allowing us to classify surface-attached cells as “on”, “near”, or “far” from *M. fragilis* with confidence.

When cells classified as D_2O-labeled (i.e. CD>0.5) were pooled from three replicate microcosms, we found a statistically significant effect of distance category (i.e. “on”, “near”, or “far” from *M. fragilis*) on CD area (Fig. 3.18; n=13 cells on *M. fragilis*, n=10 cells near *M. fragilis*, n=11 cells far from *M. fragilis*, one-way ANOVA of all three categories F-statistic 4.5988, p-value = 0.01782). However, when replicate is added as a factor to the model, neither replicate nor distance category account for variance in CD area (one-way ANOVA of all three categories, distance category p-value = 0.2255, replicate p-value = 0.2248). We are therefore uncertain whether distance category or replicate explains the observed difference in CD area between cells in different distance categories.

A previous, NanoSIMS-based study indicated that *B. subtilis* cells take up water, carbon, and nitrogen from nearby fungal hyphae in dry, oligotrophic conditions (Worrich et al., 2017). Our Raman microspectroscopy approach is consistent with these results. Unlike other single-cell resolution stable isotoping methods like NanoSIMS, Raman microspectroscopy in TS microcosms preserves pore structure since it does not require thin sectioning or dehydration of the sample. Thus our approach allowed measurement of cells not only attached to hyphae or near hyphae, but in nearby pore spaces.

Fungi are thought to be important for facilitating bacterial survival and growth in soils because (a) their hyphae help retain moisture in adjoining soil pores (Gordon et al.,

2008) and (b) they provide nutrient sources through exudation and as a substrate for decomposition (De Boer et al., 2005). By using fungus that was grown in the TS matrix and then heat-killed in place, we rule out the role of exudation in the support of bacterial survival, since exudation is carried out by living fungi. However, the dead fungus can still exude labile carbon, can be decomposed by bacteria to liberate more carbon, and can play a role in water retention. If water retention was the major mechanism by which fungi protect bacteria particularly after dry-wet cycles in soil, we would expect cells that are both *on* and *near M. fragilis* (i.e. in *M. fragilis*-adjoining pores) to show roughly equal amounts of activity after the dry-wet cycle, since the hyphae would slow dry-drown and facilitate wet-up of its whole soil "neighborhood" – the network of soil pores that it touches. That D_2O uptake was slightly but not significantly higher in cells on *M. fragilis* than in cells near *M. fragilis* suggests that the soil water retention role of fungi may indeed be an important mechanism by which fungi protect bacteria from dessication stress, and that direct attachment to dead fungal hyphae may provide an additional advantage, perhaps by providing access to a nutrient substrate during the dry-down phase which protects against the loss of dissolved nutrients during dessication.

Future Applications

The transparent soil model microcosms described in this study – wherein the locations, morphologies, growth dynamics, movements, and even metabolic states of microbes can be resolved non-destructively at the single cell level – opens up a wide variety of possible applications to important questions in soil microbial ecology. In soil and sediment ecology, previously occluded processes like microbial growth and

development, predation and lysis dynamics, migration patterns, conjugation and transduction networks, and interspecies interactions in three-dimensional porous matrices can be monitored by light and fluorescence microscopy. Because TS substrates are mostly pure and inert and do not themselves function as bioavailable sources of carbon or other nutrients, controlled amounts of nutrients can be added to the system in pore water or as "spiked-in" minerals or real soil particles, to test their effects on soil microbiota. Alternatively, the ready growth of fungi in TS microcosms suggests uses for fungal biology of soils, from elucidating the role of fungi as "highways" for bacterial movement through dry soils (Kohlmeier et al., 2005), their critical role in biomass decomposition, and as a natural sources of biomass and nutrients themselves. The compatibility of cryolite with non-destructive ^{13}C tracing suggests a variety of uses to elucidate fundamental processes in soil microbial ecology, from *in situ* tracking of trophic interactions, to monitoring carbon flows in model soils due to viral lysis, to untangling the mechanisms of the widely observed "Birch effect" by direct tracing of ^{13}C fate after dry-wet cycles (Birch,1958; Unger et al., 2010). Moreover, workers in the field may build on TS microcosm systems by combining them with their own existing methods, such as fluorescent *in situ* hybridization (FISH) to identify microbes and their locations *in situ* (a difficult task in natural soils), or fluorescent transcriptional reporter strains to track bacterial physiology in native soil-like environments. Though we have suggested a few possible uses of transparent soil microcosms, their future applications will depend on the questions and creativity of workers in the field.

Acknowledgments

We sincerely thank Fletcher Halliday (University of North Carolina at Chapel Hill) for the kind gift of the wild *Mucor fragilis* strain used in this study; Ethan Garner (Harvard University) for the *B. subtilis* codon-optimized fluorescent protein gene sequences used in strain construction; Lionel Dupuy (James Hutton Institute) for sharing detailed protocols on Nafion functionalization; the UNC Biology Department Light Microscopy Core facility for use of the Zeiss 710 confocal laser scanning microscope and Tony Purdue for training and assistance on this instrument; the UNC Hooker Light Microscopy Core facility for use of the Zeiss 880 confocal laser scanning microscope and Robert Currin for training and assistance on this instrument; Jamie Winshell (University of North Carolina at Chapel Hill) for assistance in strain construction; the Division of Microbial Ecology (University of Vienna) for use of their Zeiss AxioObserver epifluorescence microscope, Leica confocal laser scanning microscope, and Horiba high resolution confocal Raman microspectroscopy system, and Markus Schmid for training and assistance on these instruments.

Figures

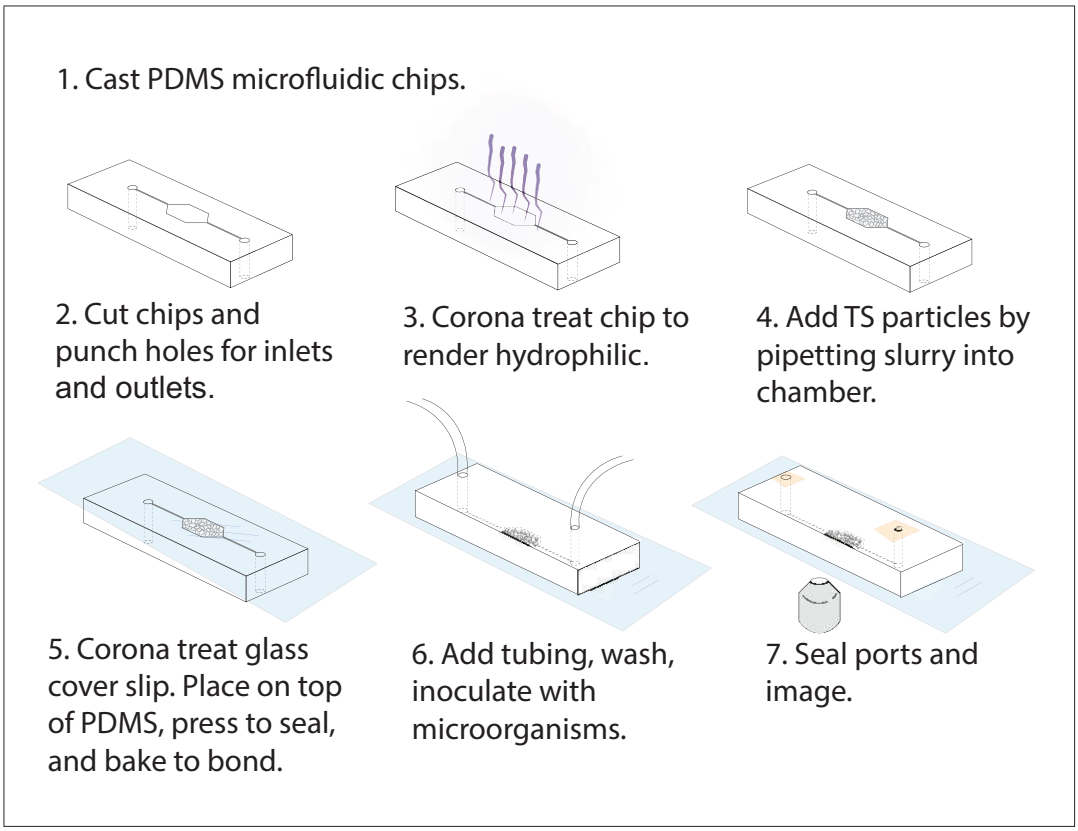

Figure 3.1: Transparent soil (TS) microcosm manufacture process.

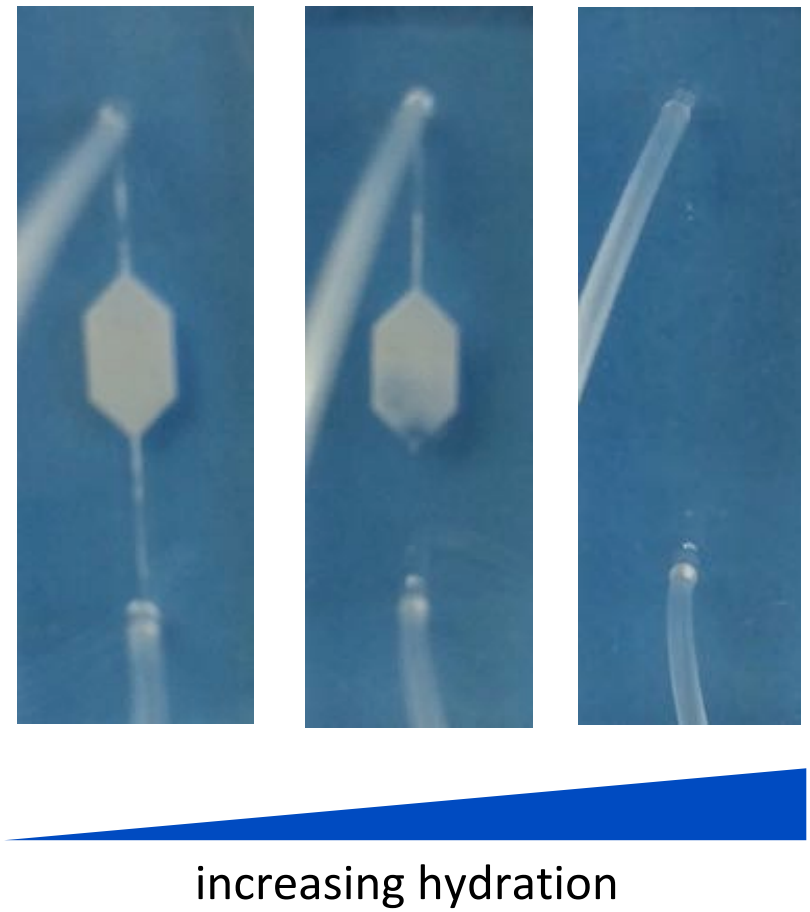

Figure 3.2: 20% ethanol added after chip manufacture hydrates dry, hydrophobic Nafion and renders it transparent. Microfluidics chamber (3 x 5 mm hexagon, with 200 μm wide channels) filled with Nafion and attached by tubing to syringe with 20% ethanol, held in syringe pump. As ethanol is slowly flowed into the microcosm by the syringe pump, the Nafion hydrates and becomes transparent. Rehydrated Nafion can then be washed with media, washing away ethanol and rendering microcosms suitable for cell culture.

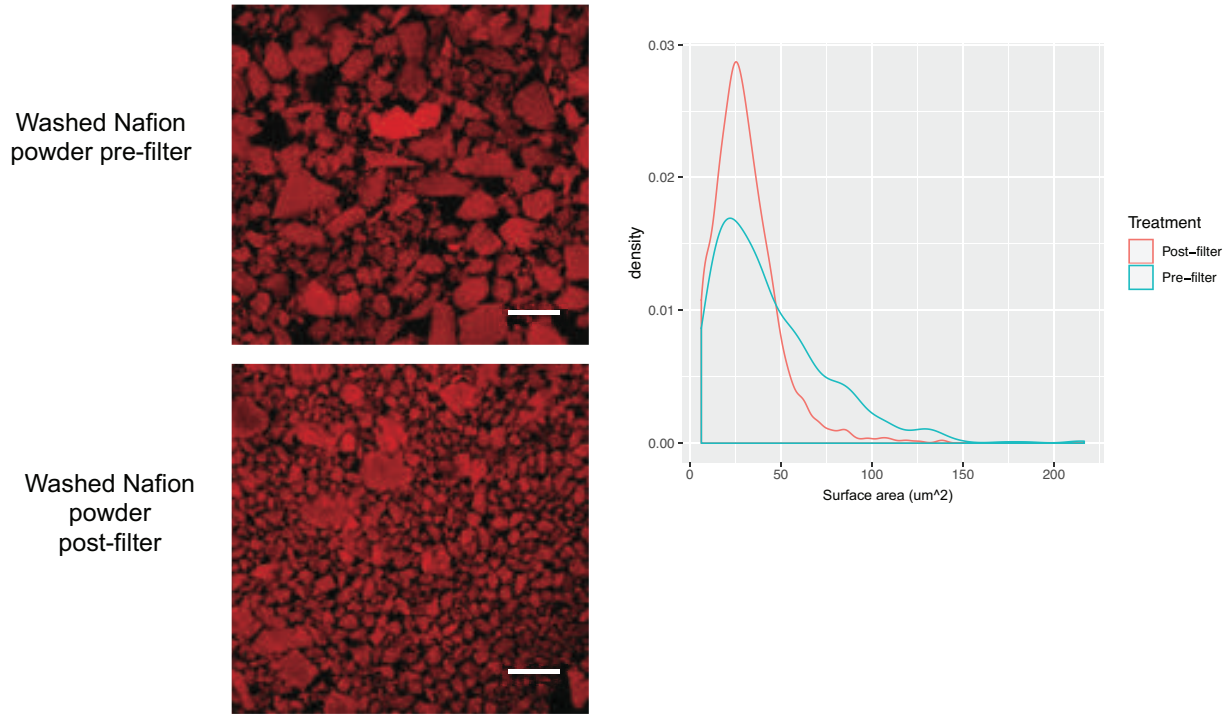

Figure 3.3: Particle size distribution of PowdION® Nafion powder before and after filtering through 40 µm cell strainer. Commercially available Nafion powder was washed (see Methods) and filtered through 40 µm cell strainer. Particles were stained with sulphorhodamine to render particles fluorescent in the RFP channel. (false-colored red). Particles were imaged by confocal microscopy and 15 µm z-stacks flattened into maximum intensity projections. Images were analyzed in Fiji image analysis software by binarizing and applying watershed process, then calculating particle area size, represented in density plot. Scale bar = 100 µm.

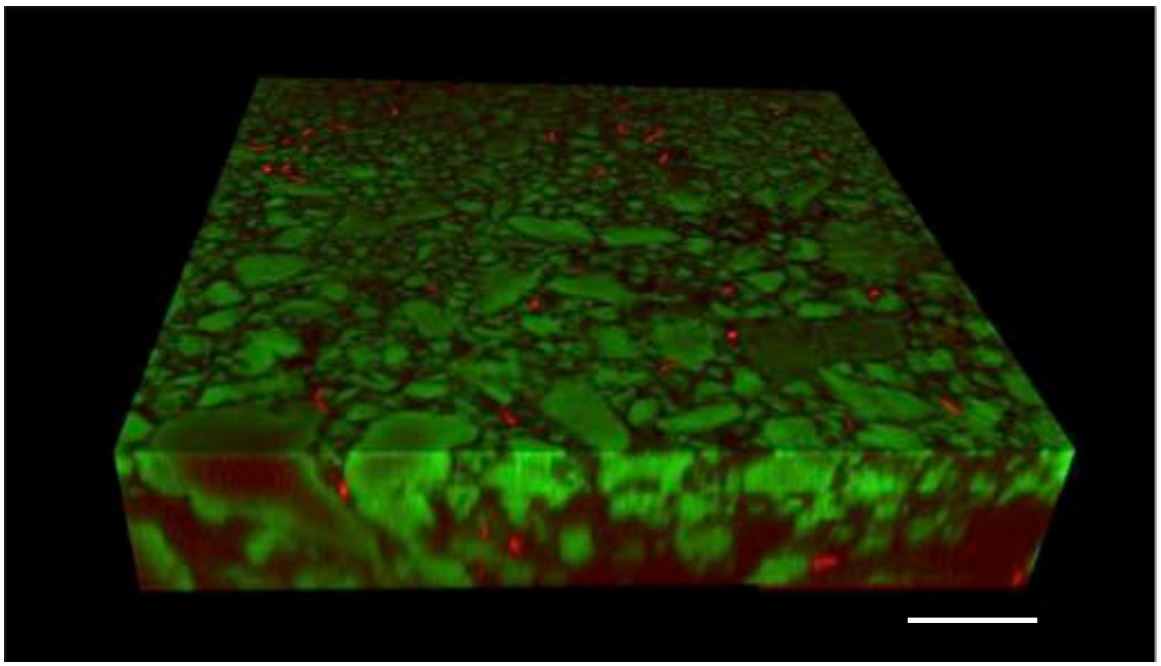

Figure 3.4: Fluorescently-labeled *E. coli* cells can be visualized to 100 µm depth in Nafion matrix by confocal microscopy. Sulphorhodamine-stained Nafion particles (false-colored green), and *E. coli* cells constitutively expressing cyan fluorescent protein (P*spac*^{C}*-cfp*, false-colored red). Three-dimensional confocal rendering obtained from 100 µm deep z-stack. Scale bar = 100 µm.

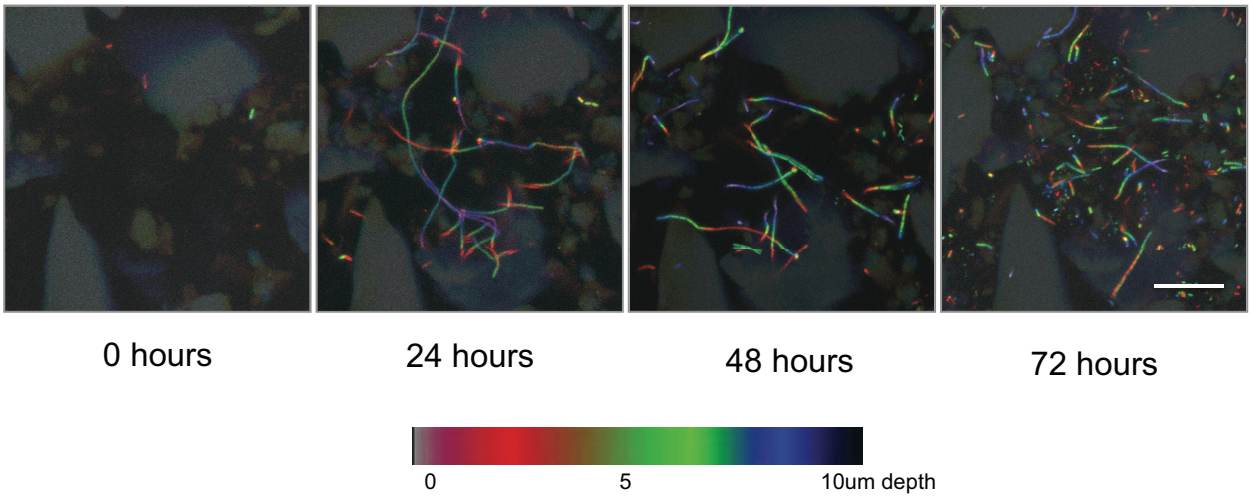

Figure 3.5: Non-destructive imaging of *B. subtilis* in Nafion matrix over time. *B. subtilis* 3610 *eps-tasA* biofilm gene mutant cells expressing constitutive YFP were inoculated into Nafion-filled microcosms in MSgg rich medium, incubated at room temperature (22°C), and imaged over time. Images are ten micron z-stacks flattened into color-coded z-projections. Scale bar = 20 μm.

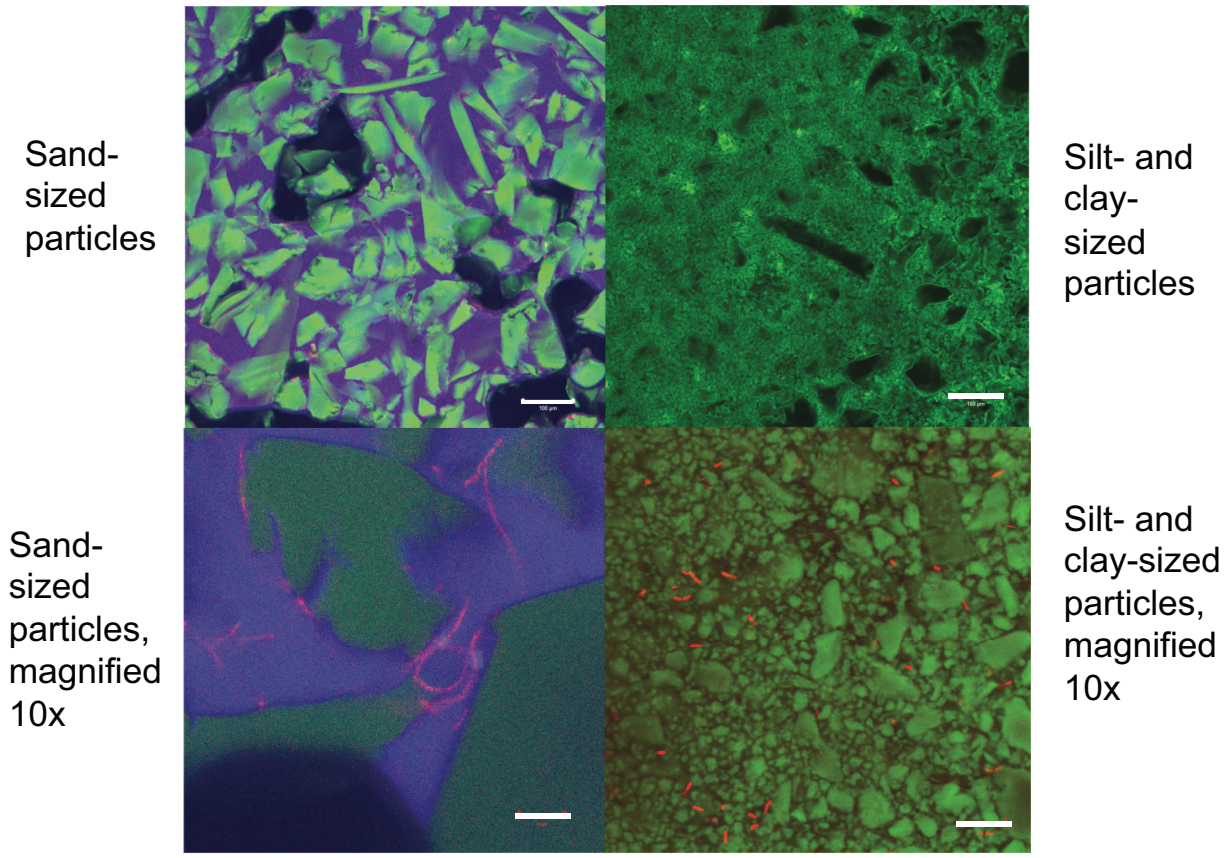

Figure 3.6: Effect of particle size on pore structure and microbial habitat. *B. subtilis* 3610 cells constitutively expressing cyan fluorescent protein were inoculated into mesocosms (5 mm wells with cover glass bottom) with different particle size distributions of Nafion (>100 µm or <30 µm fractions, obtained by dry-sieving ground Nafion through soil sieve). Mesocosms were saturated with MSgg medium and incubated at 24°C for 16 hours. Sulphorhodamine-stained Nafion particles (false-colored green), *B. subtilis* 3610 cells (false-colored red), fluorescein liquid tracer (false-colored blue). Larger particle sizes result in larger pores, putatively affording more space for *B. subtilis* to take on a more filamentous growth habit. Top scale bars = 100 µm, bottom scale bars = 10 µm.

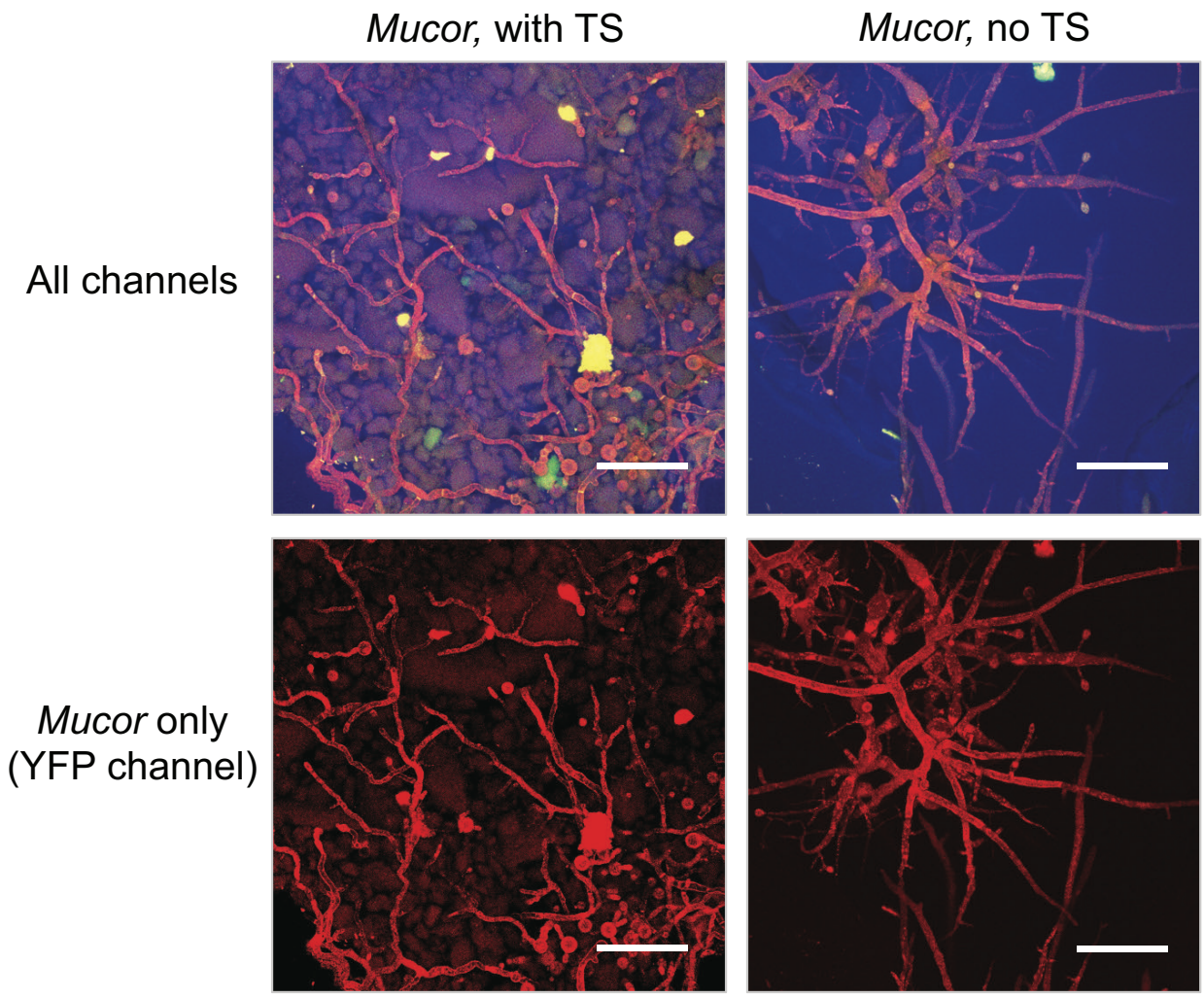

Figure 3.7: Growth in Nafion TS matrix changes *M. fragilis* morphology. *M. fragilis* spores were inoculated into microfluidic chips filled with or without Nafion (see Chapter 4) and incubated for 48 hours at 30°C in MSN minimal salts medium with 2% glucose. Confocal micrographs of 25 µm z-stacks flattened into maximum intensity projections; sulphorhodamine-stained Nafion (false-colored green), *Mucor* autofluorescence in YFP channel (false-colored red), PMT channel (false-colored blue). *Mucor* hyphae grown in TS matrix have less variation in hyphal width and more tortuous growth habit (as defined by deviation from straight lines of growth) than *Mucor* hyphae grown without TS. Scale bar=100 µm.

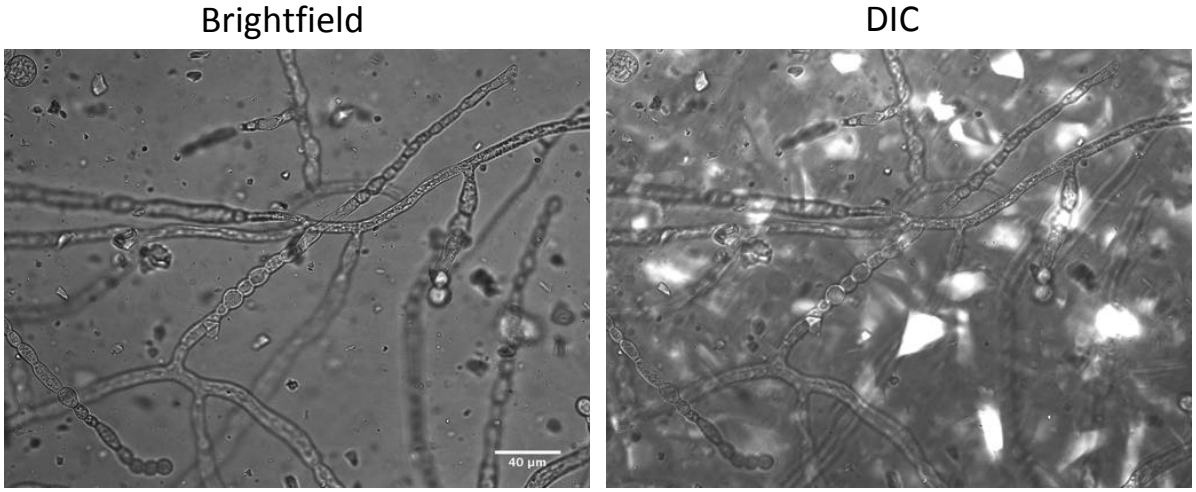

Figure 3.8: Cryolite crystals are invisible under brightfield illumination, but visible under DIC. *M. fragilis* fungus was grown from spores for 24 hours at 30°C in a microfluidic chamber packed with crystalline cryolite and saturated with aqueous minimal salts growth medium (MSN, minimal salts with free ammonium and 2% glucose). Images of the fungus were taken through the cryolite matrix, about 25 µm up from the cover slip. Images taken on Zeiss Axio Observer widefield light microscope, 40x objective, water immersion lens, under brightfield or DIC illumination. Scale bar = 40 µm.

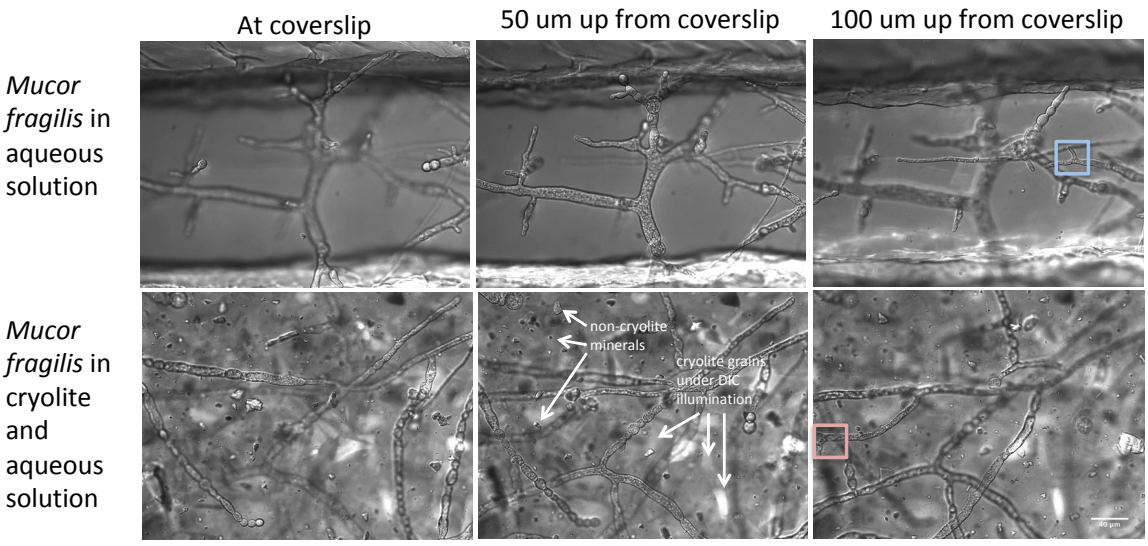
At coverslip
50 um up from coverslip
100 um up from coverslip
Mucor fragilis in aqueous solution
Mucor fragilis in cryolite and aqueous solution
non-cryolite minerals
cryolite grains under DIC illumination

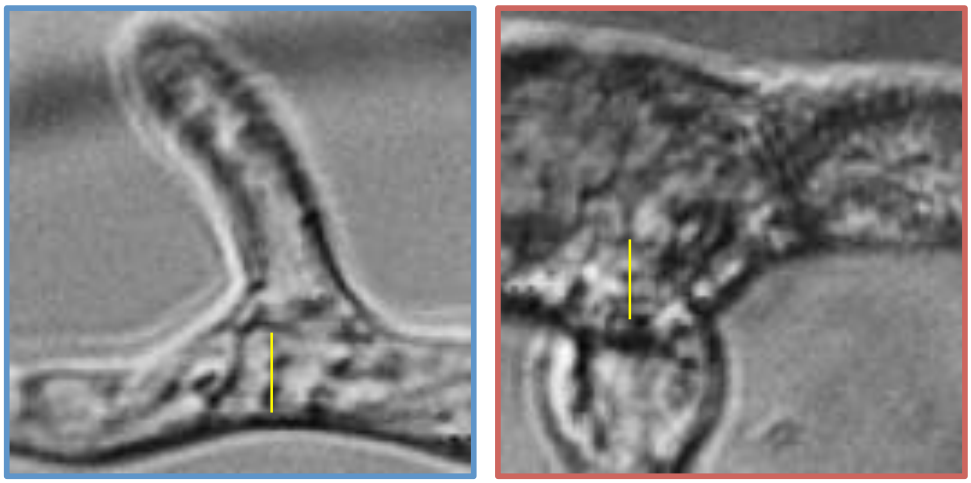

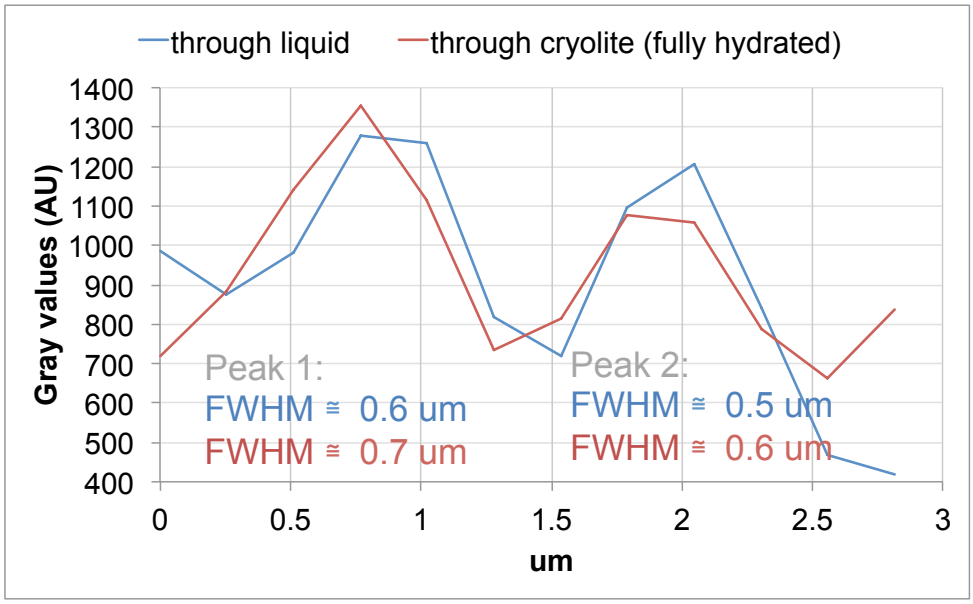
through liquid
through cryolite (fully hydrated)
Gray values (AU)
1400
1300
1200
1100
1000
900
800
700
600
500
400
0
0.5
1
1.5
2
2.5
3
um
Peak 1:
FWHM ≅ 0.6 um
FWHM ≅ 0.7 um
Peak 2:
FWHM ≅ 0.5 um
FWHM ≅ 0.6 um

Figure 3.9: Imaging through hydrated cryolite on compound microscope with DIC illumination results similar image quality and resolution as imaging through aqueous solution. *M. fragilis* was grown from spores in a microfluidic chamber packed with crystalline cryolite and saturated with aqueous minimal salts growth medium. Images of the fungus were taken through the cryolite matrix (bottom row), or through aqueous minimal salts medium alone in the inlet of the microfluidics device (top row). Images were taken on Zeiss Axio Observer widefield light microscope, 40x objective, water immersion lens, under DIC III illumination. Scale bar is 40 μm. Image resolution is 3.9 pixels/micron, 16-bit bit depth. Sub-micron fine features of the fungus such as textural bumps on the hyphal surface are resolved even through 100 μm of liquid-saturated cryolite matrix. A 3 μm line profile (yellow line in bottom images) was taken of two bumps on *M. fragilis* in liquid (blue border) and *M. fragilis* in cryolite (red border) imaged 100 μm into microfluidics chamber. Full width at half-maximum (FWHM) values were estimated for each bump as an estimate of resolution.

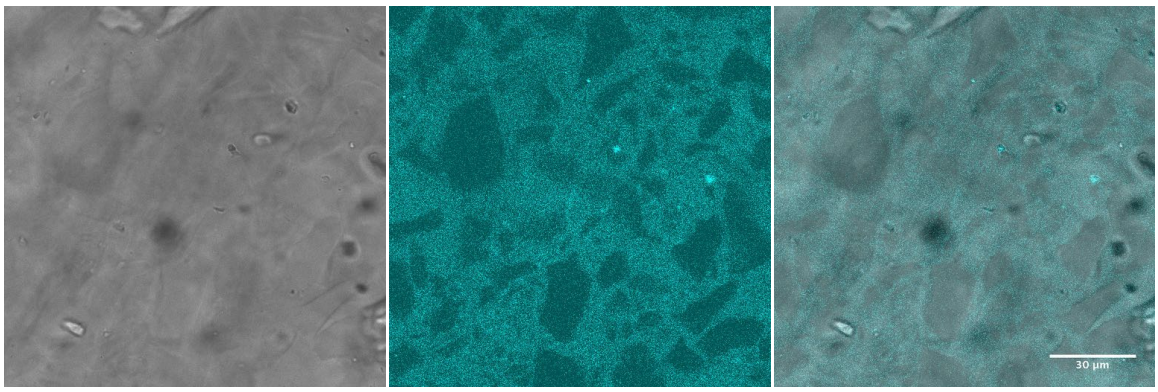

Figure 3.10: Visualization of pore space in cryolite matrix with AlexaFluor647 dye. Cryolite was packed into a microwell microscope slide, saturated with water containing 10 ug/mL AlexaFluor 647 amine fluorophore, and imaged on an inverted confocal laser scanning microscope. A single slice about 25 µm deep into the cryolite matrix is shown here. Cryolite particles are difficult to visualize in the PMT channel, but using a fluorescent liquid tracer to stain the pore space, cryolite particle edges become visible. Scale bar = 30 µm.

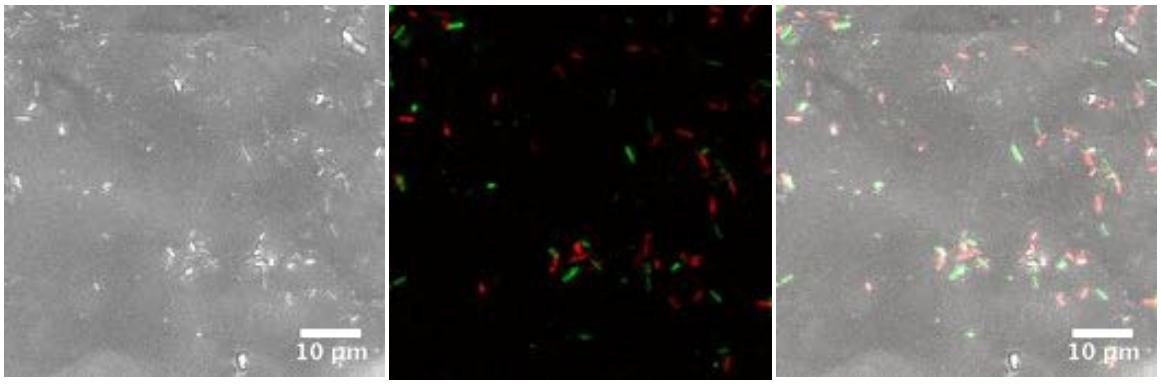

Figure 3.11: Fluorescently-labeled *Bacillus subtilis* 3610 in cryolite matrix. Maximum intensity projection of fluorescently-labeled *B. subtilis* in a packed matrix of ground crystalline cryolite, 35 μm z-stack. *B. subtilis* 3610 wild-type expressing constitutive YPet *amyE::*P*spac*^{C}*-Ypet-chlor*^{R} (green), *B. subtilis* 3610 chitosanase mutant expressing constitutive mTurquoise2 *csn::erm amyE::*P*spac*^{C}*-mTurquoise2-chlor*^{R} (red). Confocal laser scanning microscope, 40x glycerol immersion objective.

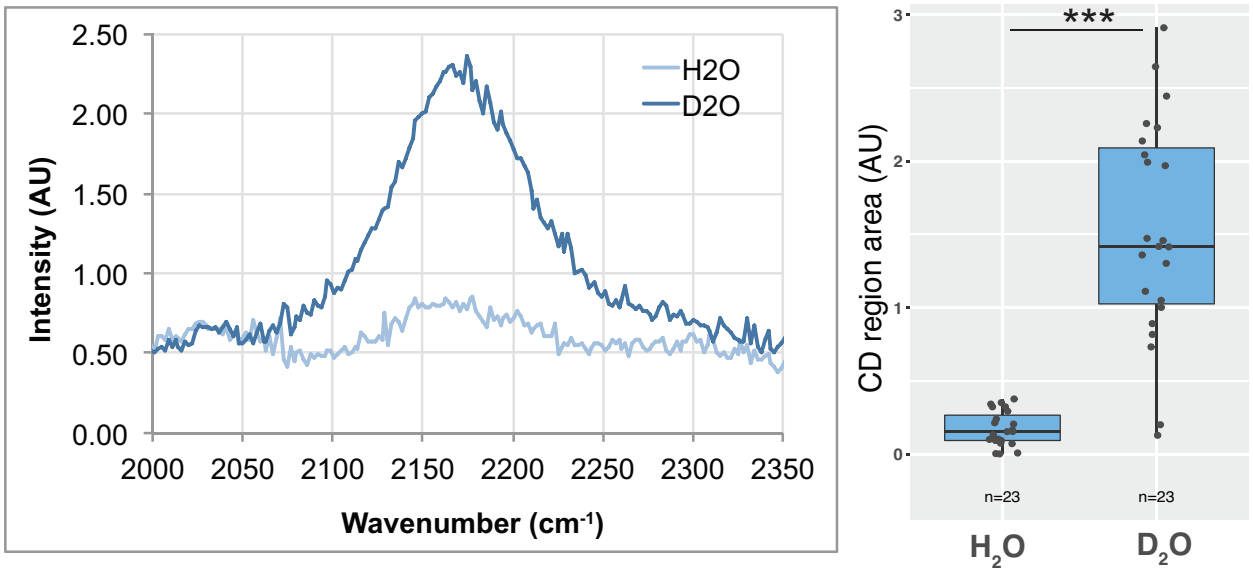

Figure 3.12: Detection of CD peak shifts and D_2O enrichment in *B. subtilis* cells in Nafion TS microcosms. *B. subtilis* 3610 cells were grown overnight at 37°C shaking in MSN minimal salts medium with 2% glucose made with either regular water or 50% heavy water (deuterium oxide, D_2O). Cells were then inoculated into separate Nafion-filled TS microcosms. Raman spectra of single cells were obtained by microspectroscopy within the Nafion matrix, from cells embedded anywhere from 15 to 85 µm deep within the matrix. Average background subtracted spectra of 23 cells grown in H_2O or D_2O (above) show a broad peak in the CD region of the spectrum between 2050 and 2300 in D_2O-labeled cells. CD region for individual cell spectra was calculated as the area under the curve between 2150 and 2200 cm^{-1}. Each dot (right) represents CD region for an individual background-subtracted cell spectrum. D_2O-labeled cells have larger CD area (One-way ANOVA F-statistic = 45.88, p-value $1.99ex10^{-8}$).

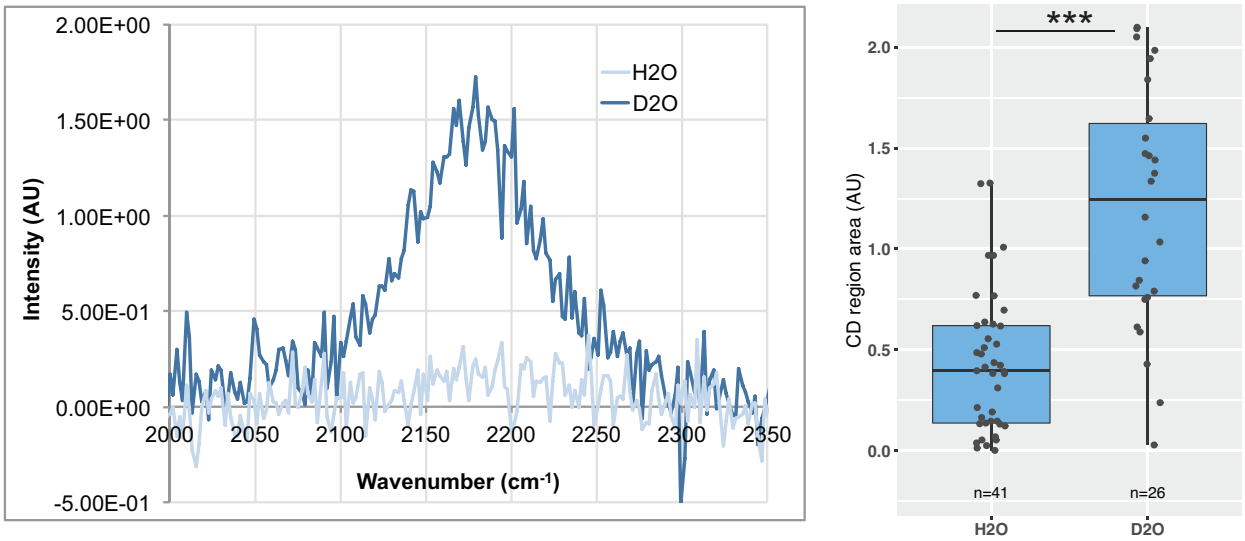

Figure 3.13: Cryolite-based TS microcosms are compatible with Raman microspectroscopy, and allow detection CD peak. *B. subtilis* 3610 cells were grown overnight at 37°C shaking in MSN minimal salts medium with 2% glucose made with either regular water or 50% heavy water (deuterium oxide, D_2O). Cells were then inoculated into separate cryolite-filled microcosms. Raman spectra of single cells were obtained by microspectroscopy within the cryolite matrix, from cells embedded anywhere from 15 to 75 µm deep within the matrix. Average background subtracted spectra of 23 cells grown in H_2O or D_2O show a broad peak in the CD region of the spectrum between 2050 and 2300 in D_2O-labeled cells. CD region for individual cell spectra was calculated as the area under the curve between 2150 and 2200 cm^{-1}. Each dot on dotplot represents CD region for an individual background-subtracted cell spectrum. D_2O-labeled cells have higher CD area (One-way ANOVA F-statistic = 33.49, p-value 2.16×10^{-7}).

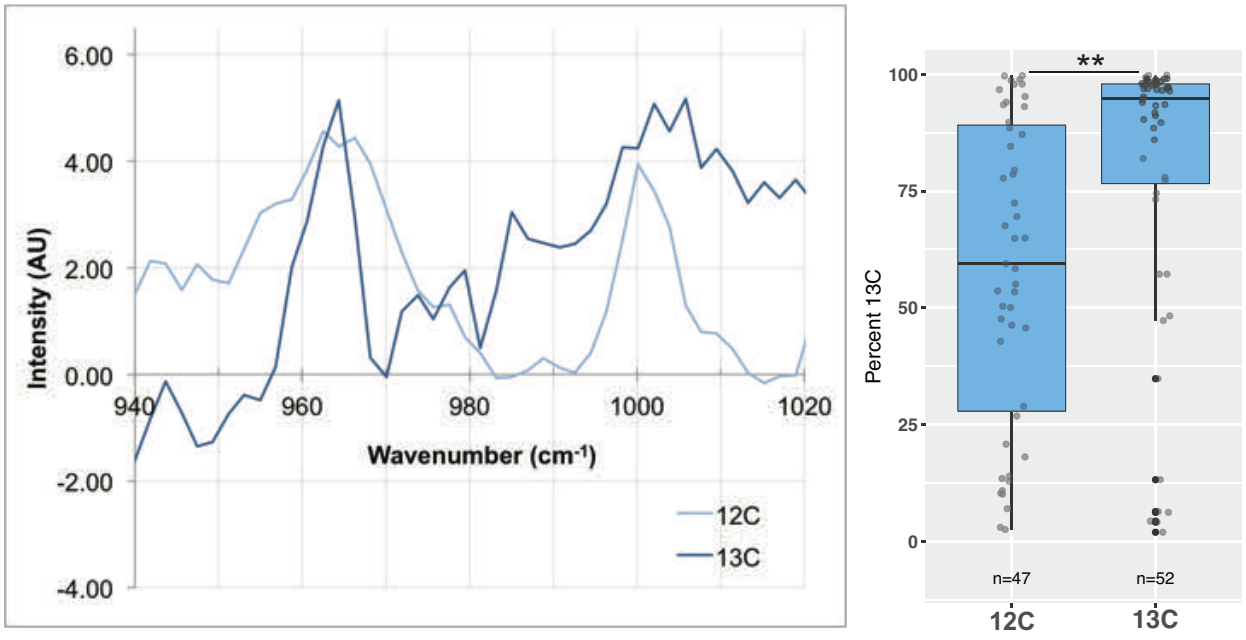

Figure 3.14: Detection of phenylalanine peak shifts and ^{13}C enrichment in *B. subtilis* in cryolite TS microcosms. *B. subtilis* 3610 cells were grown overnight at 37°C shaking in MSN minimal salts medium containing 2% of either regular ^{12}C glucose or isotopically-labeled ^{13}C glucose. Cells were then inoculated into separate Nafion-filled TS microcosms. Raman spectra of single cells were obtained by microspectroscopy within the Nafion matrix, from cells embedded anywhere from 15 to 75 µm deep within the matrix. Average background subtracted spectra of 47 or 52 cells grown in ^{12}C or ^{13}C glucose respectively are shown. Percent ^{13}C is calculated individually for each background subtracted cell spectrum as $(H_{966}/(H_{966} + H_{1003}))x100$, where H_{966} is peak height at 966 cm^{-1} (^{13}C phenylalanine peak) and H_{1003} is peak height at 1003 cm^{-1} (^{12}C phenylalanine peak). Each dot represents Percent ^{13}C for an individual background-subtracted cell spectrum. ^{13}C-labeled cells have significantly higher Percent ^{13}C values than ^{12}C-labeled cells (One-way ANOVA F-statistic = 11.124, p-value = 0.001209).

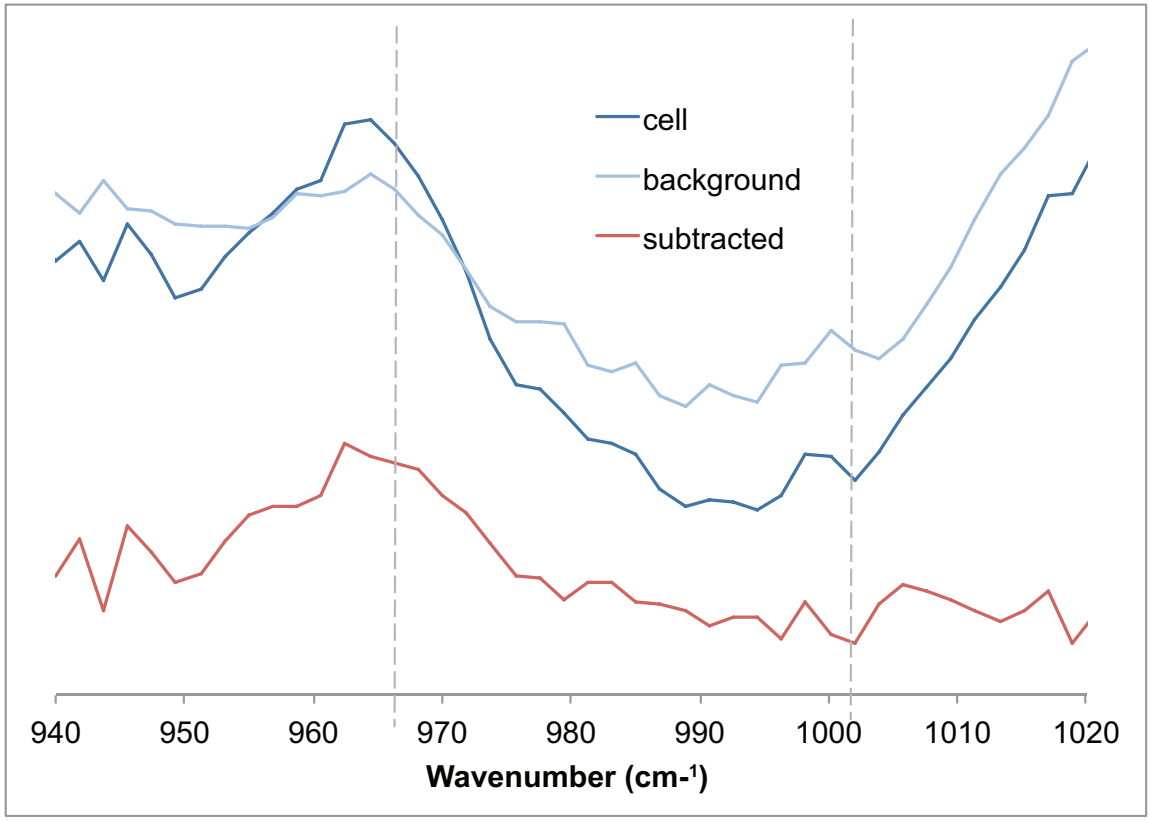

Figure 3.15: High Nafion background around 965 cm^{-1} interferes with ^{13}C phenylalanine peak at 966 nm, resulting in unlabeled ^{12}C-rich cells being misclassified as ^{13}C labeled. Representative single cell spectrum showing ^{12}C-labeled cell spectrum, a background spectrum taken 20 μm away from the cell and capturing the Raman spectrum of the Nafion matrix itself, and the subtracted spectrum (cell spectrum minus background).

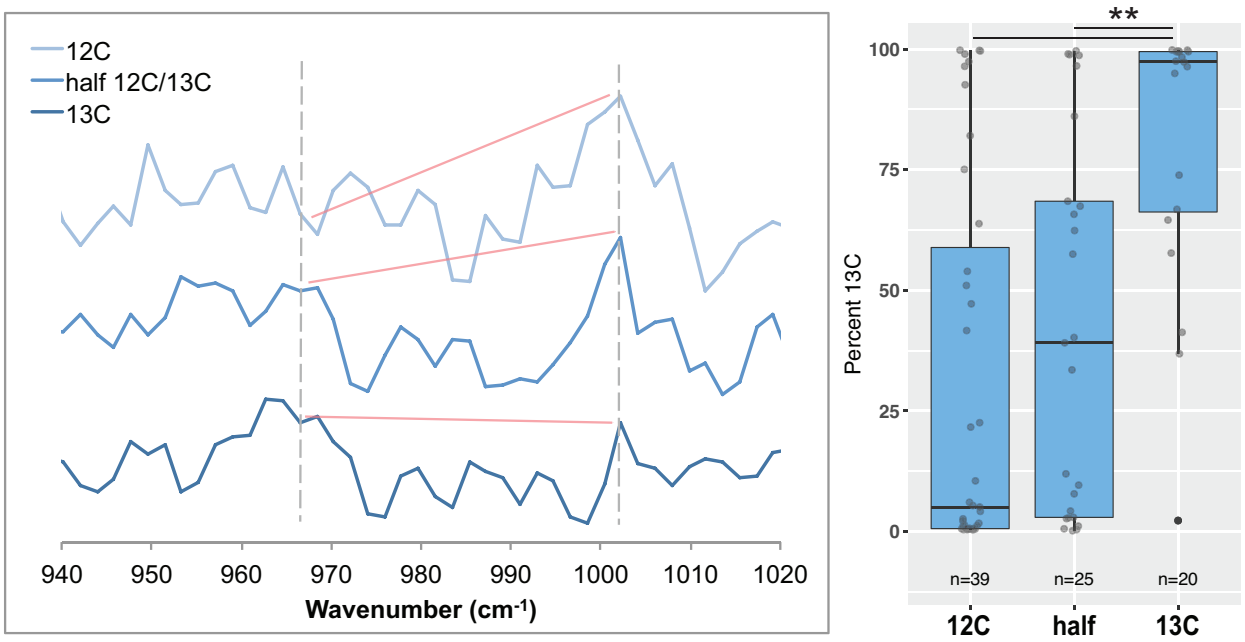

Figure 3.16: Detection of phenylalanine peak shifts and ^{13}C enrichment in *B. subtilis* in cryolite TS microcosms. *B. subtilis* 3610 cells were grown overnight at 37°C shaking in MSN minimal salts medium containing 2% of either regular ^{12}C glucose, radiolabeled ^{13}C glucose, or 1% ^{12}C glucose and 1% ^{13}C glucose (50% ^{13}C, or "half" treatment). Cells were then inoculated into separate cryolite-filled TS microcosms. Raman spectra of single cells were obtained by microspectroscopy within the cryolite matrix, from cells embedded anywhere from 15 to 85 µm deep within the matrix. Average background subtracted spectra of cells grown in ^{12}C, ^{13}C, or half-^{13}C glucose respectively are shown. Pink lines indicate the decreasing peak height of the 1003 peak relative to the 966 peak with increasing ^{13}C treatment. Percent ^{13}C is calculated individually for each background subtracted cell spectrum as $(A_{966}/(A_{966} + A_{1003}))x100$, where A_{966} is peak height at 966 cm^{-1} (^{13}C phenylalanine peak) and A_{1003} is peak height at 1003 cm^{-1} (^{12}C phenylalanine peak). Each dot on dotplot represents Percent ^{13}C for an individual background-subtracted cell spectrum. ^{13}C-labeled cells have significantly higher Percent ^{13}C values than ^{12}C-labeled cells and half-labeled cells (One-way ANOVA for comparison of all three categories F-statistic = 10.52, p-value 0.0001; Tukey-Kramer HSD p-value <0.005 when comparing ^{13}C-labeled cells to both ^{12}C- and half-labeled cells). However, half-labeled cells are difficult to distinguish from ^{12}C-labeled cells due to the large amount of variation in both distributions (Tukey-Kramer HSD p-value = 0.58 when comparing ^{12}C-labeled cells to half-labeled cells).

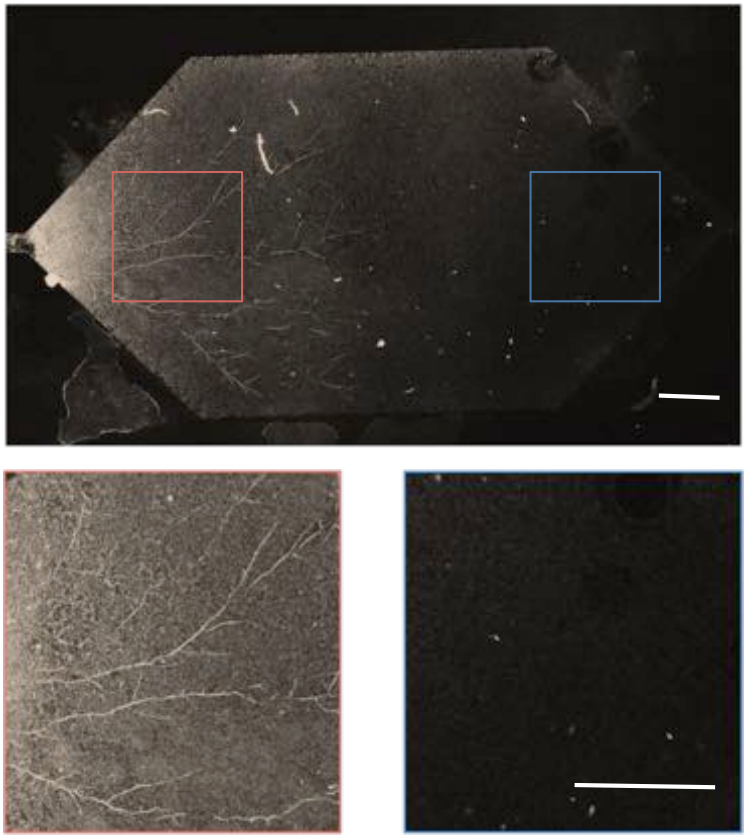

Figure 3.17: *B. subtilis* cells grown with dead *Mucor* in Nafion TS microcosm undergo a dry-wet cycle, mimicking the dry-down and wet-up of soils. Because spores were trapped within the Nafion matrix on the side where they were inoculated, one side of the microcosm is filled with hyphae, while the other side remains empty. Confocal microscopy in GFP channel shows autofluorescent *Mucor* hyphae on one side of microcosm (above, and left inset), and no growth on the other side (right inset). Scale bar is 400 μm in both top micrograph and insets. *B. subtilis* cells measured were classified as either "on" (cells attached to *M. fragilis* hyphae), "near" (cells attached to Nafion on *Mucor*-inoculated side of microcosm, within 20 μm radius of nearest hypha), or "far" (cells attached to Nafion on side of microcosm without *Mucor*). "Far" cells are 3 mm or more away from nearest *M. fragilis* hyphae.

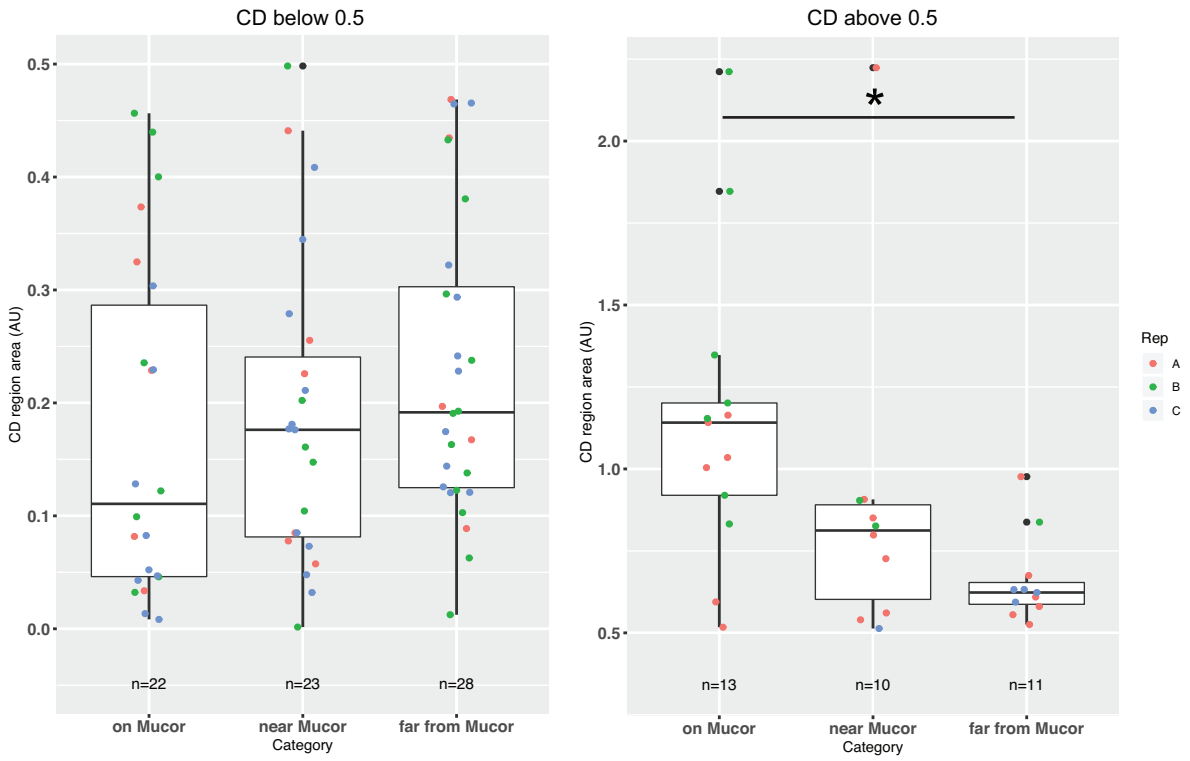

Figure 3.18: *B. subtilis* cells on *Mucor* are more metabolically active than cells far from *Mucor* after dry-wet cycle in Nafion-based transparent soil microcosms. Most cells (~60-70 percent) have no detectable activity after a dry-wet cycle, regardless of distance from *Mucor* (left panel, all cells with CD area less than 0.5, indicating no activity detectable by D_2O uptake). However, cells that did take up D_2O took up more of the label when on *Mucor* than cells far from *Mucor* (right panel, one-way ANOVA of all three categories F-statistic 4.7194, p-value 0.0160; Tukey-Kramer HSD p-value <0.0131 for cells on *Mucor* vs far from *Mucor*). Results pooled from three separate biological replicate experiments in three separate TS microcosms, indicated by color.

Criterion	Nafion	Cryolite
Biocompatible?	Yes	Yes
Inert (i.e. not easily metabolizable or decomposable by bacteria or fungi)?	Yes	Yes
Submicron resolution through 100 μm of matrix?	Yes	Yes
Bacteria visible with fluorescence through 100 μm of matrix?	Yes	Yes
Bacteria visible without fluorescence through 100 μm of matrix?	No	Yes
Ready to use without pre-treatment?	No	Yes
Particles visible under brightfield microscopy?	Yes	No
Particles visible under DIC and PMT microscopy?	Yes	Yes
Particles autofluorescent?	Yes	No
Particles visible after staining with fluorescent dye?	Yes	No
Pore water visualizable?	Yes	Yes
Commercially available?	Yes	Somewhat (see text)
Inexpensive?	No	Yes
Pure?	Yes	Somewhat (see text)
Desired particle size distributions (between 1 μm and ~5 mm) easy to obtain?	Somewhat (see text)	Yes
Amenable to drying and rewetting?	Somewhat (see text)	Yes
Cation-exchanging?	Yes	Yes
Compatible with single-cell D_2O tracing by Raman?	Yes	No
Compatible with population-level D_2O tracing by Raman?	Yes	Yes
Compatible with single-cell ^{13}C tracing by Raman?	No	No
Compatible with population-level ^{13}C tracing by Raman?	No	Yes

Table 3.1: Summary table comparing Nafion and cryolite as transparent porous substrates for applications in soil microbial ecology.

CHAPTER 4: RAPID MANUFACTURE OF MICROFLUIDIC DEVICES FOR CELL CULTURE USING CRAFT EPOXY AND STICKERS

Summary

Microfluidic devices are versatile and helpful tools for a wide variety of applications, particularly cell culture and microscopy. Here we present a method for inexpensive and rapid manufacture of microfluidic devices using vinyl-cut stickers, craft epoxy, and PDMS – a gas-permeable biocompatible silicone polymer commonly used for microfluidics device manufacture. Briefly, microfluidic devices are designed using vector drawing or free CAD software, the design is cut into adhesive vinyl stickers using a vinyl cutter, stickers are weeded and stuck to a block of PDMS, and epoxy is poured over the stickers and allowed to set to produce a master for casting PDMS-based microfluidic devices. The epoxy masters thus produced are durable, reusable, and much less expensive and easier to produce than conventional silicon microfluidic masters. Microfluidic devices with features 250 μm and larger are produced with reasonable fidelity using this method, and enable high resolution imaging of cells cultured within the devices. The depth of features produced in the final microfluidics device is constrained by the thickness of vinyl used to produce the stickers – approximately 70 μm. The method allows for rapid design iterations of devices and helps move microfluidics device manufacture out of clean rooms and into "makerspaces" and lab benches.

Introduction

Microfluidic devices have enabled many creative experiments and thereby helped answer many fundamental biological questions, particularly in microbiology and cell biology. We have developed a simple and inexpensive protocol for designing and building microfluidics devices at the lab bench at scales suitable for microbiological and mammalian cell culture. Our aim is to enable biologists and those new to microfluidics manufacture to quickly and easily design and build their own devices to advance their research goals.

Previous work has shown that durable epoxy masters can be cast from already-produced PDMS devices (Estévez-Torres et al., 2009). However, this is not useful if one is not working from an already-made PDMS device. Armani and colleagues cast epoxy masters directly from vinyl cut stickers still stuck to their backing (Armani et al., 2009). However, in our hands, the quick-cure epoxy used in that protocol bonded too quickly and strongly to the sticker backing, producing a master with poor resolution, and a number of bubbles. Pouring epoxy directly on the vinyl stickers also produces aberrations due to the buckling of the backing.

We combined and optimized these to cast reusable epoxy masters from vinyl cut stickers adhered to a cure block of PDMS. This method is appropriate to produce devices of uniform height, constrained by the height of the cut vinyl – about 70 μm. Features produced by this method can only be 250 μm wide or larger. This method is not appropriate for devices where an ultra-strong PDMS-glass bond is required – i.e. devices where strong shear forces will occur due to high flow rates.

Devices produced by this method are not as perfect as those produced by conventional silicon SU-8 masters – features have rough edges and texture of vinyl results in micropatterned roughness of final PDMS chips. However, they are a fraction of the price of silcon masters (dollars for the cost of vinyl and craft epoxy versus about $250 for a silicon master). Whether the imperfections produced by this method are tolerable will depend on the final application. For our purposes, the devices produced by this method were sufficient to enable reproducible microbial growth and high-resolution microscopy within the chambers. For some users, the method may be most helpful to rapidly and inexpensively iterate through various microfluidic designs before creating or ordering a more durable and perfect silicon master.

Protocol

1. Design master in Adobe Illustrator or TinkerCAD (free open source software).
    a. Channels and features should be designed to be not less than 250 μm.
    b. Drawing simple geometric shapes saved as independent overlapping features facilitates accurate cutting. To make a channel with an inlet, for example, draw a circle to represent the inlet and a rectangle to represent the channel and overlap the two shapes rather than merging them.
2. Cut design on vinyl cutter and carefully weed.
3. Cast PDMS block by mixing Sylgard 184 PDMS (Dow) 10:1 base to curing agent, mixing, pouring in a Petri dish or other container of appropriate size, and curing for 1 hour.

a. The amount of PDMS is not critical; the area of cast PDMS should be large enough to accommodate the vinyl-cut design, and the height of the PDMS should be 5 mm or more to facilitate strong curing.

4. Stick vinyl stickers onto cast PDMS.
    a. Use of sticker contact paper facilitates this process. Stick contact paper to front of vinyl-cut design, remove backing, and stick whole design to PDMS. Roll a PCR-plate sealer over the contact paper to ensure a strong bond of stickers to the PDMS, then carefully remove contact paper to reveal vinyl-cut design.
5. Mix craft epoxy, pour over PDMS master, and cure according to manufacturer's instruction.
    a. Using standard lab tape or Scotch tape to cover the sides of the container used for PDMS casting (for example, the Petri dish that PDMS was poured into) will facilitate the removal of the final epoxy master. Tape any Petri dish polystyrene that will come into contact with the epoxy before pouring.
    b. We used ClearCast slow-cure self-degassing epoxy, with positive results. The slow cure time leaves time to mix and for epoxy to penetrate all crevices of the vinyl-cut design, and allows time for full degassing, leaving no bubbles in the final master. A 24 hour cure time at room temperature resulted in a strong durable final master.
6. Carefully remove epoxy after curing. Remove vinyl stickers, and place in new container with mold features facing up.

7. Pour PDMS over epoxy master to make chips.
8. Punch holes and bond using plasma oven, handheld corona treater, or chemical treatment methods to finish microfluidic devices.
    a. To make TS microcosms, prepare Nafion or cryolite as detailed in Chapter 3, pipette 1:1 particle:liquid into chamber, and bond as described above (Fig. 3.1.

Results

We created four-chamber chips that allowed for four separate experiments to be run and imaged on a single microscope slide. Resultant chambers are about 50 μm deep (the width of the original vinyl used to cast the epoxy master). High quality confocal images were obtained from deep (50 μm) z-stacks of fungi cultured in chambers (Figure 4.2). This method preserved features like channels as thin as 250 μm wide (Figure 4.1). The chambers are compatible with creation of Nafion or cryolite-based “transparent soil” microcosms, by pipetting slurry into chambers – in this case, 0.75 uL volume of 1:1 particle:liquid slurry per chamber – prior to bonding (see Fig. 3.1 for microfluidics setup).

Discussion

Design features should be 250 μm or larger to avoid collapse of final features, particularly channels. Collapse occurs due to the difficulty of weeding sticker features smaller than 250 μm, and due to epoxy not fully perfusing smaller channels. Our vinyl cutter cut rectangles between 220 and 280 μm wide, indicating that the tolerance of the

method is +/- 30 μm for features 250 μm large. We found that it is to design inlets and channels as two separate features, where inlets are depicted as closed circles are channels are depicted as closed rectangles overlapping those circles. This is because the vinyl cutter then cuts those features separately, resulting in better symmetry. When the cutter cuts “lollipop” shaped features, like where inlets meet channels, the two sides of the “lollipop” become asymmetrical because of small differences in the curvature of the cutter blade.

Careful weeding of vinyl cut stickers is critical, requiring use of a sharp blade on the vinyl cutter and a deep cut setting. Adhesion of vinyl stickers to PDMS is important to avoid buckling. A firm seal can be obtained by using a plate sealer roller. Self-degassing slow set epoxy is also critical to avoid bubbles. Epoxy cannot be degassed in a vacuum chamber because bubbles produced through degassing will unstick vinyl from PDMS, resulting in buckling.

The epoxy master can be used repeatedly for PDMS casting – we have used it for a dozen uses without loss of fidelity. Washing master gently with dish soap and water is important after every few casts in order to remove impurities and oils so that final bond between PDMS and glass is strong. Bonding between PDMS devices cast using this method and glass is not as strong as PDMS cast from standard SU-8 masters, due to micropatterning of PDMS due to roughness of original vinyl. Pressing PDMS to glass firmly and evenly for about 30 seconds after plasma treatment is necessary for a strong bond.

Acknowledgments

We sincerely thank the UNC BeAM (“Be A Maker”) Network for generous, free access to vinyl cutters and vinyl, as well as training and assistance on the vinyl cutter instrument.

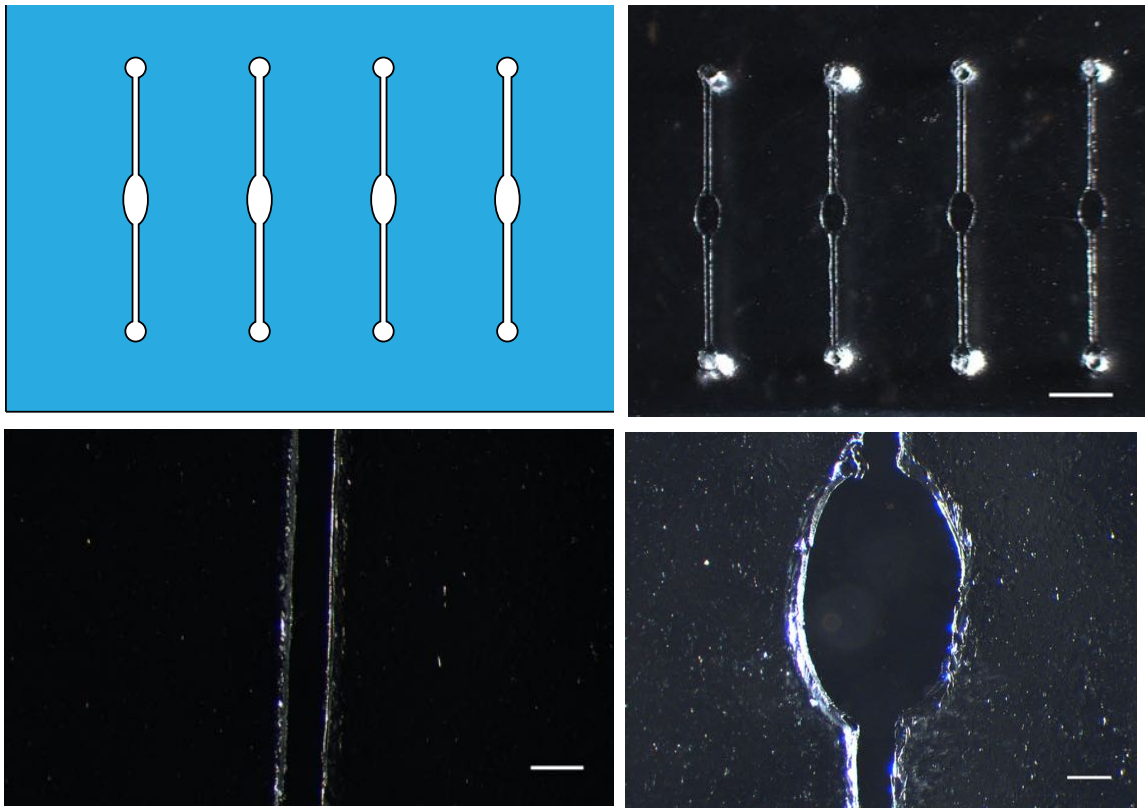

Figure 4.1: PDMS chips constructed from vinyl-cut masters. Top left: microfluidics design in Adobe Illustrator. Top right: final chambers cast in PDMS with holes punched in inlet and outlet. Scale bar = 3 mm. Bottom left: inlet channel 250 μm wide shows even width and no collapse. Scale bar = 300 μm. Bottom right: chamber shows roughness around edges but clear smooth interior surface for imaging. Scale bar = 300 μm.

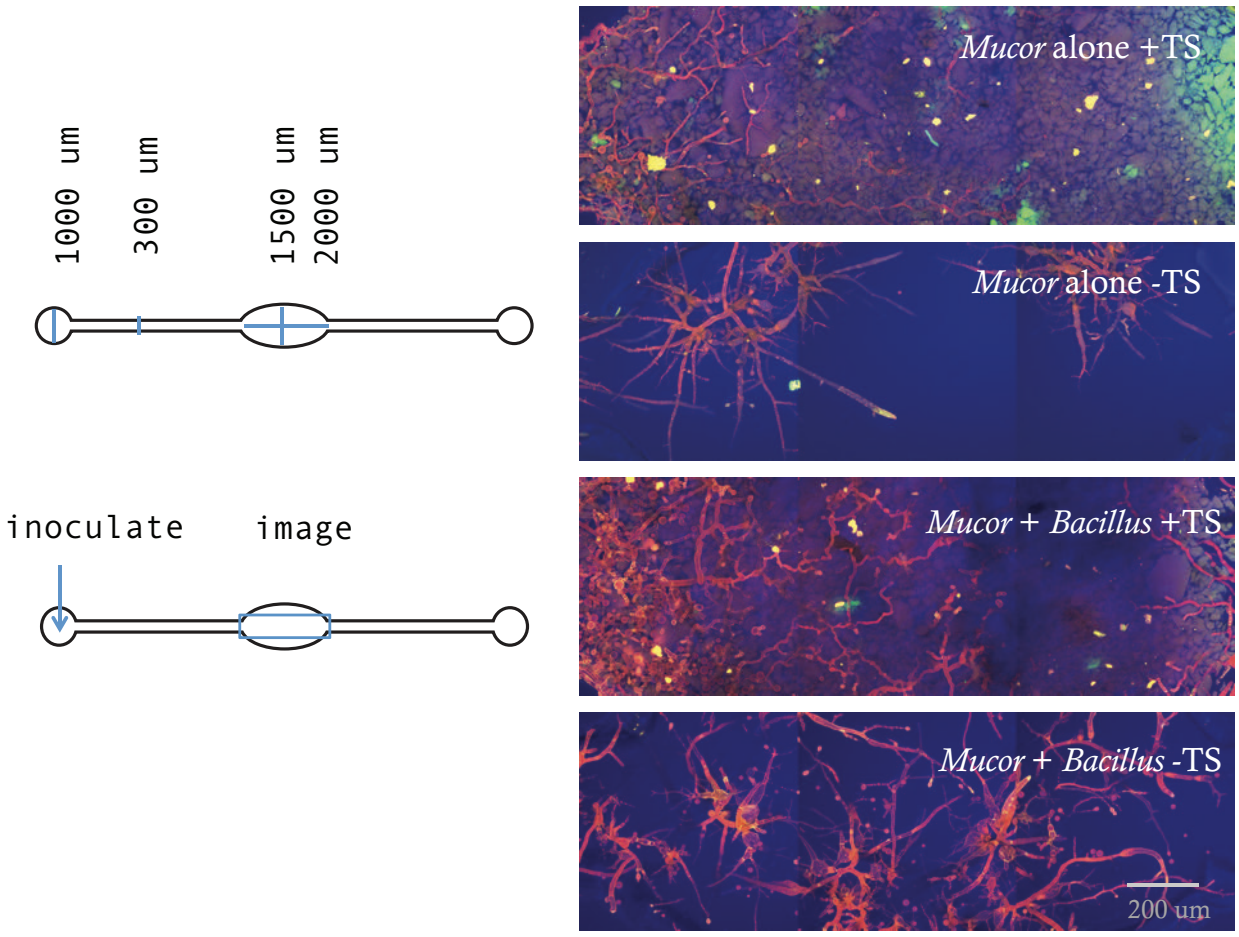

Figure 4.2: Schematic of chambers produced using vinyl cutter-epoxy PDMS casting method, and microscopy images from these chambers. Scale bar = 200 µm.

CHAPTER 5:
CONCLUSIONS AND OUTLOOK

This chapter summarizes key findings of this dissertation and offers recommendations for future work.

Key Findings

- *B. subtilis* 3610 forms biofilms on *M. fragilis* necromass, dependent on *eps-tasA* biofilm matrix production genes (Fig. 2.1, Fig. 2.2). Moreover, fungal cell wall components (chitin and chitosan) and *M. fragilis* extracts and exudates induce *tasA* biofilm gene expression (Fig. 2.3, Fig. 2.4).
- *B. subtilis* biofilm formation increases the probability that cells will form and maintain stable aggregates of nine cells or more, but does not increase the probability that cells will stick to positively charged particles or surfaces (Fig 2.7, Fig. 2.8).
- Multiple *B. subtilis* cells are required to decompose *M. fragilis* necromass. The critical number of required cells is estimated as three (Table 2.1, Fig. 2.6).
- Growing ^{13}C-labeled fungal biomass is an inexpensive and easy to obtain source of natural radiolabeled organic compounds relative to ^{13}C-labeled plant matter (p. 32).

- Raman microspectroscopy can be used to monitor uptake of ^{13}C-labeled natural fungal necromass by bacteria over time and with single-cell spatial resolution (Fig. 2.9, Fig. 2.10, Fig. 2.11).
- Though both *B. subtilis* clusters on necromass and non-associated planktonic cells take up ^{13}C from ^{13}C-labeled fungal necromass over time, we found no significant difference between the uptake dynamics of clusters and planktonic cells (Fig. 2.11).
- Transparent soil (TS) microcosms enable submicron resolution imaging of bacteria and fungi in three dimensions over time within a porous matrix (Fig. 3.4, Fig. 3.5, Fig. 3.6, Fig. 3.7, Fig. 3.8, Fig. 3.9, Fig. 3.11, Fig. 4.2).
- The transparent fluoropolymer Nafion can be rewet using 20% ethanol, 15% ethylene glycol or 0.1% Tween for TS microcosm manufacture and manipulation (Fig. 3.2).
- Nafion-based TS microcosms are compatible with Raman microspectroscopy and enable in situ single-cell detection of microbial activity as measured by uptake of D_2O (Fig 3.12). Cryolite-based TS microcosms are also compatible with Raman microspectroscopy and enable in situ detection of microbial activity as measured by uptake of D_2O, but at the population level (Fig. 3.13).
- Cryolite but not Nafion TS microcosms enable detection of carbon uptake by *populations* of bacteria in situ by Raman microspectroscopy – but not uptake by single cells (Fig. 3.14, Fig. 3.15, Fig. 3.16).

- *B. subtilis* cells attached to dead fungal biomass are more metabolically active after a dry-wet cycle in Nafion than cells far away from fungus. (Figures 3.17, 3.18)
- Nafion and cryolite both have advantages and limitations as transparent porous substrates for microbial studies (as summarized in Table 3.1).
- PDMS-based microfluidic devices with features as small as 250 μm can be manufactured using inexpensive epoxy molds cast from vinyl-cut masters. This process allows for rapid testing and iteration of designs without the need to order more expensive silicon-based microfluidics masters. These devices can be filled with TS substrate to rapidly and inexpensively produce TS microcosms at the benchtop without need for clean-room access (Fig. 3.1, Chapter 4).

Recommendations for Methodological Improvements and Extensions

Improving acquisition and analysis of Raman spectra through TS systems

The major barrier to collecting Raman spectra through porous matrices with positional accuracy has historically been the problem of refractive index mismatches (Freebody et al., 2010). Through refractive index matching between particles and liquid, Nafion- and cryolite-based TS microcosms largely overcome this difficulty. Another challenge then emerges as the primary difficulty: the substantial contribution of the TS matrix itself to the acquired cell spectra collected within the matrix.

The key methodological advance in single-cell Raman spectroscopy (SCRS) through TS matrices will be to minimize out-of-focus (i.e. “background”) contributions to cell spectra. Any gain in optics that minimizes out-of-focus contributions during

spectrum acquisition would result in a gain in single-cell Raman spectrum detection, and therefore will allow increases in either speed of acquisition, signal-to-noise ratio, or spatial resolution of the system. These gains in optics may include the optimization of pinhole size, maximization of numerical aperture (NA) of microscope objectives, or minimization of spherical aberration in objectives. Another approach would be to improve refractive index matches throughout the light path. For example, a water-immersion objective could be used to image through a Nafion film (instead of a glass coverslip, since Nafion has a close RI match with water) and then into a Nafion- or cryolite-based TS system – keeping the RI close to 1.33 throughout the system, and thereby minimizing scattering and aberrations. Gains in optics will surely include future advancement in optical microscopy in general, which can be applied to light microscopy and Raman spectroscopy through TS systems.

However, even without improvements to the optical setup used to acquire Raman spectra within TS microcosms, substantial gains could be made in cell spectrum quality through improvements in spectral analysis. In this study, our goal was to determine whether any cell signal could be detected over the background of the TS matrix at all. We did indeed detect the cell signal over the background, and used a very simple method to remove the background signal from the cell spectrum: we simply subtracted the Raman spectrum of a nearby point in x-y space from the acquired cell spectrum. However, more sophisticated techniques for removal of defocused light exist and could be applied to improve the quality of spectra obtained from cells within TS matrices, and therefore increase the amount of information that can be derived from these spectra (Everall, 2010). For example. nearest-neighbor deblurring methods, previously used to

increase the signal of the focal Raman spectrum over the background of a different out-of-focus substrate, could be applied to TS systems (Govil et al., 1991). A deconvolution-based removal of background signals based on a model of the contribution of the out-of-focus background region to final cell spectrum may also improve the final results.

This study has produced hundreds of cell spectra acquired from within TS matrices with matched background spectra, and thus provides a rich dataset for researchers interested in improving cell spectrum quality from existing spectral data acquired using existing instrumentation using new analytical approaches. Gains in these analytical approaches would improve cell spectral quality to a point where more sensitive and accurate determinations of single-cell uptake of stable isotopes could be made. Moreover, more subtle physiological signatures could potentially be detected within native cell spectra even without the addition of stable isotopes – for example, measurements of spore-formation pre-cursors within cells in a TS matrix (Huang et al., 2007). Gains in spectral quality may also enable accurate measurements of chemicals and metabolites within pore spaces in the TS matrix, producing insights not only into microbial anabolism, but also metabolite production by microbes and the spatial distribution of those metabolites.

Improving instrumentation for multi-modal image acquisition in TS systems

Improved instrumentation would be able to take advantage of the multi-modal capacity of TS microcosms. An integrated confocal laser scanning (or spinning disk) microscope with a confocal Raman microspectroscopy setup would greatly facilitate

multimodal data collection. For example, CLSM (confocal laser scanning microscopy) could be used to capture data about cell xyz position and fluorescent brightness of cells. The Raman system could then be used to measure cell spectra, allowing correlation with reporter gene status. By enabling fast and seamless collection of both data types, such a system would enable the full potential of TS systems to monitor dynamics in porous matrices. In the absence of a CLSM system, a high-quality epifluorescence microscopy setup with a motorized stage (to accurately record xyz coordinates) and high-resolution camera integrated with a confocal Raman setup would also be a great gain – especially in cryolite-based systems where the remarkable optical clarity and low autofluorescence of the substrate enables highly resolved visualization of cells even on a widefield microscope (Fig. 3.9).

Extensions to enable and improve image acquisition in unsaturated systems

The fact that air and water pores can clearly be distinguished from each other and from the particle matrix is a non-trivial advantage of TS systems over many existing soil-imaging technologies. For this study, we primarily imaged primarily through saturated TS systems, where all pores were liquid-filled and there was no air-filled pores within the system. However, a great deal of the complexity and the intriguing features of microhabitats come from the fact that most soils, most of the time, are unsaturated systems, consisting of a mix of water- and air-filled pores that offer a wide range of habitats to soil organisms and enable varying amounts of movement through soils. Improving the ability of TS systems to model unsaturated systems would therefore

advance our understanding of microbial growth and migration through unsaturated porous media.

We were able to obtain surprisingly clear and highly-resolved images of bacteria in unsaturated media as the light path followed a continuous channel of liquid i.e. the path was not interrupted by an air-filled pore (see Fig. 5.1). In principle, imaging through unsaturated TS systems could be improved by the used of adaptive optics to model and correct for the presence of air-filled pores in the system. The smaller the air pore size, the worse the optical aberration (Ji et al., 2012), so studies in unsaturated systems may benefit at least initially from using comparatively larger particle sizes (10 μm or larger) to generate larger pore spaces to lessen aberration caused by air pockets.

Multiplexing TS systems with other probes and methods

In principle, the addition of fluorescent, colorometric, or even Raman-detectable probes into the TS matrix with the liquid phase could provide valuable information about pore microenvironments and how soil microbes change those environment. For example ratiometric extracellular fluorescent pH sensors and fluorescent oxygen-quenched probes could enable *in situ* detection of pH and oxygen levels in pores. Fluorescent substrates for extracellular enzyme detection (4-MUF and 4-MUB-labeled compounds) are also intriguing candidates for *in situ* extracellular enzyme detection. However, they are pH-sensitive probes that fluoresce most brightly at pH 10, so may best be used in conjunction pH sensors to disentangle the effect of pH on 4-MUF or 4-MUB fluorescence.

Additionally, TS systems can potentially be multiplexed with existing destructive approaches for visualization of microbes in soils and sediments, such as FISH, BONCAT (bio-orthogonal non-canonical amino acid tagging, a single-cell activity measurement technique based on detection of protein translation (Hatzenpichler et al., 2014), and NanoSIMS. Though they do not enable dynamic measurements, destructive approaches may still helpful in TS systems particularly as endpoint measurements taken after a dynamic time course. For example, FISH can be used to identify cells by genus or species within a TS matrix after a non-destructive time course of those same cells undergoing growth or taking up a stable isotope. Since FISH is essentially a series of washes, perfusion of fixing and washing agents into the TS system is possible in principle, either through passive percolation or a gentle flow of liquids through the system using a syringe pump. We have not answered in this study the question of whether FISH probes tend to bind non-specifically to Nafion or cryolite, which would make FISH within TS matrices more challenging, but this would be a helpful avenue for future research.

Integrating TS systems into environmental samples, or vice versa

Outside of the context of a microfluidics device, transparent soils can be usefully incorporated into field systems or environmentally-relevant laboratory incubations. For example, Ling and colleagues developed setups where agar plugs inoculated with environmental microbes were sandwiched between polycarbonate membranes and buried back in their sediment environment. The porous polycarbonate membranes allowed flow of molecules between the microbes and the sediment environment while

keeping the microbes in place, allowing the microbes to grow in somewhat naturalistic environmental conditions while enabling them to be visualized or cultured after the incubation (Bollmann et al., 2007; Ling et al., 2015). A similar experiment using a 3D-printed "iChip" (Ling et al., 2015) where the agar plug is replaced with packed Nafion or cryolite and inoculated with microbes is possible. The microcosm can be buried in within real soil, then the setup dismantled, and imaged through polycarbonate (which is optically clear when wet) into the microcosm. The optical problems caused by drying of the TS system in regular "field" conditions suggest that an easily wettable cryolite-based system that can be slightly rewet prior to imaging may be a better candidate than Nafion for such environmental incubations. Alternatively, this type of setup may be better suited to answering questions in sediment microbial ecology, where the system is always saturated and can easily be imaged through.

Instead of placing TS systems in "the field", another option is to bring "the field" into TS systems. For example, I found that adding small amounts – between about 1 and 10% of total particle volume – of natural soil grains or silica particles to a TS system still allowed imaging through the system (Fig. 5.2). This suggests that TS microcosms can be "spiked" with small amounts of minerals of interest (magnetite, heavy metals, iron-containing compounds, etc.) or soil solutes of interest (dissolved organic compounds extracted from various soils, for instance) and still act as relatively transparent matrices for visualizing cells. Again, larger particles sizes are preferred for spike-ins, as they reduce optical aberration; tiny micron particles like clays (2 μm or less) scatter light much more strongly than larger particles. Alternatively, an incubation of cells in a TS microcosm with "soil tea" (an extract of soil solutes obtained by washing

soil particles in water and filtering out particles) may allow the growth and visualization of cells in a natural soil pore-water-like medium.

Other interesting “spike-ins” are fluorescently-labeled polysaccharides, either tethered to beads or not (Arnosti, 2003). These polysaccharides enable the clear visualization of complex natural carbon sources within the TS matrix. The uptake and detection of fluorescently-labeled polysaccharides in the periplasm of marine bacteria is a novel discovery suggesting that the size of molecules that are able to be imported into cells is larger than previously expected (Reintjes et al., 2017). Whether a similar phenomenon occurs in soil bacteria is yet to be determined, and could be facilitated by incubation of soil microbes with fluorescently-labeled polysaccharides within TS microcosms.

One important parameter of the TS substrates used in this study that has not been thoroughly characterized is their surface properties. Sorption isotherm characterizations of both these substrates would be useful for predicting mineral-microbe and mineral-metabolite interactions (Pett-Ridge, 2019, personal communication), by characterizing which ions and chemicals tend to bind to the substrates, and how strongly.

Recommendations for Future Biological Studies

Though this study has focused on terrestrial soil systems, advances in our understanding of soils at the microscale owe a great deal to analogous research in sediments, and vice versa. As porous systems, soils and sediments share many characteristics, as well as important differences. Therefore many methodological

advances and biological questions and discoveries relevant to one will be relevant to both.

The following is a (by no means exhaustive) list of possible biological questions enabled by TS microcosms:

- Migration and predation in porous media: How do hydration conditions, mineral types, pore sizes, nutrient conditions, and/or cell physiological state enable or constrain bacterial migration through porous media in three dimensions? What genes are necessary for migration in these conditions, and what genes have been shown to be necessary for migration in liquid or in agar, but play a different role in porous matrices? How do protists, nematodes, tardigrades, and other microscopic soil fauna migrate through these matrices? How does ease of migration enable or constrain predation in these systems?
- Interspecies interactions: How do microbially-produced metabolites travel through porous media – particularly unsaturated porous media? How large is the "sphere of influence" of a single metabolite-producing cell or cluster of cells in these media? How do bacteria interact differently in porous media than on agar plates?
- Genetic exchange: How does conjugation- or transduction-based genetic exchange occur in porous media? Can DNA sorbed to minerals be taken up by microbes even in unsaturated conditions?
- Virus-bacteria dynamics: How does the addition of bacteriophage structure the population of a soil microbial community within a porous matrix? How narrow is the host range of bacteriophages when measured at the micron scale? Are the

nutrients released by viral lysis of a bacterium taken up by its neighbors – and if so, how close do they have to be for that uptake to occur?

- Development over time: How do soil microbes with interesting developmental trajectories (*Myxococcus xanthus* which forms multicellular aggregates, *Streptomyces coelicolor* which form spore bodies) develop over time in porous media, in ways that differ interestingly from their development on agar plates? How do different nutrient sources or different starting densities affect their development in such a system?
- Microbial responses to drying and rewetting: What microscale processes explain the Birch effect, which is observed at the macroscale? (The Birch effect is the widely observed pulse of carbon dioxide and nitrous oxide released from dry soils immediately after rewetting). Is this pulse of gases produced due to a pulse of microbial respiration due to mobilization of dissolved organic carbon, which then becomes available to cells upon wetting? Or is it due to a pulse of microbial respiration due to nutrient release from cell lysis of neighbors due to osmotic shock from a sudden wetting event?
- Extracellular enzyme distributions: How do consortia of microbes producing different extracellular enzymes have to be spatially distributed in porous media in order to decompose complex natural biomass and necromass? In what conditions do extracellular enzyme-producers thrive in porous media, and in what conditions do non-producers have a fitness advantage?
- Fungal-bacterial interactions (enabled by *in situ* isotopic labeling of fungi): What is the “zone of influence” of any given fungus in terms of exudates or

decomposition products i.e. how far do these molecules travel within a porous matrix and how do they affect neighboring bacteria? Might bacteria use fungal hyphae not only to cross otherwise non-traversable air pockets through the soil ("the fungal highway" [Kohlmeier et al., 2005]) but also to gather nutrients during their travel ("fast food on the fungal highway")?

- Soil minerals as terminal electron acceptors: How does the distribution of minerals affect the distribution of soil microbes who may use those minerals as terminal electron acceptors for anaerobic respiration? Is the distribution of those minerals only important in anaerobic (water-logged) conditions, or do they also constrain bacterial distributions in aerobic conditions?
- Activity versus uptake: how soon do cells become active given a rehydration or nutrient amendment event, relative to how soon they begin taking up carbon or other nutrients?
- Culturability: Does cultivation of soil microbes within a porous matrix itself enhance culturability of microbes that have not been cultivable in liquid on agar media?

Again, the future of transparent soil microcosms and their applications will depend upon the questions and creativity of workers in the field. One might say that the earth is the limit.

Figures

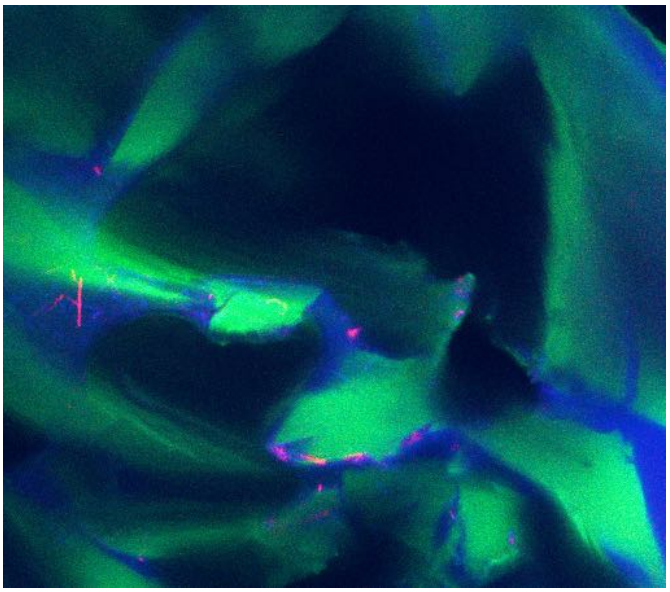

Fig. 5.1: *B. subtilis* 3610 cells in an unsaturated Nafion-based TS microcosm. *B. subtilis* 3610 cells constitutively expressing cyan fluorescent protein were inoculated into Nafion-filled mesocosms (Nafion particles in 5 mm wells with cover glass bottom). Mesocosms were saturated with MSgg rich biofilm-inducing medium and incubated at 24°C for 4 hours, and allowed to air-dry over that period in a biological safety hood to produce a partially-hydrated system. Mesocosm was imaged by confocal microscopy, using a 40x water immersion objective; this z-slice (0.75 µm thick) was taken 10 µm into the TS matrix from the coverslip. Sulphorhodamine-stained Nafion particles false-colored green, *B. subtilis* 3610 cells false-colored red, fluorescein liquid tracer false-colored blue, and air pockets are visible as black space. Notice bacteria suspended within liquid-filled pores and "bridges" between particles. Image size = 106 x 106 µm.

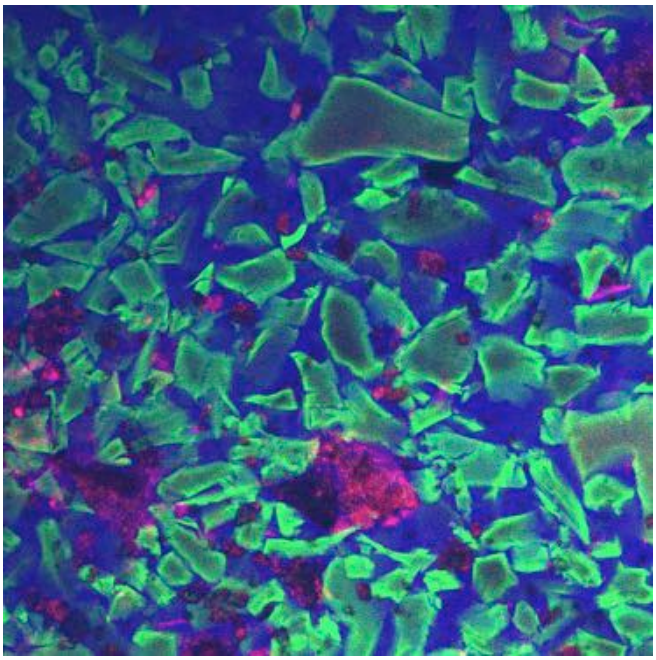

Fig. 5.2: Nafion TS microcosm with 10% natural soil particles. Acidic oak-hickory hardwood forest clay soil from Mason Farm Preserve (Chapel Hill, NC) was sieved to particles sizes below 100 μm and added to a slurry of Nafion and water to about 10% total volume. Mesocosm was imaged by confocal microscopy, using a 10x air objective; this z-slice (3 μm thick) was taken 10 μm into the TS matrix from the coverslip. Sulphorhodamine-stained Nafion particles false-colored green, CFP channel (highlighting CFP-bright natural soil aggregates) false-colored red, and fluorescein liquid tracer false-colored blue. Image size = 850 x 850 μm.

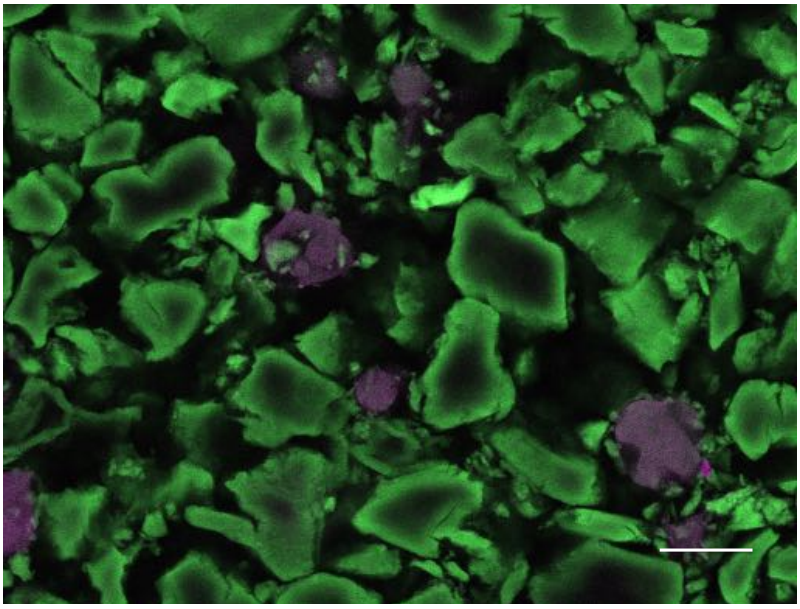

Fig. 5.3: Fluorescently-labeled xylan beads in a Nafion-based TS microcosm. Fluorescently-labeled xylan (FITC-bright) tethered to agarose beads were added to a Nafion-based TS microcosm. Mesocosm was imaged by confocal microscopy, using a 10x air objective; this z-slice (3 μm thick) was taken 10 μm into the TS matrix from the coverslip. Sulphorhodamine-stained Nafion particles false-colored green, xylan beads false-colored violet. Scale bar = 100 μm.

APPENDIX: THE WORDS UNDER THE WORDS

How bottomless and deep is the well from which we draw the everyday miracle of being alive. If I had the courage, that's what I would tell people when they asked me what my PhD research was about. It's like when someone asks "How are you?" but then sometimes they ask "How *are* you?" and you hear in their voice and see in the tilt of their head that they're expressing a curiosity and care for what you feel you cannot ordinarily say at a house party or in a dissertation – "the words under the words", as poet Naomi Shihab Nye writes.

If there are words under words like "Raman spectroscopy", "zygomycete", "chitosanase", "bootstrap confidence interval", and "cryolite", they might be "elusive", "frustrating", and "it took me all night, then I stumbled to the U-bahn at dawn". For me, in the dark of another long hour in the microscope room, they have sometimes been, "if only I'd known", "I should have known", and "how could I have known" – "mistake", "failure", "loss", "I did not sufficiently control", "I could not accurately predict". Which is another way of saying: "strange", "intricate", "unfathomable", and – most of all – "possible". The Oxford English Dictionary does not define it as "to participate in an unfinished unfolding, or to immerse in the immense". Beneath that immersion still is something muddy, swelling, primary, and unspeaking, whose closest extant phylogenetic relatives in the English language might be "thank you" and "wow".

My dissertation defense celebration included a "Dissertation Remix Station", with scissors, glue, magazines, and a single printed copy of this dissertation. Guests were invited to cut words and phrases from the dissertation and make their own poems and collages out of it. Many wonderful creative works were thus produced; I will share here

just one. My sister, Sachi Partin, composed a poem (below) that somehow managed to distill to its essence what 150 pages of scientific writing could not directly say. I take this as evidence that fails to support the common hypothesis that scientific writing is literal, while poetry is oblique.

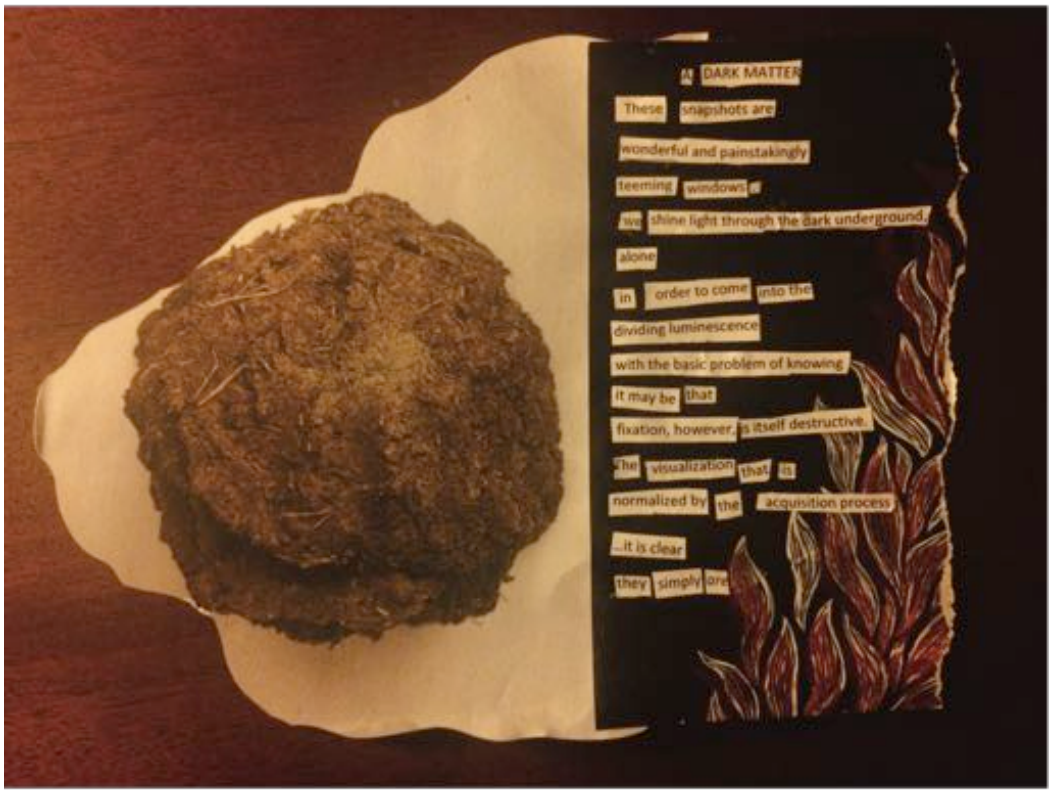

"A Dark Matter" by Sachi Partin
These snapshots are
wonderful and painstakingly
teeming windows.
we shine light through the dark underground,
alone
in order to come into the
dividing luminescence
with the basic problem of knowing.
it may be that
fixation, however, is itself destructive.
The visualization that is
normalized by the acquisition process
…it is clear
they simply *are*.

When my friend Alexis Pauline Gumbs says, “Thank you for teaching me that poetry and experiment are not metaphors for each other but in fact the same exact practice”, I say, “Thank you for the same”, and wonder if this is one part of what she means. Between the lines and under the words of all scientific literature are supplemental materials and appendices, the dark story of what did not obey laws and did not hold still for the camera, what could not be replicated, what was given freely by unmerited grace, what made it all possible but never got cited. The ordinary operations by which what counts as reality gets to count as reality. What is grasped from the abundance to fit inside, what spills over, what vastly exceeds.

The appendices and the supplementary materials are where scientists put what bears on the findings, but exceeds what can be said in the scientific manuscript. They are pieces without which the manuscript and its conclusions can – ostensibly – survive. But without the words under the words, something does not survive. Or, to allow Naomi Shihab Nye to finish what she had earlier begun to say:

> “Answer, if you hear the words under the words –
> otherwise it is just a world with a lot of rough edges,
> difficult to get through, and our pockets full of stones.”

REFERENCES

Allison, S. D., Lu, L., Kent, A. G., & Martiny, A. C. (2014). Extracellular enzyme production and cheating in Pseudomonas fluorescens depend on diffusion rates. *Frontiers in Microbiology*, *5*(APR), 169. https://doi.org/10.3389/fmicb.2014.00169

Ams, D. A., Fein, J. B., Dong, H., & Maurice, P. A. (2004). Experimental Measurements of the Adsorption of *Bacillus subtilis* and *Pseudomonas mendocina* Onto Fe-Oxyhydroxide-Coated and Uncoated Quartz Grains. *Geomicrobiology Journal*, *21*(8), 511–519. https://doi.org/10.1080/01490450490888172

Armani, M., Probst, R., & Shapiro, B. (2009). Fabricating Micro-Fluidic Channels Using a Vinyl Sign Plotter. In K. E. Herold & A. Rasooly (Eds.), *Lab-on-a-Chip Technology (Vol. 1): Fabrication and Microfluidics* (Vol. 1). Caister Academic Press, U.K. Retrieved from https://www.caister.com/hsp/abstracts/loc1/02.html

Arnosti, C. (2003). Fluorescent derivatization of polysaccharides and carbohydrate-containing biopolymers for measurement of enzyme activities in complex media. *Journal of Chromatography B: Analytical Technologies in the Biomedical and Life Sciences*, *793*(1), 181–191. https://doi.org/10.1016/S1570-0232(03)00375-1

Arnosti, Carol. (2011). Microbial Extracellular Enzymes and the Marine Carbon Cycle. *Annual Review of Marine Science*, *3*(1), 401–425. https://doi.org/10.1146/annurev-marine-120709-142731

Atkinson, J. A., Pound, M. P., Bennett, M. J., & Wells, D. M. (2019, February 1). Uncovering the hidden half of plants using new advances in root phenotyping. *Current Opinion in Biotechnology*. Elsevier Current Trends. https://doi.org/10.1016/j.copbio.2018.06.002

Bardgett, R. D., Freeman, C., & Ostle, N. J. (2008, August 10). Microbial contributions to climate change through carbon cycle feedbacks. *ISME Journal*. Nature Publishing Group. https://doi.org/10.1038/ismej.2008.58

Barnard, R. L., Osborne, C. A., & Firestone, M. K. (2013). Responses of soil bacterial and fungal communities to extreme desiccation and rewetting. *The ISME Journal*, *7*(11), 2229–2241. https://doi.org/10.1038/ismej.2013.104

Baveye, P. C., Otten, W., Kravchenko, A., Balseiro-Romero, M., Beckers, É., Chalhoub, M., … Vogel, H.-J. (2018). Emergent Properties of Microbial Activity in Heterogeneous Soil Microenvironments: Different Research Approaches Are Slowly Converging, Yet Major Challenges Remain. *Frontiers in Microbiology*, *9*, 1929. https://doi.org/10.3389/fmicb.2018.01929

Beauregard, P. B., Chai, Y., Vlamakis, H., Losick, R., & Kolter, R. (2013). Bacillus subtilis biofilm induction by plant polysaccharides. *Proceedings of the National Academy of Sciences*, *110*(17), E1621–E1630.

https://doi.org/10.1073/pnas.1218984110

Berry, D., Mader, E., Lee, T. K., Woebken, D., Wang, Y., Zhu, D., … Wagner, M. (2015). Tracking heavy water (D2O) incorporation for identifying and sorting active microbial cells. *Proceedings of the National Academy of Sciences of the United States of America*, *112*(2), E194-203. https://doi.org/10.1073/pnas.1420406112

Bertaux, J., Gloger, U., Schmid, M., Hartmann, A., & Scheu, S. (2007). Routine fluorescence in situ hybridization in soil. *Journal of Microbiological Methods*, *69*(3), 451–460. https://doi.org/10.1016/j.mimet.2007.02.012

Birch, H. F. (1958). The effect of soil drying on humus decomposition and nitrogen availability. *Plant and Soil*, *10*(1), 9–31. https://doi.org/10.1007/BF01343734

Blank, G., Al-Khayat, M., & Ismond, M. A. H. (1987). Germination and heat resistance of Bacillus subtilis spores produced on clove and eugenol based media. *Food Microbiology*, *4*(1), 35–42. https://doi.org/10.1016/0740-0020(87)90016-5

Bollmann, A., Lewis, K., & Epstein, S. S. (2007). Incubation of environmental samples in a diffusion chamber increases the diversity of recovered isolates. *Applied and Environmental Microbiology*, *73*(20), 6386–6390. https://doi.org/10.1128/AEM.01309-07

Branda, S. S., González-Pastor, J. E., Ben-Yehuda, S., Losick, R., & Kolter, R. (2001). Fruiting body formation by Bacillus subtilis. *Proceedings of the National Academy of Sciences of the United States of America*, *98*(20), 11621–11626. https://doi.org/10.1073/pnas.191384198

Brenan, C. J. H., Hunter, I. W., & Brenan, J. M. (1997). Noninvasive Confocal Raman Imaging of Immiscible Liquids in a Porous Medium. *Analytical Chemistry*, *69*(1), 45–50. https://doi.org/10.1021/ac960654j

Brenner, S. (2002). Life sentences: Detective Rummage investigates. *Genome Biology*, *3*(9), comment1013.1. Retrieved from https://www-ncbi-nlm-nih-gov.libproxy.lib.unc.edu/pmc/articles/PMC139404/

Bribes, J. -L, El Boukari, M., & Maillols, J. (1991). Application of Raman spectroscopy to industrial membranes. Part 2–Perfluorosulphonic membrane. *Journal of Raman Spectroscopy*, *22*(5), 275–279. https://doi.org/10.1002/jrs.1250220507

C. Xie, J. Mace, M. A. Dinno, Y. Q. Li, W. Tang, R. J. Newton, & Gemperline, P. J. (2005). Identification of Single Bacterial Cells in Aqueous Solution Using Confocal Laser Tweezers Raman Spectroscopy. https://doi.org/10.1021/AC0504971

Chen, M., & Alexander, M. (1973). Survival of soil bacteria during prolonged desiccation. *Soil Biology and Biochemistry*, *5*(2), 213–221. https://doi.org/10.1016/0038-0717(73)90004-7

Cui, L., Yang, K., Li, H.-Z., Zhang, H., Su, J.-Q., Paraskevaidi, M., … Zhu, Y.-G. (2018). Functional Single-Cell Approach to Probing Nitrogen-Fixing Bacteria in Soil Communities by Resonance Raman Spectroscopy with $^{15}N_2$ Labeling. *Analytical Chemistry*, *90*(8), 5082–5089. https://doi.org/10.1021/acs.analchem.7b05080

da Costa, R. R., Hu, H., Pilgaard, B., Vreeburg, S. M. E., Schückel, J., Pedersen, K. S. K., … Poulsen, M. (2018). Enzyme Activities at Different Stages of Plant Biomass Decomposition in Three Species of Fungus-Growing Termites. *Applied and Environmental Microbiology*, *84*(5), e01815-17. https://doi.org/10.1128/AEM.01815-17

Dal Ferro, N., & Morari, F. (2015). From Real Soils to 3D-Printed Soils: Reproduction of Complex Pore Network at the Real Size in a Silty-Loam Soil. *Soil Science Society of America Journal*, *79*(4), 1008. https://doi.org/10.2136/sssaj2015.03.0097

Dashtban, M., Schraft, H., Syed, T. A., & Qin, W. (2010). Fungal biodegradation and enzymatic modification of lignin. *International Journal of Biochemistry and Molecular Biology*, *1*(1), 36–50. Retrieved from http://www.ncbi.nlm.nih.gov/pubmed/21968746

Davidson, E. A., & Janssens, I. A. (2006). Temperature sensitivity of soil carbon decomposition and feedbacks to climate change. *Nature*, *440*(7081), 165–173. https://doi.org/10.1038/nature04514

De Boer, W., Folman, L. B., Summerbell, R. C., & Boddy, L. (2005, September 1). Living in a fungal world: Impact of fungi on soil bacterial niche development. *FEMS Microbiology Reviews*. Narnia. https://doi.org/10.1016/j.femsre.2004.11.005

Deng, J., Orner, E. P., Chau, J. F., Anderson, E. M., Kadilak, A. L., Rubinstein, R. L., … Shor, L. M. (2015). Synergistic effects of soil microstructure and bacterial EPS on drying rate in emulated soil micromodels. *Soil Biology and Biochemistry*, *83*, 116–124. https://doi.org/10.1016/j.soilbio.2014.12.006

Dorgan, K. M. (2018). Kinematics of burrowing by peristalsis in granular sands. *The Journal of Experimental Biology*, *221*(Pt 10), jeb.167759. https://doi.org/10.1242/jeb.167759

Downie, H. F., Valentine, T. A., Otten, W., Spiers, A. J., & Dupuy, L. X. (2014). Transparent soil microcosms allow 3D spatial quantification of soil microbiological processes *in vivo*. *Plant Signaling & Behavior*, *9*(10), e970421. https://doi.org/10.4161/15592316.2014.970421

Downie, H., Holden, N., Otten, W., Spiers, A. J., Valentine, T. A., Dupuy, L. X., … Peitgen, H. (2012). Transparent Soil for Imaging the Rhizosphere. *PLoS ONE*, *7*(9), e44276. https://doi.org/10.1371/journal.pone.0044276

Drescher, K., Nadell, C. D., Stone, H. A., Wingreen, N. S., & Bassler, B. L. (2014). Solutions to the public goods dilemma in bacterial biofilms. *Current Biology*, *24*(1),

50–55. https://doi.org/10.1016/j.cub.2013.10.030

Drescher, K., Shen, Y., Bassler, B. L., & Stone, H. A. (2013). Biofilm streamers cause catastrophic disruption of flow with consequences for environmental and medical systems. *Proceedings of the National Academy of Sciences*, *110*(11), 4345–4350. https://doi.org/10.1073/pnas.1300321110

Eichorst, S. A., Strasser, F., Woyke, T., Schintlmeister, A., Wagner, M., & Woebken, D. (2015). Advancements in the application of NanoSIMS and Raman microspectroscopy to investigate the activity of microbial cells in soils. *FEMS Microbiology Ecology*, *91*(10), fiv106. https://doi.org/10.1093/femsec/fiv106

Eickhorst, T., & Tippkötter, R. (2008). Improved detection of soil microorganisms using fluorescence in situ hybridization (FISH) and catalyzed reporter deposition (CARD-FISH). *Soil Biology and Biochemistry*, *40*(7), 1883–1891. https://doi.org/10.1016/J.SOILBIO.2008.03.024

Estévez-Torres, A., Yamada, A., & Wang, L. (2009). An inexpensive and durable epoxy mould for PDMS Chips and Tips. *Lab on a Chip*. Retrieved from http://blogs.rsc.org/chipsandtips/2009/04/22/an-inexpensive-and-durable-epoxy-mould-for-pdms/?doing_wp_cron=1558756058.9302821159362792968750

Everall, N. J. (2010). Confocal Raman microscopy: common errors and artefacts. *The Analyst*, *135*(10), 2512. https://doi.org/10.1039/c0an00371a

Fike, D. A., Gammon, C. L., Ziebis, W., & Orphan, V. J. (2008). Micron-scale mapping of sulfur cycling across the oxycline of a cyanobacterial mat: a paired nanoSIMS and CARD-FISH approach. *The ISME Journal*, *2*(7), 749–759. https://doi.org/10.1038/ismej.2008.39

Flessa, K. (1972). Notes on cryolite: A medium for the study of burrowing organisms. *Limnology and Oceanography*, *17*(1), 134–135. Retrieved from https://aslopubs.onlinelibrary.wiley.com/doi/pdf/10.4319/lo.1972.17.1.0134

Fontaine, S., Mariotti, A., & Abbadie, L. (2003). The priming effect of organic matter: a question of microbial competition? *Soil Biology and Biochemistry*, *35*(6), 837–843. https://doi.org/10.1016/S0038-0717(03)00123-8

Francoeur, A. A., & Dorgan, K. M. (2014). Burrowing behavior in mud and sand of morphologically divergent polychaete species (Annelida: Orbiniidae). *The Biological Bulletin*, *226*(2), 131–145. https://doi.org/10.1086/BBLv226n2p131

Freebody, N. A., Vaughan, A. S., & Macdonald, A. M. (2010). On optical depth profiling using confocal Raman spectroscopy. *Analytical and Bioanalytical Chemistry*, *396*(8), 2813–2823. https://doi.org/10.1007/s00216-009-3272-0

Ganiyu, A. A., Rashid, A. S. A., & Osman, M. H. (2016). Utilisation of transparent synthetic soil surrogates in geotechnical physical models: A review. *Journal of Rock*

Mechanics and Geotechnical Engineering, *8*(4), 568–576. https://doi.org/10.1016/j.jrmge.2015.11.009

Gordon, H., Haygarth, P. M., & Bardgett, R. D. (2008). Drying and rewetting effects on soil microbial community composition and nutrient leaching. *Soil Biology and Biochemistry*, *40*(2), 302–311. https://doi.org/10.1016/j.soilbio.2007.08.008

Govil, A., Pallister, D. M., Chen, L.-H., & Morris, M. D. (1991). Optical Sectioning Raman Microscopy. *Applied Spectroscopy*, *45*(10), 1604–1606. https://doi.org/10.1366/0003702914335201

Grossart, H.-P., Tang, K. W., KiÃ¸rboe, T., & Ploug, H. (2007). Comparison of cell-specific activity between free-living and attached bacteria using isolates and natural assemblages. *FEMS Microbiology Letters*, *266*(2), 194–200. https://doi.org/10.1111/j.1574-6968.2006.00520.x

H. Koschwanez, J., R. Foster, K., & W. Murray, A. (2011). Sucrose Utilization in Budding Yeast as a Model for the Origin of Undifferentiated Multicellularity. *PLoS Biology*, *9*(8), e1001122. https://doi.org/10.1371/journal.pbio.1001122

Hallsworth, J. E., Heim, S., & Timmis, K. N. (2003). Chaotropic solutes cause water stress in Pseudomonas putida. *Environmental Microbiology*, *5*(12), 1270–1280. https://doi.org/10.1111/j.1462-2920.2003.00478.x

Hatzenpichler, R., Scheller, S., Tavormina, P. L., Babin, B. M., Tirrell, D. A., & Orphan, V. J. (2014). *In situ* visualization of newly synthesized proteins in environmental microbes using amino acid tagging and click chemistry. *Environmental Microbiology*, *16*(8), 2568–2590. https://doi.org/10.1111/1462-2920.12436

Helliwell, J. R., Sturrock, C. J., Mairhofer, S., Craigon, J., Ashton, R. W., Miller, A. J., … Mooney, S. J. (2017). The emergent rhizosphere: imaging the development of the porous architecture at the root-soil interface. *Scientific Reports*, *7*(1), 14875. https://doi.org/10.1038/s41598-017-14904-w

Hobley, L., Harkins, C., MacPhee, C. E., & Stanley-Wall, N. R. (2015). Giving structure to the biofilm matrix: an overview of individual strategies and emerging common themes. *FEMS Microbiology Reviews*, *39*(5), 649–669. https://doi.org/10.1093/femsre/fuv015

Holden, P. A., Ritz, K., & Young, I. (2012). The Architecture and Biology of Soils: Life in Inner Space - by Ritz, K. & Young, I. *European Journal of Soil Science*. https://doi.org/10.1111/j.1365-2389.2012.01454.x

Holden, P. A. (2011). How do the microhabitats framed by soil structure impact soil bacteria and the processes that they regulate? In *The architecture and biology of soils: life in inner space*. https://doi.org/10.1079/9781845935320.0118

Huang, S., Chen, D., Pelczar, P. L., Vepachedu, V. R., Setlow, P., & Li, Y. (2007).

Levels of Ca2+-dipicolinic acid in individual bacillus spores determined using microfluidic Raman tweezers. *Journal of Bacteriology*, *189*(13), 4681–4687. https://doi.org/10.1128/JB.00282-07

Huang, W. E., Ward, A. D., & Whiteley, A. S. (2009). Raman tweezers sorting of single microbial cells. *Environmental Microbiology Reports*, *1*(1), 44–49. https://doi.org/10.1111/j.1758-2229.2008.00002.x

Intergovernmental Panel on Climate Change. (2013). Carbon and other biogeochemical cycles. In Intergovernmental Panel on Climate Change (Ed.), *Climate Change 2013 the Physical Science Basis: Working Group I Contribution to the Fifth Assessment Report of the Intergovernmental Panel on Climate Change* (Vol. 9781107057, pp. 465–570). Cambridge: Cambridge University Press. https://doi.org/10.1017/CBO9781107415324.015

Intergovernmental Panel on Climate Change. (2018). Special Report on Global Warming of 1.5C. *Global Warming of 1.5 °C: Special Report*, (October 2018), 1–33. Retrieved from https://www.ipcc.ch/report/sr15/

Iskander, M., Bathurst, R. J., & Omidvar, M. (2015). Past, Present, and Future of Transparent Soils. *Geotechnical Testing Journal*, *38*(5), 20150079. https://doi.org/10.1520/GTJ20150079

Iskander, Magued. (2010). Introduction to Transparent Soils (pp. 1–4). Springer, Berlin, Heidelberg. https://doi.org/10.1007/978-3-642-02501-3_1

Ji, N., Sato, T. R., & Betzig, E. (2012). Characterization and adaptive optical correction of aberrations during in vivo imaging in the mouse cortex. *Proceedings of the National Academy of Sciences*, *109*(1), 22–27. https://doi.org/10.1073/pnas.1109202108

Kakumanu, M. L., Cantrell, C. L., & Williams, M. A. (2013). Microbial community response to varying magnitudes of desiccation in soil: A test of the osmolyte accumulation hypothesis. *Soil Biology and Biochemistry*, *57*, 644–653. https://doi.org/10.1016/J.SOILBIO.2012.08.014

Kosmulski, M. (2009). Surface Charging and Points of Zero Charge, Surfactant Science Series. CRC Press. Retrieved from https://www.crcpress.com/Surface-Charging-and-Points-of-Zero-Charge/Kosmulski/p/book/9781420051889

Kouzai, Y., Mochizuki, S., Saito, A., Ando, A., Minami, E., & Nishizawa, Y. (2012). Expression of a bacterial chitosanase in rice plants improves disease resistance to the rice blast fungus Magnaporthe oryzae. *Plant Cell Reports*, *31*(4), 629–636. https://doi.org/10.1007/s00299-011-1179-7

Kubiëna, W. (1938). *Micropedology,*. Ames Ia.: Collegiate Press. Retrieved from https://www.worldcat.org/title/micropedology/oclc/1579778

Kumar B. N., V., Guo, S., Bocklitz, T., Rösch, P., & Popp, J. (2016). Demonstration of Carbon Catabolite Repression in Naphthalene Degrading Soil Bacteria via Raman Spectroscopy Based Stable Isotope Probing. *Analytical Chemistry*, *88*(15), 7574–7582. https://doi.org/10.1021/acs.analchem.6b01046

Lafuente, B., Downs, R. T., Yang, H., & Stone, N. (2016). The power of databases: The RRUFF project. In *Highlights in Mineralogical Crystallography* (pp. 1–29). https://doi.org/10.1515/9783110417104-003

Leis, A. P., Schlicher, S., Franke, H., & Strathmann, M. (2005). Optically transparent porous medium for nondestructive studies of microbial biofilm architecture and transport dynamics. *Applied and Environmental Microbiology*, *71*(8), 4801–4808. https://doi.org/10.1128/AEM.71.8.4801-4808.2005

Lewis, R. J. (Ed.). (2007). *Hawley's Condensed Chemical Dictionary*. Wiley. https://doi.org/10.1002/9780470114735

Li, M., Ashok, P. C., Dholakia, K., & Huang, W. E. (2012). Raman-Activated Cell Counting for Profiling Carbon Dioxide Fixing Microorganisms. *The Journal of Physical Chemistry A*, *116*(25), 6560–6563. https://doi.org/10.1021/jp212619n

Li, M., Huang, W. E., Gibson, C. M., Fowler, P. W., & Jousset, A. (2013). Stable Isotope Probing and Raman Spectroscopy for Monitoring Carbon Flow in a Food Chain and Revealing Metabolic Pathway. *Analytical Chemistry*, *85*(3), 1642–1649. https://doi.org/10.1021/ac302910x

Li, M., Xu, J., Romero-Gonzalez, M., Banwart, S. A., & Huang, W. E. (2012). Single cell Raman spectroscopy for cell sorting and imaging. *Current Opinion in Biotechnology*, *23*(1), 56–63. https://doi.org/10.1016/j.copbio.2011.11.019

Lin, J. D., Lemay, M. A., & Parfrey, L. W. (2018). Diverse Bacteria Utilize Alginate Within the Microbiome of the Giant Kelp Macrocystis pyrifera. *Frontiers in Microbiology*, *9*, 1914. https://doi.org/10.3389/fmicb.2018.01914

Lindblad, E. B., & Duroux, L. (2017). Mineral Adjuvants. In *Immunopotentiators in Modern Vaccines* (pp. 347–375). Academic Press. https://doi.org/10.1016/b978-0-12-804019-5.00018-9

Ling, L. L., Schneider, T., Peoples, A. J., Spoering, A. L., Engels, I., Conlon, B. P., … Lewis, K. (2015). A new antibiotic kills pathogens without detectable resistance. *Nature*, *517*(7535), 455–459. https://doi.org/10.1038/nature14098

Lopez-Sangil, L., Hartley, I. P., Rovira, P., Casals, P., & Sayer, E. J. (2018). Drying and rewetting conditions differentially affect the mineralization of fresh plant litter and extant soil organic matter. *Soil Biology and Biochemistry*, *124*, 81–89. https://doi.org/10.1016/J.SOILBIO.2018.06.001

Ma, L., Shi, Y., Siemianowski, O., Yuan, B., Egner, T. K., Mirnezami, S. V., …

Cademartiri, L. (2019). Hydrogel-based transparent soils for root phenotyping in vivo. *Proceedings of the National Academy of Sciences of the United States of America*, 201820334. https://doi.org/10.1073/pnas.1820334116

Mairhofer, S., Pridmore, T., Johnson, J., Wells, D. M., Bennett, M. J., Mooney, S. J., & Sturrock, C. J. (2017). X-Ray Computed Tomography of Crop Plant Root Systems Grown in Soil. *Current Protocols in Plant Biology*, *2*(4), 270–286. https://doi.org/10.1002/cppb.20049

Mairhofer, S., Zappala, S., Tracy, S., Sturrock, C., Bennett, M. J., Mooney, S. J., & Pridmore, T. P. (2013). Recovering complete plant root system architectures from soil via X-ray µ-Computed Tomography. *Plant Methods*, *9*(1), 8. https://doi.org/10.1186/1746-4811-9-8

Man, A., Şerban Gâz, A., Mare, A. D., Berţa, L., Serban, A., & Florea, G. (2017). Effects of low-molecular weight alcohols on bacterial viability. *Revista Română de Medicină de Laborator*, *25*, 2017. https://doi.org/10.1515/rrlm-2017-0028

McLoon, A. L., Guttenplan, S. B., Kearns, D. B., Kolter, R., & Losick, R. (2011). Tracing the domestication of a biofilm-forming bacterium. *Journal of Bacteriology*, *193*(8), 2027–2034. https://doi.org/10.1128/JB.01542-10

Metzner, R., Eggert, A., van Dusschoten, D., Pflugfelder, D., Gerth, S., Schurr, U., … Jahnke, S. (2015). Direct comparison of MRI and X-ray CT technologies for 3D imaging of root systems in soil: potential and challenges for root trait quantification. *Plant Methods*, *11*(1), 17. https://doi.org/10.1186/s13007-015-0060-z

Moilanen, D. E., Piletic, I. R., & Fayer, M. D. (2007). Water Dynamics in Nafion Fuel Cell Membranes: the Effects of Confinement and Structural Changes on the Hydrogen Bond Network. *The Journal of Physical Chemistry. C, Nanomaterials and Interfaces*, *111*(25), 8884–8891. https://doi.org/10.1021/jp067460k

Muhamadali, H., Chisanga, M., Subaihi, A., & Goodacre, R. (2015). Combining Raman and FT-IR Spectroscopy with Quantitative Isotopic Labeling for Differentiation of *E. coli* Cells at Community and Single Cell Levels. *Analytical Chemistry*, *87*(8), 4578–4586. https://doi.org/10.1021/acs.analchem.5b00892

Musat, N., Foster, R., Vagner, T., Adam, B., & Kuypers, M. M. M. (2012). Detecting metabolic activities in single cells, with emphasis on nanoSIMS. *FEMS Microbiology Reviews*, *36*(2), 486–511. https://doi.org/10.1111/j.1574-6976.2011.00303.x

Nielsen, C. K., Kjems, J., Mygind, T., Snabe, T., & Meyer, R. L. (2016). Effects of Tween 80 on Growth and Biofilm Formation in Laboratory Media. *Frontiers in Microbiology*, *7*. https://doi.org/10.3389/FMICB.2016.01878

Nunan, N., Wu, K., Young, I. M., Crawford, J. W., & Ritz, K. (2003). Spatial distribution of bacterial communities and their relationships with the micro-architecture of soil.

FEMS Microbiology Ecology, *44*(2), 203–215. https://doi.org/10.1016/S0168-6496(03)00027-8

O'Callaghan, F. E., Braga, R. A., Neilson, R., MacFarlane, S. A., & Dupuy, L. X. (2018). New live screening of plant-nematode interactions in the rhizosphere. *Scientific Reports*, *8*(1), 1440. https://doi.org/10.1038/s41598-017-18797-7

Oates, P. M., Castenson, C., Harvey, C. F., Polz, M., & Culligan, P. (2005). Illuminating reactive microbial transport in saturated porous media: Demonstration of a visualization method and conceptual transport model. *Journal of Contaminant Hydrology*, *77*(4), 233–245. https://doi.org/10.1016/j.jconhyd.2004.12.005

Or, D., Phutane, S., & Dechesne, A. (2007). Extracellular Polymeric Substances Affecting Pore-Scale Hydrologic Conditions for Bacterial Activity in Unsaturated Soils. *Vadose Zone Journal*, *6*(2), 298. https://doi.org/10.2136/vzj2006.0080

Pauly, H., & Bailey, J. C. (1999). *Genesis and evolution of the Ivigtut cryolite deposit, SW Greenland*. Copenhagen (Denmark): Commission for Scientific Research in Greenland. Retrieved from https://www.worldcat.org/title/genesis-and-evolution-of-the-ivigtut-cryolite-deposit-sw-greenland/oclc/490728074

Peter, M. G. (2005). Chitin and Chitosan in Fungi. In E. J. Vandamme, S. De Baets, & A. Steinbüchel (Eds.), *Biopolymers Online*. Weinheim, Germany: Wiley-VCH Verlag GmbH & Co. KGaA. https://doi.org/10.1002/3527600035.bpol6005

Pold, G., & DeAngelis, K. M. (2013, June 3). Up against the wall: The effects of climate warming on soil microbial diversity and the potential for feedbacks to the carbon cycle. *Diversity*. Multidisciplinary Digital Publishing Institute. https://doi.org/10.3390/d5020409

Priest, F. G. (1977). Extracellular enzyme synthesis in the genus Bacillus. *Bacteriological Reviews*, *41*(3), 711–753. Retrieved from http://www.ncbi.nlm.nih.gov/pubmed/334155

Reintjes, G., Arnosti, C., Fuchs, B. M., & Amann, R. (2017). An alternative polysaccharide uptake mechanism of marine bacteria. *The ISME Journal*, *11*(7), 1640–1650. https://doi.org/10.1038/ismej.2017.26

Rice, C. D., Dykstra, M. A., & Feil, P. H. (1992). Microbial contamination in two antimicrobial and four control brands of alginate impression material. *The Journal of Prosthetic Dentistry*, *67*(4), 535–540. Retrieved from http://www.ncbi.nlm.nih.gov/pubmed/1507139

Ritz, K. (2011). Views of the underworld: in situ visualization of soil biota. In *The architecture and biology of soils: life in inner space*. https://doi.org/10.1079/9781845935320.0001

Rivas, L. A., Parro, V., Moreno-Paz, M., & Mellado, R. P. (2000). The Bacillus subtilis

168 csn gene encodes a chitosanase with similar properties to a Streptomyces enzyme. *Microbiology*, *146*(11), 2929–2936. https://doi.org/10.1099/00221287-146-11-2929

Robinson, D. (2012). Measuring Roots: An Updated Approach. Edited by S. Mancuso. Berlin, Germany: Springer-Verlag (2012), pp. 382, £135.00. ISBN 978-3-642-22066-1. *Experimental Agriculture*, *48*(3), 466–467. https://doi.org/10.1017/s0014479712000294

Rosenberg, E., Keller, K. H., & Dworkin, M. (1977). Cell density dependent growth of Myxococcus xanthus on casein. *Journal of Bacteriology*, *129*(2), 770–777. Retrieved from http://www.ncbi.nlm.nih.gov/pubmed/402357

Saima, Kuddus, M., Roohi, & Ahmad, I. Z. (2013). Isolation of novel chitinolytic bacteria and production optimization of extracellular chitinase. *Journal of Genetic Engineering and Biotechnology*, *11*(1), 39–46. https://doi.org/10.1016/j.jgeb.2013.03.001

Shimosaka, M., Nogawa, M., Wang, X., Kumehara, M., & Okazaki, M. (1995). Production of Two Chitosanases from a Chitosan-Assimilating Bacterium, Acinetobacter sp. Strain CHB101. *Applied and Environmental Microbiology*, *61*(2), 438–442. https://doi.org/10.1128/aem.70.8.4522-4531.2004

Siala, A., & Gray, T. R. G. (1974). Growth of Bacillus subtilis and Spore Germination in Soil Observed by a Fluorescent-antibody Technique. *Journal of General Microbiology*, *81*(1), 191–198. https://doi.org/10.1099/00221287-81-1-191

Slessarev, E. W., Lin, Y., Bingham, N. L., Johnson, J. E., Dai, Y., Schimel, J. P., & Chadwick, O. A. (2016). Water balance creates a threshold in soil pH at the global scale. *Nature*, *540*(7634), 567–569. https://doi.org/10.1038/nature20139

Stanford Nano Shared Facilities | Stanford University. (n.d.). Retrieved May 25, 2019, from https://snsf.stanford.edu/equipment/xsa/nanosims.html

Stefanie Kohlmeier, †, Theo H. M. Smits, †, Roseanne M. Ford, ‡, Christoph Keel, §, Hauke Harms, ∥ and, & Lukas Y. Wick*, ∥. (2005). Taking the Fungal Highway: Mobilization of Pollutant-Degrading Bacteria by Fungi. https://doi.org/10.1021/ES047979Z

Thom, B. C., Bureau, M., & Ayers, S. H. (1916). Effect of pasteurization on mold spores, *VI*(4).

Tielen, P., Rosenau, F., Wilhelm, S., Jaeger, K.-E., Flemming, H.-C., & Wingender, J. (2010). Extracellular enzymes affect biofilm formation of mucoid Pseudomonas aeruginosa. *Microbiology*, *156*(7), 2239–2252. https://doi.org/10.1099/mic.0.037036-0

Tielen, Petra, Kuhn, H., Rosenau, F., Jaeger, K.-E., Flemming, H.-C., Wingender, J., …

Sandvik, L. (2013). Interaction between extracellular lipase LipA and the polysaccharide alginate of Pseudomonas aeruginosa. *BMC Microbiology*, *13*(1), 159. https://doi.org/10.1186/1471-2180-13-159

Tötzke, C., Kardjilov, N., Manke, I., & Oswald, S. E. (2017). Capturing 3D Water Flow in Rooted Soil by Ultra-fast Neutron Tomography. *Scientific Reports*, *7*(1), 6192. https://doi.org/10.1038/s41598-017-06046-w

Traving, S. J., Thygesen, U. H., Riemann, L., & Stedmon, C. A. (2015). A Model of Extracellular Enzymes in Free-Living Microbes: Which Strategy Pays Off? https://doi.org/10.1128/AEM.02070-15

Tushcel, D. (2017). Why are the Raman spectra of crystalline and amorphous solids different? *Spectroscopy*, *32*(3), 26–33. Retrieved from http://www.spectroscopyonline.com/why-are-raman-spectra-crystalline-and-amorphous-solids-different

Unger, S., Máguas, C., Pereira, J. S., David, T. S., & Werner, C. (2010). The influence of precipitation pulses on soil respiration – Assessing the "Birch effect" by stable carbon isotopes. *Soil Biology and Biochemistry*, *42*(10), 1800–1810. https://doi.org/10.1016/J.SOILBIO.2010.06.019

van Dusschoten, D., Metzner, R., Kochs, J., Postma, J. A., Pflugfelder, D., Bühler, J., … Jahnke, S. (2016). Quantitative 3D Analysis of Plant Roots Growing in Soil Using Magnetic Resonance Imaging. *Plant Physiology*, *170*(3), 1176–1188. https://doi.org/10.1104/pp.15.01388

Vereecken, H., Schnepf, A., Hopmans, J. W., Javaux, M., Or, D., Roose, T., … Young, I. M. (2016). Modeling Soil Processes: Review, Key Challenges, and New Perspectives. *Vadose Zone Journal*, *15*(5), 0. https://doi.org/10.2136/vzj2015.09.0131

Vu, B., Chen, M., Crawford, R. J., & Ivanova, E. P. (2009). Bacterial Extracellular Polysaccharides Involved in Biofilm Formation. *Molecules*, *14*(7), 2535–2554. https://doi.org/10.3390/molecules14072535

Wagner, M., & Haider, S. (2012). New trends in fluorescence in situ hybridization for identification and functional analyses of microbes. *Current Opinion in Biotechnology*, *23*(1), 96–102. https://doi.org/10.1016/j.copbio.2011.10.010

Wang, Y., Song, Y., Tao, Y., Muhamadali, H., Goodacre, R., Zhou, N.-Y., … Huang, W. E. (2016). Reverse and Multiple Stable Isotope Probing to Study Bacterial Metabolism and Interactions at the Single Cell Level. *Analytical Chemistry*, *88*(19), 9443–9450. https://doi.org/10.1021/acs.analchem.6b01602

Wei E. Huang, Robert I. Griffiths, Ian P. Thompson, Mark J. Bailey, and, & Whiteley, A. S. (2004). Raman Microscopic Analysis of Single Microbial Cells. https://doi.org/10.1021/AC049753K

Weiss, M. S., Kreusch, A., Schiltz, E., Nestel, U., Welte, W., Weckesser, J., & Schulz, G. E. (1991). The structure of porin from Rhodobacter capsulatus at 1.8 A resolution. *FEBS Letters*, *280*(2), 379–382. Retrieved from http://www.ncbi.nlm.nih.gov/pubmed/1707373

West, S. A., Diggle, S. P., Buckling, A., Gardner, A., & Griffin, A. S. (2007). The Social Lives of Microbes. *Annual Review of Ecology, Evolution, and Systematics*, *38*(1), 53–77. https://doi.org/10.1146/annurev.ecolsys.38.091206.095740

Wieder, W. R., Bonan, G. B., & Allison, S. D. (2013). Global soil carbon projections are improved by modelling microbial processes. *Nature Climate Change*, *3*(10), 909–912. https://doi.org/10.1038/nclimate1951

Woese, C. R., & Fox, G. E. (1977). Phylogenetic structure of the prokaryotic domain: the primary kingdoms. *Proceedings of the National Academy of Sciences of the United States of America*, *74*(11), 5088–5090. https://doi.org/10.1073/pnas.74.11.5088

Worrich, A., Stryhanyuk, H., Musat, N., König, S., Banitz, T., Centler, F., … Wick, L. Y. (2017). Mycelium-mediated transfer of water and nutrients stimulates bacterial activity in dry and oligotrophic environments. *Nature Communications*, *8*(1), 15472. https://doi.org/10.1038/ncomms15472

Yannarell, S. M., Grandchamp, G. M., Chen, S.-Y., Daniels, K. E., & Shank, E. A. (2019). A dual-species biofilm with emergent mechanical and protective properties. *Journal of Bacteriology*, JB.00670-18. https://doi.org/10.1128/jb.00670-18

Yasbin, R. E., & Young, F. E. (1974). Transduction in Bacillus subtilis by bacteriophage SPP1. *Journal of Virology*, *14*(6), 1343–1348. Retrieved from http://www.ncbi.nlm.nih.gov/pubmed/4214946

Zhu, P., Wang, Q., Jaimes-Lizcano, Y. A., & Papadopoulos, K. (2014). Packed-Bed Capillary Microscopy on BP-Oil-Spill Oil in Porous Media. In *Oil Spill Remediation* (pp. 189–219). Hoboken, NJ: John Wiley & Sons, Inc. https://doi.org/10.1002/9781118825662.ch8